Development and Manufacturing of Scaffold-less Constructs for Tendon/Ligament Repair

by

Michael J. Smietana

A dissertation submitted in partial fulfillment
of the requirements for the degree of
Doctor of Philosophy
(Biomedical Engineering)
in the University of Michigan
2014

Doctoral Committee:

Associate Professor Lisa M. Larkin, Co-Chair
Professor Ellen M. Arruda, Co-Chair
Assistant Professor Kenneth M. Kozloff
Associate Professor Jan P. Stegemann

Dedication

To my family for all their love and support

Table of Contents

List of Tables

List of Figures

Abstract

Soft tissues, such as rotator cuff tendons and the anterior cruciate ligament (ACL), integrate with the subchondral bone through a complex multi-tissue interface that functions to minimize the formation of stress concentrations and enable the efficient transfer of load between tendon or ligament and bone. Current rotator cuff tendon and ACL repair techniques, requiring the reattachment of the tendon/ligament to its original bony footprint, fail to regenerate this interface. Instead, the repaired insertion site transitions from tendon/ligament to bone through a disorganized, fibrovascular scar tissue with weak mechanical properties, leaving it prone to failure and compromising long-term clinical outcomes. To improve tendon-bone integration following rotator cuff repairs, the objective of this thesis was to utilize a scaffold-less tissue engineered construct to promote the regeneration of the tendon-bone interface and develop a reproducible, automated manufacturing system to facilitate the advancement of the construct towards clinical use. Matrix organization and mechanical properties of the regenerated enthesis were evaluated in both acute (immediate repair) and chronic (repair 4 weeks post injury) supraspinatus tear rat models. Utilization of tissue-engineered constructs resulted in superior enthesis regeneration compared to current mechanical fixation techniques.

Next, to enhance the reproducibility and uniformity of existing multi-phasic scaffold-less construct fabrication methodologies, protocol standards and a novel delamination system were developed and later extrapolated for use with human derived constructs. The novel construct fabrication methods yielded an increased number of engineered constructs of consistent size and mechanical properties. Temporal gene expression confirmed the commitment of human derived constructs toward tendon and bone-like tissues. Lastly, to facilitate the eventual

large-scale commercial production of our multiphasic tissues, a novel semi-closed bioreactor system was developed and validated. The use of the bioreactor successfully facilitated the co-culture and integration of two distinct tissue types in a single chamber without any direct user manipulation. The findings described in this thesis will lead to the development of a new soft-tissue-to-bone repair strategy to improve functional tendon/ligament repair outcomes and provide the framework for expediting the clinical and commercial translation of our tissue engineering technologies.

Chapter 1
Introduction

1.1 Specific Aims

Rotator cuff injuries are one of the most common orthopedic disorders affecting the shoulder with approximately 75,000 repair procedures performed each year in the United States [169]. Rotator cuff tears typically involve the supraspinatus tendon at the tendon-bone insertion (enthesis) and are often the cause of significant pain and weakness. Due to the complex anatomy of the shoulder, degenerative changes within the joint and relative hypo-vascularity of the tendon, large tears (>3 cm) do not heal on their own and often require surgical intervention to improve symptomatic injuries. Current primary repair techniques utilize suture to reattach and securely fix the ruptured tendon to its bony insertion. Failure rates, however, with these techniques are unacceptably high (20-94%) and are likely due, at least in part, to the inability to regenerate the native tissue properties of the enthesis during repair. Healing at the enthesis, with current fixation methods, forms a notably weaker, less-organized fibrovascular tissue rather than a mechanically and compositionally graded tissue interface. The organized heterogeneity of the enthesis serves to minimize strain concentrations at this interface and enables load transfer between the soft tissue and bone. Failure to promote native enthesis regeneration can leave the repair site prone to failure and compromise long-term clinical outcomes. As such, there is a need for tissue engineering strategies to recapitulate the enthesis to improve functional outcomes following repair.

Our lab has established a scaffold-less method for engineering 3D tissue constructs derived from mesenchymal stem cells (MSCs). *In vitro*, MSCs are differentiated towards tendon/ligament and bone pathways to form early stage and initially extensible constructs that rapidly remodel *in vivo* to form mature, functional replacement tissues. The combination of these two distinct tissue types in co-culture forms a bi-phasic construct that when used in a sheep ACL repair model quickly integrates with the host tissue and re-establishes a functional enthesis [105]. The success of our constructs to regenerate the tendon/ligament-bone interface of the ACL prompted the investigation of our tissue in a rotator cuff repair model to enhance regeneration of the native tendon insertion site thereby improving repair outcomes.

Additionally, for effective translation of this technology for clinical use, well-characterized and reproducible manufacturing processes must be established that are suited for large-scale commercial production and are compliant with current FDA regulations. Following the development of suitable methodologies, incorporation of these practices into a closed and automated bioreactor system can provide a means to generate efficient, reproducible, and safe constructs in a cost-effective way. The consideration and transition of current laboratory methodologies towards translational manufacturing strategies early in the developmental process can significantly lessen the technical, regulatory, and commercial hurdles plaguing the field of tissue engineering and regenerative medicine.

As such, the goal of this thesis was to design and utilize our scaffold-less constructs to improve enthesis regeneration following rotator cuff repair and to develop a standardized process and manufacturing system for closed, commercially relevant, construct production. To achieve this goal, I have completed the following aims:

Aim 1: Evaluate the efficacy of scaffold-less constructs to regenerate the enthesis following acute and chronic rotator cuff repair.

Aim 2: Develop standardized and clinically relevant methodologies for uniform and reproducible construct fabrication.

Aim 3: Design, build, and evaluate a commercially relevant bioreactor system for closed, automated bone-ligament-bone (BLB) construct fabrication.

The purpose of this thesis is to significantly advance the commercialization of this technology and hopefully hasten its clinical availability for the treatment of musculoskeletal injuries involving the ACL and rotator cuff tendons.

1.2 Rotator Cuff Injury, Repair, and Existing Limitations

1.2.1 Rotator Cuff Injury

The rotator cuff functions to stabilize the glenohumeral joint and control shoulder movement. The rotator cuff is comprised of four muscles and associated tendons that include the supraspinatus, infraspinatus, teres minor and subscapularis (Figure 1.1A**)**. Rotator cuff tendon tears are one of the most common injuries affecting the shoulder, with over 75,000 repair procedures performed annually in the United States [169]. Rotator cuff tears most commonly involve partial thickness or full thickness rupture of the supraspinatus tendon near the tendon-to-bone interface of the humeral head [78] (Figure 1.1B).

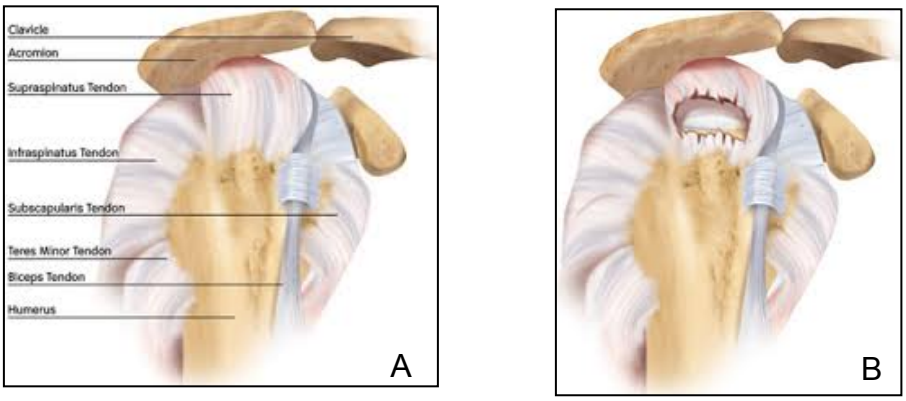

Figure 1.1 Rotator Cuff Anatomy A) Native shoulder, and B) Full-thickness supraspinatus tendon tear. (http://www.smith-nephew.com/patient/health-concerns/sports-injuries/shoulder-injuries/rotator-cuff-tear/)

The two main mechanisms of rotator cuff injury are acute and chronic tears. Acute tears account for less than 10% of all rotator cuff tears and arise as a result of sudden high-impact motions, or are usually sustained following a fall or shoulder dislocation [12]. Most rotator cuff tears (~90%) are chronic in nature and occur as the result of repetitive wear over time [161]. Patient age has been implicated as a key contributing factor for the increased frequency and size of chronic rotator cuff tears in the elderly population [20,75,144,161]. A cadaveric study showed that 30% of people over age 60 displayed signs of degenerative tears compared to only 6% of those younger than 60 [90].

Rotator cuff injuries typically involve one or more tendon tears leading to a loss of function, instability, pain, and compromised joint mechanics [78]. Due to the hypo-vascularization and degenerative weakening of the tendon with age, as well as, the complex anatomy and extensive range of motion associated with the shoulder joint, tears of the rotator cuff tendons do not heal [58,60,108,143,144,182]. Treatment of rotator cuff injuries can be managed conservatively with anti-inflammatory medication, steroid injections, and physical therapy aimed to reduce pain and restore strength [23]. However, for those with large tears (>3cm), persistent pain, or shoulder weakness, surgical intervention is typically recommended to restore joint mechanics [89].

1.2.2 Current Rotator Cuff Repair Techniques

The current standard of treatment for symptomatic rotator cuff tears includes early primary anatomic repair followed by controlled rehabilitation [59]. Repair procedures most commonly involve arthroscopic tendon-bone fixation techniques that rely on suture materials and suture anchors [43,120,172]. Regardless of the specific suture configuration used, the goal of the surgery is to anatomically secure the ruptured tendon to its anatomic footprint to improve shoulder strength and function [4,168,172]. While the repair of acute, small to medium tears have had suitable outcomes with existing techniques, repair of chronic, large (3-5cm) or massive tears (>5cm, 2 tendons) have been associated with significant failure rates [7,118,144].

Repairs of chronic rotator cuff injuries often fail to form a robust attachment at the tendon-to-bone repair site, making it prone to continued failure [166]. Excessive tension placed on the initial repair site can gradually pull the healing tendon away from the bone, forming a gap that can result in complete repair failure, or a re-tear [26]. Clinical studies have reported unacceptably high re-tear failure rates ranging from 20-94% [53,60] depending on the size of tear [33,66,79], tissue quality [51,67,68,79,85,87,137,138], and time between injury and repair [11,12,19,46,55,74,76]. Chronic injuries in particular present additional challenges that include significant retraction of detached tendon, poor quality of remaining tendon, limited vascularization, muscle atrophy, fatty infiltration, and osteolysis at the insertion site that can further complicate repair outcomes [33,67,72,187]. To reduce the high occurrence of re-tears and improve tendon repair outcomes, several tissue-engineering strategies designed to promote tendon-bone integration and/or augment mechanics at the repair site have been developed [7,40,136].

1.2.3 Rotator Cuff Repair: Augmentation with Biologic Scaffolds

To improve primary repair outcomes of large rotator cuff defects, several commercially available biologic and synthetic scaffold devices have been utilized to mechanically reinforce and enhance the body's own healing potential for

integrating the tendon to bone [39,147]. A recent publication by Ricchetti et al., extensively reviews the current basic science and clinical understanding of several ECM scaffolds currently used to enhance tendon attachment to bone [136].

Extracellular matrix (ECM)-derived scaffolds are the most widely used scaffolds for rotator cuff repair and are commonly derived from acellularized small intestinal sub-mucosa (SIS) or dermis tissue, from both allogeneic and xenogeneic sources [8,35,41]. Used as patches or overlays to augment existing suture techniques, these scaffolds aim to provide temporary mechanical support to "off-load" the repair site at early time points until sufficient tendon attachment has occurred [42,96,97]. However, variations in the structural composition of the scaffold (i.e. collagen crosslinking) can greatly affect the matrix degradation rates *in vivo*[9]. The failure to match the scaffold's degradation rates with a sufficient amount and/or quality of new matrix production can result in a weakening of the scaffold's overall mechanical properties and limit its usefulness for repair.

In a recent study performed by Derwin et al., four commercially available ECM scaffolds were evaluated at time of repair using a canine infraspinatus tear model [41]. The results of this study showed that the elastic moduli of all four matrices were initially an order of magnitude lower than the native canine tendon and, upon implantation, rapidly decreased their mechanical properties as a result of premature graft resorption. This suggests that the mechanical role of these scaffolds for use as an augmenting device and their ability to enhance tendon-bone attachment may be limited. Additionally, the high compliance associated with these materials would likely result in considerable stretching of the material under physiologic muscle loading and limit its use in primary rotator cuff repair [41].

In addition to providing a mechanical structure, the ECM scaffold's natural composition, unique 3D structure, and ability for remodeling *in vivo* may provide a chemical and structural environment capable of instructing host cells to enhance healing at the site of repair. However, despite encouraging results as a

graft patch in animal models, sub-optimal results were observed in human trials [80,149,171]. In a randomized control trial performed by Iannotti et al., augmentation with small intestinal submucosa (SIS) failed to improve frequency of re-tear, tendon healing, or clinical outcome scores [80]. The sub-optimal results have been primarily attributed to a mismatch in mechanical properties, rapid matrix remodeling found in the chronically degenerated shoulder joint environment, and lack of functional tendon-to-bone integration [41].

More recently, free biceps tendon autografts have been used in repair, particularly in exceptionally large retracted tears, in which anatomic re-attachment is impossible [32,117,121,135]. However, the use of autogenic tissues, especially from most at-risk elderly patients, is limited by tissue availability, donor site morbidity, and poor tissue quality. Additionally, the availability, associated costs of processing, and risk of immune response from residual genetic material further diminishes the potential use of allogeneic or xenogeneic grafts and scaffold tissues for rotator cuff repair [139].

To date, the utilization of tendon grafts and ECM derived materials to improve function and integration at the tendon-bone attachment site has encountered limited clinical success [31,41]. Alternative strategies and factors are needed to improve the biological fixation of the tendon to the bone to improve overall stability and functionality of the repair.

1.2.4 ACL Injury and Repair

The anterior cruciate ligament (ACL) connects the femur to the tibia and is the most commonly injured ligament of the knee with an estimated 200,000 injuries occurring each year in the US, especially in younger female athletes [18] (Figure 1.2). The ACL mediates load transfer and provides overall knee stability by limiting excessive anterior tibial translation and internal knee rotation. The ACL does not heal on its own following injury due in part to a lack of vascularization. Surgical intervention is often required to restore knee stability. Over 100,000

reconstructive surgeries are performed yearly in the US, with expenditures exceeding 5 billion dollars [25,124,170].

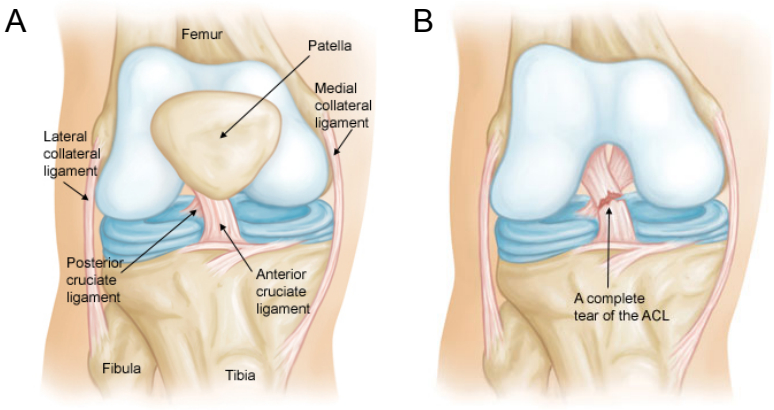

Figure 1.2 Anatomy of the Knee A) Native ACL, and B) Torn ACL (http://orthoinfo.aaos.org/topic.cfm?topic=a00549)

Current reconstruction techniques utilize allogeneic or autogenic tendon grafts secured into anatomically placed tibial and femoral bone tunnels to restore ACL function [116]. Grafts most commonly used include the hamstring tendon (HT) graft and the bone-patellar tendon-bone (BPTB) graft isolated from the central third of the patellotibial junction. However, the higher risk of revision surgery with HT grafts and the ability of BPTB grafts, to more effectively integrate with subchondral bone of the tunnels have made BPTB grafts the current gold-standard for repair [50,125].

Despite favorable outcomes following ACL repair, graft failure rates have been reported as high as 25% due in part to poor graft fixation [37,45,134]. Long-term, follow-up studies of ACL reconstructed patients have shown continued knee laxity and only a 63% return to pre-injury activity [6]. Additionally, the incidence of early-onset osteoarthritis (OA) within 7-14 years has been reported as high as 50% [95,129,145]; and more recently, a study by Barenius et al., revealed a 3-fold increase in the prevalence of OA after ACL reconstruction compared to the contralateral knee [10].

Compared to the native ACL, current tendon graft tissues exhibit vastly different mechanical and viscoelastic properties that often exceed the native tissue stiffness and strength [105,139]. Recent evidence suggests that an overly stiff ECM can shield the endogenous cells or infiltrating host cells within these structures from strains necessary for proper graft-bone integration and growth of new ligamentous tissue [49,64,111,127]. Suboptimal tissue mechanics, limited tissue availability, and donor-site morbidity associated with the use of autologous grafts, as well as the additional risk of disease transmission with allogeneic tissues, has led to the development of novel tissue-engineering graft alternatives for ACL repair.

Current tissue engineering strategies for ACL repair often rely on the use of exogenous scaffold materials to match the native tissue properties [127]. Again, the over-design of these graft materials for initial strength and stiffness, compounded with variable degradation rates and risk of immune rejection, limit their ability to integrate with native bone and regenerate the damaged ligament tissue.

Mechanical fixation of tendon grafts to bone is commonly performed with interference screws, which often fail to preserve or re-establish the anatomic insertion site following surgery. Consequently, the resultant attachment site is considered the weak point during early post-operative healing and is prone to pullout failure under normal knee motion [100,113,140,142]. Regeneration of the native tissue interface is important for improving graft strength and maturation of healing tissue and is critical for restoring normal knee kinematics and improving long-term outcomes following repair [101].

1.3 Tendon/Ligament to Bone Interface - Enthesis

1.3.1 Enthesis Structure and Function

Tendons (connecting muscle to bone) and ligaments (connecting bone to bone) attach to the bone via an indirect or direct insertion site [16]. Indirect insertions,

also known as fibrous insertions, superficially attach the tendon or ligament to the bone via the periosteum and are characterized by collagenous fibers known as Sharpey's fibers that traverse directly from the tendon or ligament deep into the bone [126]. Fibrous attachments are often broad, distributing force over a large area and reducing stress concentration at the interface. Examples of indirect entheses include the medial collateral ligament (MCL) and the deltoid tendon insertion of the humerus.

Direct insertion sites are characterized by a heterogeneous and regional distribution of cells, matrix, and mineral content [100,148,155,166]. The composition and structure of this insertion site is shared by both rotator cuff tendons of the shoulder and cruciate ligaments of the knee and are considered biochemically and morphologically similar [36,179]. Direct entheses connect the tendon or ligament to bone via a characteristic fibrocartilage region over a length of approximately 100μm-1mm. [180]. This interface, also referred to as a fibrocartilaginous insertion, exhibits a functionally graded zonal arrangement composed of four regions that include: 1) tendon or ligament, 2) un-mineralized fibrocartilage, 3) mineralized fibrocartilage, and 4) bone (Figure 1.3) [15,16,180].

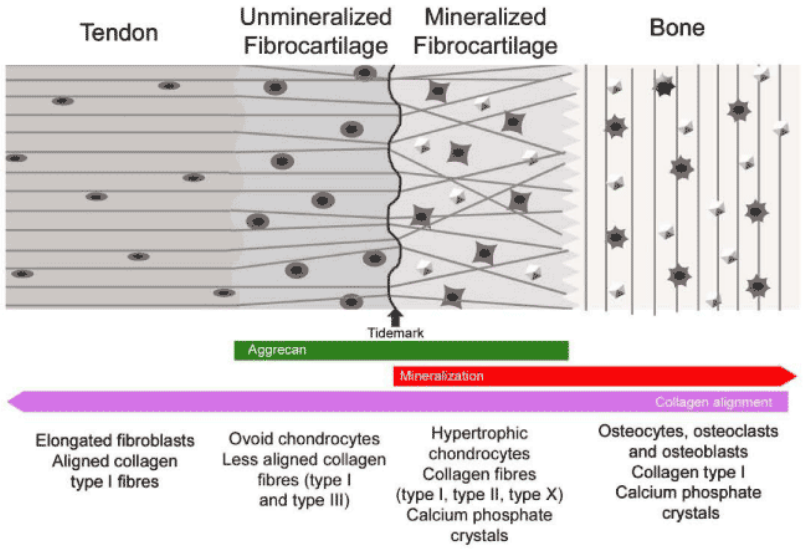

Figure 1.3 Structural and Compositional Zonal Arrangement of the Enthesis (http://omicsonline.org/2161-0533/2161-0533-S1-003.php?aid=4930)

The tendon or ligament (zone 1) consists of elongated, spindle-shaped fibroblasts embedded in a highly aligned extracellular matrix (ECM) composed of primarily type I collagen with small amounts of type III and V collagen, elastin, and proteoglycans such as decorin [88]. The un-mineralized fibrocartilage region (zone 2) contains ovoid fibrochondrocytes and consists of type II, and III collagen with small amounts of type I, IX, and X collagen along with the proteoglycans aggrecan and decorin [165]. The mineralized fibrocartilage region (zone 3) contains hypertrophic fibrochondrocytes and significant amounts of type I, II and X collagen and aggrecan. Calcium phosphate crystals and mineral deposits are also contained within this region [148,155]. Collagen fibril alignment is more disorganized here compared to both tendon and un-mineralized fibrocartilage regions [164]. The border between mineralized and non-mineralized fibrocartilaginous regions is identified by a ‘‘tidemark’’, a basophilic line that represents the mineralization front. The last region, bone (zone 4), consists of osteoblasts, osteocytes and osteoclasts and is mainly composed of type 1 collagen and a large mineral content [165].

The mechanical properties of bone and tendon are significantly different. Bone is stiff with a modulus of 20 GPa whereas tendon is extensible with a stiffness around 200 MPa [162]. The presence of a fibrocartilaginous transition region is designed to reduce stress concentrations that would otherwise form at the interface of two dissimilar materials [150,164].

The varied mechanical properties across the tendon/ligament insertion site are related to gradations in collagen fiber orientation and mineral content. Highly aligned collagen fibers become more disorganized across the insertion as the fibers angularly integrate with the bone, reducing tissue stiffness (Figure 4) [164]. This structural gradation results in a region between tendon and bone that is approximately half as stiff as the tendon [100]. The compliance of the region between tendon and bone may serve to dissipate energy during load transfer and help prevent injury [61,100]. Nearer to the bone region, the increasing mineral

content of the insertion site causes stiffening of the collagen fibers and increases tissue stiffness approaching that of the bone [61].

Interdigitation of the fibrocartilage region with the bone increases the surface area of the attachment and, along with its ability to resist changes in cross-sectional area, is thought to reduce stress concentrations at this interface [61]. Additionally, the structural and mechanical differences across this zone gradually dissipate fiber bending and stretch-induced narrowing of the tendon that can arise during movement away from the tendon-bone junction [14,17,150]. As a result, the likelihood of failure of the fibrocartilaginous zone, if healthy, is drastically reduced with failure occurring more often in the tendon/ligament region or subchondral bone [57].

1.3.2 Enthesis Healing Following Repair

The structure and function of the native enthesis is essential for mediating load at the tendon/ligament bone interface. As such, its regeneration following repair is critical for optimal outcomes. Failure to regenerate may leave the attachment site prone to failure, limiting clinical outcomes such as the return of normal shoulder function [61,93].

Despite efforts to improve tendon-bone healing, current rotator cuff repair practices involving suture with or without scaffold augmentation fail to restore the native enthesis [101,141]. Instead, current mechanical fixation techniques develop a disorganized fibrovascular tissue with inferior mechanical properties between the tendon and bone [29,56,141,166] (Figure 1.4). The loss of this complex fibrocartilaginous insertion at the tendon-bone interface has been implicated in the high frequency of tendon re-tears following primary rotator cuff repair [74,100,122,164].

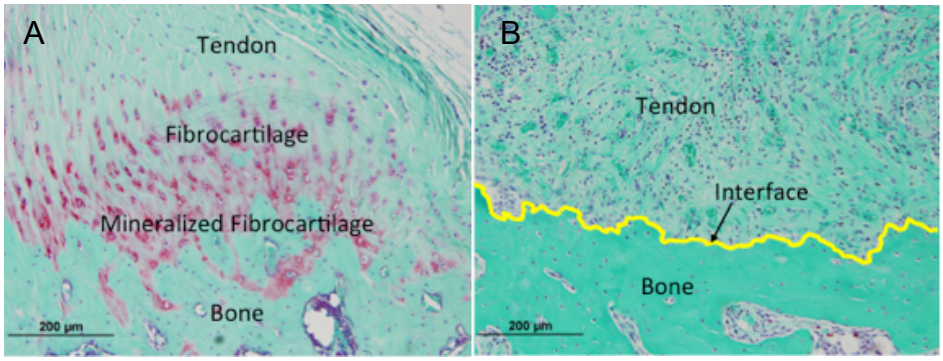

Figure 1.4 Safranin O Staining of RC Enthesis A) Native RC enthesis, and B) RC enthesis following suture repair.

Formation of this fibrous tissue following repair occurs over three stages: inflammation (0-7 days), repair (5-14 days), and remodeling (>14 days) [100]. First, in the inflammation stage, a substantial infiltration of fibroblast and inflammatory cells occurs at the site of injury and increases angiogenesis. The ECM contains some cartilage-like cells and is composed of primarily fibronectin, glycosaminoglycans, and type III collagen [163]. Collagen fiber orientation and tensile mechanical properties of the tendon are significantly decreased, resulting in no integration with bone and the lack of a fibrocartilage insertion zone.

During the repair stage, collagen fibers begin to integrate with the bone but overall tissue quality remains poor and disorganized compared to native [63]. The tissue is composed of granulation tissue and contains chondrocyte-like cells and fibroblasts [56]. Several growth factors are up-regulated to induce cell proliferation and matrix deposition at the site of repair including fibroblast growth factor basic (FGF-b), bone morphogenetic proteins (BMP-12 -13, and -14), platelet derived growth factor-B (PDGF-B), and transforming growth factor-B1 (TGF-B1) [181].

In the remodeling stage, the newly formed tissue remains disorganized and hypercellular [62]. Following 4 weeks repair in a rat model, the tendon had integrated with bone but no fibrocartilage region was observed [62]. At 8 weeks, the repair site was more organized than previous time points but did not resemble the graded fibrocartilage structure of the native enthesis [163]. Although structural

properties reached two thirds of normal levels, the material properties of the tissue remained an order of magnitude weaker than in control groups [29]. By 16 weeks, the healing tissue still had not functionally integrated with the bone. The tendon attached to the bone through a fibrovascular scar with a sharp boundary between soft tissue and bone and was structurally and compositionally different than the native enthesis tissue [3,101].

Like the rotator cuff, repair of the ACL with current grafting techniques also fails to recreate a fibrocartilaginous enthesis. Instead, the graft often heals with a fibrovascular scar at the graft-tunnel interface that exhibits poor mechanical stability and remains a primary cause of ACL graft failure [2]. Furthermore, suboptimal long-term ACL outcomes and increased risk of OA may be due in part to poor graft-bone integration and an inability to effectively transfer load [48]. As such, the re-establishment of a native-like enthesis is crucial for improving the long-term success and functionality of the reconstructed knee.

As described, current surgical procedures for both rotator cuff and ACL repairs fail to regenerate the compositional, geometrical, and biomechanical properties of the native enthesis to the level needed for normal joint function and tissue regeneration [126]. As a result, researchers have begun to design new strategies focused on recreating the functional properties of the native enthesis to improve repair success and improve long-term outcomes [98,154].

1.3.3 Native Enthesis Development

Understanding the biological and mechanical processes regulating the development of the native tendon-bone interface may be useful in identifying new tissue engineering strategies for improving enthesis repair. In a recent *in situ* hybridization study by Galatz et al., the spatial and temporal expression of ECM genes involved in rotator cuff development were examined utilizing a murine model [52]. The study reports the formation of tendon and bone masses at 15.5 days post-conception but a transition zone was not observed until 7 days after

birth. Furthermore, significant enthesis maturation did not occur until day 21 postnatally. The formation of a direct insertion site is believed to occur through endochondral ossification. The tendon/ligament initially attaches to the hyaline cartilage of bone and as ossification occurs, a fibrocartilaginous region develops at the tendon-bone interface. The formation of this fibrocartilage zone is due to fibroblast metaplasia as a result of mechanical stimuli at the insertion site [83,167]. The influence that mechanical load has on enthesis formation during post-natal development underlines the important role mechanical stimuli may play in regenerating the insertion site during repair.

In a separate study, muscle loading during tendon enthesis development has been shown to significantly impact insertion maturation in a murine model [77]. Botulinum toxin injection, which causes muscle paralysis, resulted in less mineralization, impaired fibrocartilage formation, diminished collagen alignment, and inferior mechanical properties compared to saline controls at post-natal time points [77]. However, paralysis at early time points did not result in significant differences in enthesis structure suggesting that mechanical load is not needed for initiation of enthesis development but is a critical factor in directing enthesis maturation [77].

In addition to mechanical cues, chemical factors are also known to be important in enthesis development. Proteins including Indian hedgehog (Ihh) and parathyroid hormone-related protein (PTHrP) have been implicated in regulating chondrocyte hypertrophy and mineralization[100,162]. Graded expression of these factors at the tendon-bone interface may regulate spatial gradients between mineral and un-mineralized fibrocartilage zones[162]. Transcription factors SOX-9 and scleraxis (Scx) are associated with chondrogenesis and tenogenesis respectively [152,160]. Cells forming the insertion site originate from both SOX-9 and Scx lineages and the localization of these genes at the tendon-bone interface defines the tendon/fibrocartilage transition [160]. Scx expression at this site has

also been shown to regulate BMP-4 expression in tendon cells. Inhibition of BMP-4 expression in Scx positive cells failed to initiate enthesis development [21].

The combination of these works demonstrates that the development of a functionally graded enthesis is driven by and responsive to both biologic and mechanical signals. As such, tissue-engineering strategies targeting these signaling pathways post-injury may be useful for stimulating the required cells, ECM, and mechanical properties necessary for native-like repair.

1.4 Strategies to Improve Tendon-Bone Healing *In Vivo*

Recent tissue-engineering approaches to improve soft-tissue/bone healing at the tendon-bone interface are typically designed to augment current repair techniques *in vivo*. Treatments often rely on the singular or combined use of growth factors and cells with existing suture or scaffold-augmented fixation techniques to modulate the repair site and facilitate the formation of the native insertion site. These biologic approaches have been extensively reviewed by several researchers[3,13,114]. Examples of specific applications as they relate to rotator cuff repair are described below:

1.4.1 Growth Factor Therapies

To enhance rotator cuff healing *in vivo*, the application of various growth factors capable of modulating the biology at site of repair have been investigated [114]. Fibroblast growth factor basic (FGF-2) is known to stimulate angiogenesis as well as influence matrix synthesis and is up-regulated during early stages of tendon healing [3,71]. Local application of FGF-2 in a fibrin sealant following acute injury and repair of the supraspinatus tendon in a rat model resulted in accelerated healing at the tendon-bone interface compared to the fibrin sealant alone in the contralateral shoulder [81]. At 2 weeks, histological scorings of repair sites demonstrated improved cellularity, vascularity, and fiber maturity and were correlated with improved mechanical strength when compared to fibrin only

treatment. However, differences were not observed at the later 4 and 6 week time points. Additionally, despite the improvement in attachment strength, a fibrocartilaginous region characteristic of the native tendon-bone interface was not recreated.

In a similar study by the same group, FGF-2 fibrin sealant was applied to a rat tendon-bone interface and repaired with a commercially available acelluarized dermal graft (GraftJacket)[82]. At 2 weeks, repair with FGF-2 showed similar histological scores and strength compared to graft repairs without growth factor. However at 6 and 12 weeks, repair with FGF-2 formed a cartilaginous tissue at the tendon-bone interface accompanied with improved repair failure strength. Despite the presence of fibrocartilage, the insertion site still did not recreate the complexity of the direct insertion found in the unoperated control shoulders.

TGF-B isoforms have also been shown to alter healing at the tendon-bone interface with varied results [84]. Application of TGF-B1 (and suppression of isoforms 2 and 3) at repair sites resulted in increased fibrous scar tissue formation and a decrease in mechanical properties; while the use of TGF-B3 and suppression of isoforms 1 and 2, resulted in no significant change compared to controls. In a separate study, however, prolonged exposure to TGF-B3 in a heparin/fibrin-based delivery system positively enhanced the structural and material properties of the tendon-bone interface following repair [107]. Decreased scar formation and increased fibrocartilage formation, collagen alignment, and interface strength have also been reported with the use TGF-B3 administered at site of repair within osteoconductive calcium-phosphate matrix[86].

In vivo, growth factor signaling pathways may be regulated and may interact with each other to coordinate control of cell function. FGF-2, for example, is known to alter gene expression of several growth downstream factors including TGF-B and BMP-2 [13]. As such, signaling of a single growth factor is unlikely to mediate

native-like tissue regeneration alone and has led researchers to the use of platelet rich plasma (PRP) therapies to improve enthesis repair.

PRP, isolated from autologous blood, forms a dense plasma matrix that can be applied at the repair site. PRP is known to contain several growth factors that have been shown to play a critical role in the tendon healing process including: TGF-B, bFGF, PDGF, vascular endothelial growth factor, connective tissue growth factor, and epidermal growth factor [3]. In a recent study by Ersen et al., the use of PRP in a rat supraspinatus tear model resulted in improved load to failure and stiffness at the repair site [47]. However, histological differences were not observed between groups repair treated with and without PRP.

While the use of growth factor based strategies commonly results in increased matrix synthesis and structural improvements at the repair site, the resultant tissue often consists of fibrous scar tissue rather than an organized, fibrocartilage gradient characteristic of the native enthesis. Further optimization related to the mode of delivery, timing of release, and ideal concentrations is needed for these strategies to be successful. As such, surgeons continue to rely on existing suture fixation techniques with sub-optimal outcomes. Alternative cell-based therapies, capable of sensing and responding to the local chemical and mechanical environments, may be needed to improve enthesis repair.

1.4.2 Cell-Based Therapies

One of the most common cells used in current cell-based therapies is the mesenchymal stem cell (MSC). MSCs are characterized by their unique ability to self-renew and differentiate *in vitro* into several different specialized tissue lineages including bone, tendon, cartilage, muscle, ligament, and adipose tissue [27,184]. MSCs can be easily isolated from an autologous or allogeneic bone marrow aspiration and are considered to be anti-inflammatory and/or immuno-modulatory upon implantation. More recently, resident MSC populations have also been harvested from adipose tissues which may be a more accessible

donor source for MSC isolation [44]. *In vivo*, MSCs are capable of directly participating in the healing response or signaling local or distant host processes.

The use of MSCs to improve tendon-bone healing following rotator cuff injury has recently been examined in a rat model [69]. Following the detachment of the supraspinatus tendon, bone marrow derived MSC contained in a fibrin sealant carrier were injected into the repair site and the tendon subsequently repaired with suture [69]. Results, at both 2 and 4 week time points, showed no histological difference in cartilage formation, collagen orientation, failure strength, or stiffness of the enthesis compared to controls [69]. Additional signals or differentiation factors are likely needed for effective interface repair. Undifferentiated MSC alone may not be enough to stimulate the desired regenerative response.

In a follow-up study also performed by Gulotta et al., MSCs were transduced with adenoviral-mediated scleraxis, a transcription factor implicated in tenogenesis and native enthesis development, before being integrated into a fibrin sealant carrier and injected into the repair site[70]. Despite the lack of histological improvement at 2 weeks following repair, increases in both load to failure and stiffness were observed compared to non-transduced MSC injected controls. At 4 weeks, the biomechanics continued to improve, and histologically, the formation of fibrocartilage was observed at the tendon-bone interface. However, the organization of this tissue and amount of fibrocartilage present was still significantly less than in the native enthesis. Nonetheless, the application of differentiated MSCs may be a useful tool for inducing the native healing response following rotator cuff repair and holds promise for future cell-based strategies utilizing these cells.

Despite the potential of the described *in vivo* techniques to improve tissue healing at the tendon-bone interface, many of these strategies continue to rely on existing suture-fixation techniques and frequently fail to re-create the native anatomy of the rotator cuff enthesis. The inability to restore this interface

compromises repair success and long-term clinical outcomes following tendon/ligament injury [99]. As such, novel tissue engineering approaches capable of regenerating the graded fibrocartilaginous structure and mechanics of the native enthesis are needed for orthopedic repair.

1.5 *In Vitro* Scaffold-Based Strategies for Enthesis Repair

To improve regeneration of the tendon-bone insertion site following repair, several *in vitro* tissue-engineering strategies have been developed to replicate the functionally graded properties of the enthesis for subsequent implantation *in vivo* [186]. These approaches mimic the zonal arrangement of the native tissue by imploring stratified or graded scaffold designs described in the following sections [154].

1.5.1 Stratified Scaffold Designs

Stratified scaffold designs for enthesis regeneration typically consist of various cells, growth factors, or other signals continuously arranged in pre-defined regions specific for the generation of distinct tissue types. The goals of stratified scaffold designs are to integrate these regions and form a graded fibrocartilaginous transition zone following implantation. Work by Spalazzi et al., successfully produced a co-cultured 3D scaffold composed of three distinct but continuous phases arranged in succession. The first phase served as the tendon region and consisted of poly- (lactic-co-glycolic acid) (PLGA) (10:90) matrix seeded with ACL derived fibroblasts [158,159]. The second region was the fibrocartilaginous region composed of PLGA (85:15) and seeded with chondrocytes. The third region served as the bone region and was composed of sintered PLGA (85:10) and 45S5 glass microspheres and was seeded with osteoblasts. Deposition of collagen 1 was observed throughout the tendon and fibrocartilage regions with significant amounts of mineral in the bone region. Subcutaneous implantation of the constructs resulted in continuity across all three phases with mineralized tissue in the bone regions and distinct

fibrocartilage and tendon regions [156,157]. The results of these studies demonstrated the ability of a multi-phasic construct consisting of appropriate cells and matrix composition to form a functionally graded tissue following implantation. However, the ability of this stratified scaffold to integrate with the host or grafted tissue in a tendon/ligament repair model has not been evaluated. Moreover, the utilization of scaffold materials with variable degradation rates and mechanical properties may shield the cells from signals required for optimal tissue regeneration upon implantation.

Paxton et al. describes an alternative scaffold design for the creation of a whole multi-tissue construct composed of an artificial ligament mid-substance attached between two osteoconductive anchors [123]. Fibroblasts seeded into a fibril gel are guided through cell-mediated tension around two bio-resorbable bone cement anchors (Brushite) producing ligament/bone-like tissue interfaces. Increasing the collagen content of the ligament region, through the addition of growth factors (ascorbic acid, proline, and TGF-B), led to an increase in the attachment strength at this interface. The ability of this strategy to form a ligament mid-substance and two relevant ligament/bone interfaces allows this technology to directly replace the damaged tissue at the site of repair eliminating the need to integrate with the damaged tendon/ligament tissue or replacement tendon graft. However, the ability of this construct to regenerate a fibrocartilaginous enthesis following implantation has not been evaluated.

1.5.2 Graded Scaffold Designs

Opposed to stratified scaffold designs that rely on integration of distinct, pre-defined regions upon implantation to recreate the graded properties of the enthesis, graded scaffold designs utilize spatially arranged biochemical or biophysical signals to gradually control cell differentiation and matrix synthesis *in vitro*. In a study performed by Phillis et al., fibroblasts were seeded onto a scaffold substrate conjugated with a linearly graded increase of a bone transcription factor, Runx2. Regions of low Runx2 concentration were associated

with more tendon-like phenotype, while higher concentrations trans-differentiated towards osteoblast-like cells [128]. The results showed a gradual change in phenotype over the length of the scaffold. However, the formation of a fibrocartilaginous transition was not recreated.

In a similar study, MSC were cultured onto a polymeric scaffold to engineer composite osteochondral tissues [174]. Silk microspheres formed two inversely proportional linear gradients across the construct controlling the delivery of BMP-2 and IGF-1. The proximal and distal ends of the scaffold contained the highest concentrations of BMP-2 and IGF-1, respectively, which both decreased across the construct length. This gradual change of local growth factor release resulted in graded differences of calcium and glycosaminoglycan (GAG) deposition, characteristic of bone and cartilage regions, respectively. Collagen type-I, II, and X gene expressions were also similarly graded across the two construct regions, mimicking the native composition of the osteochondral interface. The results of this study validate the ability of controlled growth factor release to generate tissue gradients *in vitro* and may be applicable in generation of other tissue interfaces such as the tendon-bone interface.

Biophysical gradients can also be used to form functionally graded interface tissues *in vitro* [92,186]. In a study by Li et al., a mineralization gradient of calcium phosphate was incorporated into electrospun PLGA nanofibers [91]. The formation of this gradient was associated with stiffness variations across the scaffold length. Seeding this scaffold with adipose-derived MSCs resulted in the graded expression of osteogenic cell markers, with regions of highest stiffness and mineral content being most bone-like. Interestingly, formation of this osteogenic gradient was achieved without osteogenic inducing culture medium suggesting that compositional and mechanical gradations alone may be sufficient to promote cell differentiation and influence cell behavior.

Each of the scaffold-based strategies described emphasize the influence local environmental factors (generated *in vitro* or following implantation) have on the formation of graded tissue properties. However, use of these strategies (stratified or graded in design) is limited as they are routinely designed to match the native properties of the tendon, bone, and/or insertion site, potentially shielding the repair site from signals necessary for proper enthesis regeneration. Additionally, the degeneration of the scaffold material often does not match the rate of new tissue synthesis and can impair the rate and course of new tissue development and maturation. Furthermore, the use of exogenous scaffolding materials can trigger a foreign body reaction leading to material rejection and/or increased amounts of fibrotic scar tissue at site of repair.

Due to these imitations and the inability of current scaffold-techniques to fully regenerate native enthesis following repair, alternative tissue engineering strategies are needed. A scaffold-less method to engineer an initially compliant multi-phasic tissue graft, composed of physiologically relevant tissue interfaces and capable of sensing and responding to local environmental signals, may be well suited for regeneration of the native functional tendon-bone interface.

1.6 Scaffold-less Tissue Engineering – STEL Approach

Previous work from our lab, the Skeletal Tissue Engineering Laboratory (STEL), has demonstrated the successful fabrication of a multiphasic bone-ligament-bone (BLB) graft for ligament repair, without the use of exogenous or stiff, scaffolding materials [104,105]. Regionally distinct areas of bone and ligament form viable tissue interfaces *in vitro* that are capable of quickly remodeling upon implantation. (Figure 1.5)

Figure 1.5 Scaffold-Less BLB Construct

The utilization of this initially compliant graft in both medial collateral (MCL) and anterior cruciate ligament (ACL) repair models has shown that the graft quickly incorporates into native tissue and develops a viable enthesis shortly following repair [105]. Significant improvements in construct size, composition, morphology, and mechanics were observed at increased ACL recovery time points, as described in the work of Ma et al. [106]. Briefly, BLB outcomes, following 6 months recovery, restored approximately 52% of native tissue modulus and were histologically similar to the native ACL tissue. Results at later 9 month recovery time points compared to existing autologous patella tendon graft techniques, demonstrated superior tissue regeneration and knee mechanics [106].

However, despite the success of this BLB tissue in an ACL repair model, the translation of these results to a rotator cuff repair model is unknown. Additionally, to further the advancement of this technology towards clinical use, a regulatory compliant, standardized, and commercially viable manufacturing process is needed. Achievement of these goals could significantly streamline the long-term success of this tissue engineering product for both tendon and ligament repair.

1.7 Summary

The approach, outlined in the aforementioned aims, seeks to advance the commercial manufacturing and clinical translation of a compliant multi-phasic tissue construct for tendon/ligament repair. The use of a compliant scaffold-free graft that can respond to local mechanical and biological environments has the potential to improve tendon/ligament-to-bone regeneration and subsequent repair outcomes following rotator cuff and ACL injury. However, despite considerable

amounts of research in the field and the development of numerous tissue-engineering strategies, there are relatively few products currently available to patients or in late-stage clinical trials. This slow progress in development is due part to a lack of proficiency in translating bench-scale methods to robust, cost-effective manufacturing processes that comply with current good manufacturing processes (CGMP) guidelines and ensure the reproducibility, efficacy, and safety of the final tissue engineering product for human use.

Utilizing a rat model, Chapter 2 of this thesis, will evaluate the efficacy of our scaffold-less construct to regenerate the native enthesis following an acute, and more clinically relevant, chronic, full thickness supraspinatus tear. It is hypothesized that utilization of our construct will regenerate an enthesis that more closely resembles the native structural properties compared to current suture repair techniques.

Next, Chapter 3 and Chapter 4 will describe the advancement of existing laboratory protocols for the production of uniform, reproducible, and clinically relevant scaffold-less constructs. The development of such a well-characterized system will provide consistent, high-quality constructs and lessen the difficulty for adapting fabrication methodologies into CGMP-compliant and scalable manufacturing processes required for human use.

Chapter 5 will describe the translation of the reproducible bench-scale manufacturing processes of Chapter 3 into a novel bioreactor system for semi-closed, automated BLB fabrication. The development of this bioreactor will minimize contamination risk, eliminate user-variability, and provide means to economically scale construct production for commercial construct use.

In summary, this thesis describes a novel treatment strategy for the regeneration of the tendon/ligament-to-bone interface, which may be critical for improving current rotator cuff repair outcomes following injury. These findings may provide

a new paradigm for the treatment of other musculoskeletal injuries requiring the reattachment of soft-tissue-to-bone. Furthermore, the approach outlined in this report for scaffold-less construct manufacturing demonstrates the practicality of employing translatable and scalable processes early in the product development stage as a means to overcome existing challenges in the commercialization and clinical advancement of new tissue engineering technologies.

Chapter 2
Utilization of Scaffold-less Constructs for Tendon-Bone Interface Regeneration

2.1 Introduction

Rotator cuff (RC) tears are one of the most common orthopedic disorders in the US with over 70,000 repair procedures performed annually [169]. Tears of the rotator cuff tendons often fail to heal spontaneously and are frequently the cause of significant shoulder pain and impaired shoulder function [114]. Current repair techniques utilize an open or arthroscopic suture technique to reattach the tendon to bone. Failure rates, however, especially in full thickness large (3-5cm) or massive tears (>5cm, 2 tendons), are unacceptably high (20-94%) [53,108]. Complications including tendon retraction, muscle atrophy, and fatty infiltration have been known to limit the successfulness of the repair [33,67,72,187]. Additionally, healing of the tendon-bone insertion (enthesis) with current techniques often results in a notably weaker fibrovascular scar rather than a normal enthesis and may explain the high prevalence of repair failures [26].

The native enthesis consists of a compositionally and mechanically graded fibrocartilage transition zone designed to minimize stress concentrations at the tendon-bone interface. Using a rat supraspinatus rotator cuff model, Thomopoulos et al., demonstrated that the biology and zonal arrangement of the enthesis is not regenerated following rotator cuff repair [166]. Rather, a sharp boundary was histologically observed, with disorganized collagen fibers and a fibrocartilaginous region, representing a significant deviation from the native enthesis anatomy. The structural repair and regeneration of a native enthesis

and return of normal biomechanics is paramount for improving functional outcomes and reducing the risk of recurrent structural failure after repair. As such, several tissue-engineering approaches have been developed to improve the biological healing and regeneration of the enthesis following RC repair.

To improve the healing response at the enthesis, Derwin et al. described several commercially available extracellular matrix (ECM) scaffolds currently used clinically for rotator cuff repair [41]. While the inherent biochemical properties of these scaffold materials have the potential to modulate host processes and influence the biology of the repair, the scaffold's properties, which are degraded over time, often do not match the rate of new extracellular matrix production. Additionally, a structurally native fibrocartilage enthesis often fails to regenerate and, as such, alternative strategies are needed to improve enthesis repair of rotator cuff injuries.

More recently, stratified and functionally graded scaffold-based approaches have been developed to pre-engineer the native tendon/ligament-to-bone interface *in vitro* [154,186]. In these studies, the spatial distribution of mechanical properties, biological factors, and/or cell populations are used to direct the formation of gradients designed to mimic the tendon insertion site *in vitro* or following subcutaneous implantation. Evaluation of these graded scaffolds in an *in vivo* rotator cuff repair model, however, has not been performed, and the degradation characteristics of the scaffold and biocompatibility has not been defined to date.

As an alternative to current scaffold based approaches, our lab has developed an initially compliant, scaffold-less tissue engineered bone-ligament-bone construct that relies on the local biologic and mechanical environments to direct the regeneration of the tendon or ligament-to-bone insertion. Previous work in sheep ACL and rat MCL repair models have shown that the osteogenic regions of our construct quickly integrate with the host tissue and rapidly remodel forming a graded tendon/ligament-to-bone transition that undergoes hypertrophy to match

the native footprint (Figure 2.1**)**.

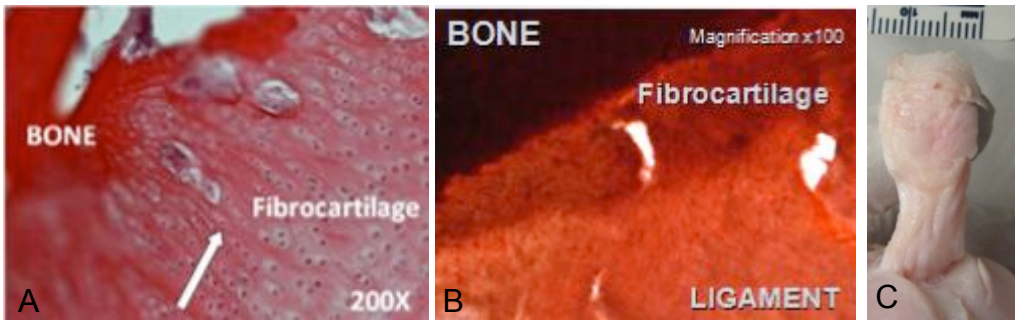

Figure 2.1 Ligament/Bone Interface of BLB Construct Explant A) H&E showing ligament integration into bone through Sharpey's fibers (arrow) and fibrocartilage-like region at 2-months, B) Alizarin Red staining of ligament -bone interface showing mineralization gradient at 2 months, and C) Femoral insertion of explanted BLB graft at 9-months. Construct diameter significantly increased in size from initial construct diameter (approx. 3mm).

While the results of these studies in the ACL are encouraging, it is unclear if they can be extrapolated to a rotator cuff model. The objective of this study was to evaluate the efficacy of our osteogenic scaffold-less constructs to regenerate the native matrix organization and mechanical strength of the enthesis in both acute (immediate repair) and chronic (repair 4 weeks post injury) supraspinatus tears in a rat model. We hypothesized that utilization of the tissue-engineered tendon construct would better regenerate the fibrocartilage transition zone, collagen organization, and tendon attachment strength of the native enthesis in both acute and chronic tear repairs compared to suture repair alone.

2.2 Materials & Methods

2.2.1 Animal Model & Design

The University of Michigan Institutional Animal Care and Use Committee (IACUC) approved this study. Female Fisher 344 rats, approximately 150-200 g in mass, were used in this study. For recreating an acute supraspinatus tendon tear, right shoulders underwent a full thickness supraspinatus tenectomy using a transacromial approach [29]. Chronic supraspinatus tendon tears were created by encasing the detached end of the supraspinatus tendon in a small piece of

silicone tubing and allowing the animal to recover for 4 weeks. The encasement with the silicone tubing prevented attachment to the surrounding connective tissue so that the cut end of the tendon could easily be identified and repaired at a later date. The left contralateral shoulders were used as non-surgical controls for each treatment group. Both acute and chronic tendon tears were repaired with either a Mason-Allen suture technique (suture repair group) or a modified trans-osseous technique utilizing a tissue engineered construct (construct repair group). At 8 weeks (n=43) following repair of the tendon, animals were euthanized with an overdose of sodium pentobarbital and assessed for biomechanical and structural repair of the injury site.

2.2.2 Preparation of Solutions and Media

All media and solutions were prepared and stored at 4°C prior to use. Media were warmed in a heated water bath to 37°C before utilized in the culture of cells. Media were prepared, as previously described, with slight modifications [104,153]. Growth medium (GM) consisted of Dulbecco's Modified Eagle Medium (DMEM; Gibco, Rockville, MD, Cat# 10565-042) supplemented with 20% Fetal Bovine Serum (FBS; Gibco, Rockville, MD, Cat# 10437-028) and 2% antibiotic-antimycotic (Sigma, St. Louis, MO, Cat# A9909). Osteogenic GM consisted of GM supplemented with 600ng/ml bFGF, and 40 ng/ml dexamethasone. Differentiation medium (DM) consisted of DMEM supplemented with 7% Horse Serum Albumin (HS, Gibco, Rockville, MD, Cat# 16050-122) and 2% antibiotic-antimycotic. Osteogenic DM consisted of DM, plus the addition of 0.13 mg/ml ascorbic acid-2 phosphate, 0.05 mg/ml L-proline, 400 ng/ml dexamethasone and 2 ng/ml transforming growth factor-beta (TGF-b; Peprotech, Rocky Hill, NJ, Cat# 100-21).

2.2.3 Bone Marrow Isolation and Cell Expansion

Bone marrow stromal cells were isolated and expanded according to a previously described protocol [104,153]. Briefly, rat femurs were removed from the animal and cut at the proximal and distal metaphysis. The marrow contents were extracted

through centrifugation (900 g for 10 min) and cultured on 100 mm tissue culture treated polystyrene plates (BD Falcon). Plates were fed osteogenic GM and incubated at 37°C, 95% humidity, and 5% CO_2. After 72 hours, plates were rinsed with DPBS and fed with fresh GM, removing the non-adherent cells. The remaining adherent cell population was cultured to 80% confluence, at which time cells were enzymatically removed from the 100 mm plate using a 0.25% trypsin-EDTA solution (Gibco), passaged, and seeded onto 100 mm plates at a density of 5 x 10^3 cells/cm^2. Following 3-4 passages, the cultured cells were utilized for construct fabrication.

2.2.4 Preparation of Self-Organized Constructs

Methods for creating scaffold-less three-dimensional tissues have been previously described by our lab [104,105,153]. Bone-like constructs, instead of tendon/ligament-like constructs, were used in this study based on their ability to specifically regenerate the tendon-bone interface in an ACL repair model. Briefly, MSCs plated onto 100 mm cell culture dishes at 21x10^3 cells/cm^2 and suspended in 8 mls of osteogenic GM supplemented with 0.13 mg/ml ascorbic acid-2 phosphate and 0.05 mg/ml L-proline. The dishes were placed in a 37°C, 5% CO_2 incubator and medium changed every 2–3 days. After approximately 5 days, the cells became confluent and osteogenic differentiation medium (DM) was substituted for GM to induce monolayer delamination. As the monolayer delaminated, it was transferred to a Sylgard coated dish and constrained between two minutien pins placed approximately 60 mm apart. The monolayer was fully self-assembled into a 60 mm long cylindrical construct within 1-2 days. One week following delamination, constructs were approximately 0.9 mm in diameter and cut into 6 mm long segments for use in rotator cuff repairs (Figure 2.2A). The medium was again changed every 2-3 days until the construct was used for implantation.

2.2.5 Surgical Technique

Rats were anaesthetized using 2% isoflurane and the right shoulder was shaved and scrubbed with povidone iodine. An incision was made from a point 2-3 mm distal to the head on the humerus to approximately 5 mm proximal along the deltoid muscle. The biceps muscle and deltoid muscle were cut longitudinally to expose the supraspinatus muscle. The acromion was cut and moved to expose the enthesis of the supraspinatus on the humeral head. The supraspinatus was isolated and a sagittal cut was made at the tendon-bone interface, detaching the tendon from its insertion. For suture repairs, two 0.6 mm crossing tunnels were drilled into the greater tuberosity footprint. A 4-0 Vicryl suture (Ethilon) was used to suture the detached supraspinatus tendon back onto its original insertion point. For the construct repairs, a 0.9 mm bone tunnel was drilled directly through the middle of supraspinatus insertion footprint and guided out to the lateral aspect of the humeral head. A tissue-engineered graft (~6 mm in length) was pulled into the bone tunnel and anchored to the periosteum on the lateral aspect of the humerus with 9-0 silk sutures (Ethilon) (Figure 2.2 B).

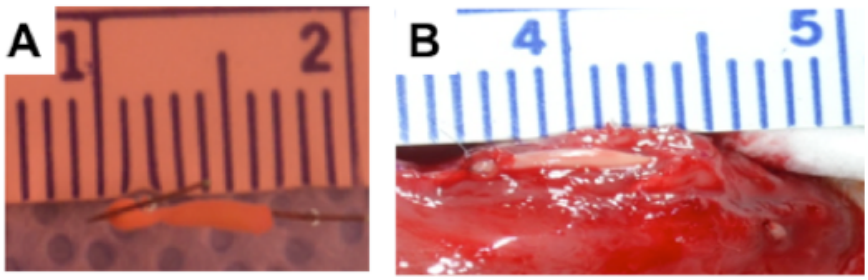

Figure 2.2 *In vitro* Tissue Engineered Constructs A) Construct prior to implantation and B) Construct inserted into humeral bone tunnel during repair of acute rotator cuff tear.

A small hole was made in the remaining supraspinatus tendon with #5 forceps and the construct was pulled into the hole, such that the graft lay on the posterior aspect of the tendon. The end of the construct was sutured to the supraspinatus tendon with 9-0 silk sutures. The deltoid and biceps muscle were closed using 7-0 sutures and the skin was closed with staples. Animals were fed ad libitum and allowed full cage activity. Analgesic, Carprofen (5 mg/kg), was administered following induction of anesthesia and every 24 hours for 48 hours post-surgery.

Eight weeks following surgical repair of the tendon the animals were euthanized with sodium pentobarbital and both shoulders were removed for biomechanical and histological analyses.

2.2.6 Biomechanical Testing

Biomechanical testing was performed on freshly dissected supraspinatus tendons while still attached to the humerus. Prior to testing, the supraspinatus muscle belly was carefully removed from the supraspinatus tendon and the cross sectional area of the tendon was measured using a digital micrometer. To prevent the fracture of the humeral physis during mechanical testing, the humerus was potted with polymer into a custom-designed grip. The specimen was then placed into a Dynamic Mechanical Analyzer (RSA-III, TA Instruments) for uniaxial tensile testing. The end of the tendon was secured to a screw grip using sandpaper and cyanoacrylate. The specimen was attached to a 35 N load cell and aligned uniaxially. The specimen was loaded to failure at a rate of 0.3 mm/sec or approximately 0.10/sec. Samples were tested at room temperature and were continuously moistened via a PBS drip throughout testing. The ultimate load-to-failure and location of failure (enthesis or tendon mid-substance) were recorded. The stiffness for each specimen was calculated from the linear region of the load-deformation curve. Statistical analysis was performed by two-way ANOVA with significance as $P < 0.05$. Data from the contralateral shoulders were combined for each injury group. Data are presented as mean ± standard error.

2.2.7 Histomorphometric Analysis

Following recovery, the supraspinatus tendon with the humerus still attached was carefully dissected from the surrounding tissue under a microscope leaving the supraspinatus muscle intact. Following dissection, samples were fixed in 10% neutral buffered formalin for 48 hours, decalcified in EDTA for 48 hours, and subsequently washed in phosphate-buffered saline solution. The samples were dehydrated and embedded in paraffin for sectioning. To facilitate comparisons between groups, an orientation of 90° between the humerus and supraspinatus

muscle was maintained for each sample during embedding. Serial sections 12-μm thick, containing the repaired tendon and greater tuberosity of the humerus, were cut in the coronal plane and stained with picosirius red, safranin-O, and hematoxylin and eosin (H&E). Using an Olympus B light microscope, digital images of the stained slides were taken using a SPOT RT camera (Diagnostic Instruments, Sterling Heights, Michigan). Five representative slides for each stain and specimen were prepared. Each slide was evaluated using polarized and non-polarized light and analyzed by 3 different people.

To evaluate collagen organization in the repaired tendon enthesis, sections stained with picrosirius red were imaged under monochromatic polarized light. The birefringence of collagen fibers was semi-quantitatively analyzed, based on brightness, to determine differences in collagen deposition and maturation at the site of repair [34,86]. Five representative tissue sections across the full width of the tendon-bone interface were analyzed for each shoulder. The polarization plane was rotated until maximum brightness was obtained to account for variations in specimen orientation on the slide. Digital images were taken of each tissue section at X10 magnification during a single imaging session under identical imaging parameters. The images were imported into Image J software and underwent 8-bit digitalization. Non-collagenous material was shown as black (zero) and collagenous material was assigned a gray scale value from 1-255. Higher gray-scale values signify more organized and mature collagen. Using the Image J software, ten rectangular areas (50 x 50 μm) were randomly selected in the tendon directly adjacent to the tendon-bone interface. Mean gray scale values for each region were averaged for each specimen to obtain a brightness value. Statistical analysis of specimen brightness was performed by two-way ANOVA with P value < 0.05 considered significant. Data are presented as mean ± standard error.

The area of fibrocartilaginous material at the tendon-bone interface was assessed by use of safranin O stained sections. Safranin O stains sulfated

proteoglycans reddish-purple, a property referred to as metachromasia. Digital images of the stained sections were imported into Image J and areas of metachromasia were meticulously outlined and measured using the Image J software at a X4 magnification (National Institutes of Health, Bethesda, Maryland, USA). Measured areas were averaged for suture and construct repaired shoulders and contralateral controls. Statistical analysis of total area of fibrocartilage was performed by two-way ANOVA with P value < 0.05 considered significant. Data are presented as mean ± standard error.

2.3 Results

2.3.1 Gross Morphology

At the time of necropsy, there was continuity between the tendon and bone in all acute and chronic repairs with no detectable differences between groups. All animals appeared healthy and showed no signs of infection. The cross-sectional area of the enthesis was measured and was not significantly different between each group in either acute or chronic injury repairs (3.4±0.8 mm^2).

2.3.2 Biomechanical Testing

Minimums of 5 samples for each treatment group were tested uniaxially until failure. In the acute injury repair groups, four of the suture-repaired specimens (n=8) failed at the enthesis, while the rest of the suture-repaired specimens and all the construct-repaired specimens (n=5) failed at the tendon mid-substance. In the chronic injury repair group, three suture-repaired specimens (n=5) failed at the enthesis while the rest of the suture-repaired specimens and the entire construct repair group (n=5) failed at the tendon mid-substance. All non-operative contralateral shoulders failed at the tendon mid-substance during testing.

Following 8 weeks recovery, acute and chronic injuries repaired with either suture or construct techniques displayed no differences in stiffness between groups. All repair groups were significantly less stiff than their respective contra-

lateral shoulders and not significantly different from each other (Figure 2.3). The mean stiffness of the tendon-bone interface in the acute injury repair groups was as follows: contra-lateral (23.2±1.5 N/mm, n=13), suture repair (12.9±0.8 N/mm, n=8), and construct repair (14.0±0.7 N/mm, n=5). The suture and construct repaired shoulders achieved 56% and 60% of native contralateral stiffness respectively. The mean stiffness of the tendon-bone interface in the chronic injury repair groups was as follows: contra-lateral (21.7±1.2 N/mm, n=10), suture repair (9.3±1.6 N/mm, n=5), and construct repair (10.1±0.6 N/mm, n=5). The suture and construct repaired shoulders achieved 43% and 46% of native contralateral stiffness, respectively.

The maximum load-to-failure was not significantly different between acute and chronic injuries repair with suture or tissue constructs. Each group was significantly less than its respective non-operative contralateral shoulder and not significantly different from the other group (Figure 2.3). The maximum load-to-failure for acute injury repair was as follows: contra-lateral (25.0±1.7 N, n=13), suture repair (18.8±1.3 N, n=8), and construct repair (17.0±2.8 N, n=5). This corresponded to approximately 75% and 68% of the contralateral failure load for suture and construct repairs, respectively. Maximum load to failure for chronic injury repair groups was as follows: contra-lateral (22.9±1.4 N, n=10), suture repair (14.0±2.3 N, n=5), and construct repair (12.9±2.1 N, n=5), respectively. The suture and construct repaired shoulders achieved 61% and 56% of contralateral shoulder load to failure, respectively.

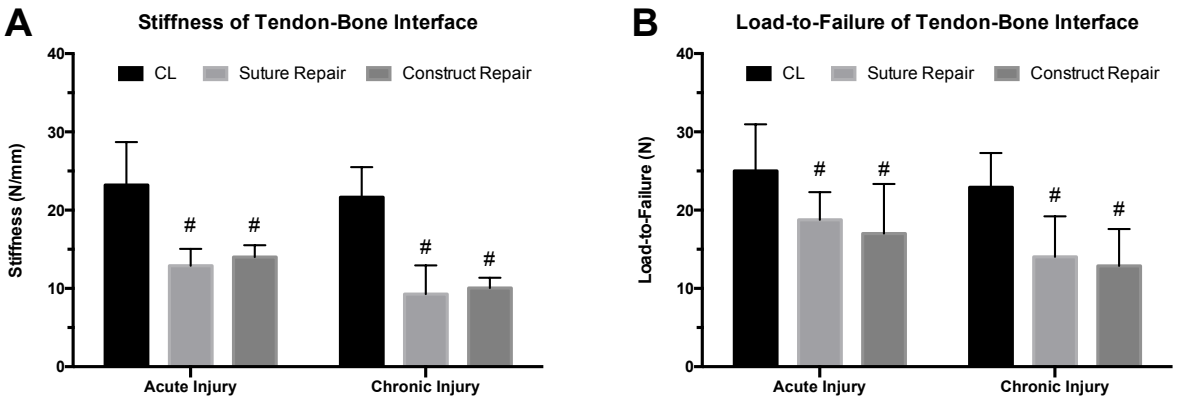

Figure 2.3 Mechanics of Tendon-Bone Interface Following Acute and Chronic Injury Repair A) Stiffness of contralateral (CL), suture repaired, and construct repaired shoulders and B) Load to Failure of contra-lateral (CL), suture repaired, and construct repaired shoulders. (#) Denotes statistical significance compared to CL shoulder (P<0.05). Data are shown as mean ± S.E. for each group.

2.3.3 Histomorphometric Analysis

Collagen birefringence was semi-quantitatively analyzed, based on brightness, to evaluate collagen organization at the tendon-bone interface. Five specimens were analyzed for each treatment group. Contralateral shoulders of acute and chronic injured shoulders were not significantly different and were combined for analysis. Suture and construct repaired shoulders, although significantly more disorganized (shown in picrosirius red staining) than contralateral shoulders, were not significantly different to each other in either acute or chronic injury groups (Figure 2.4). Additionally, although repaired chronic injuries trended towards lower gray scale values, no significant difference in collagen organization was observed between repaired acutely or chronically injured shoulders. Suture repairs of acute injuries had a mean brightness gray scale value of 70±1 gray scale units, while construct repairs had value of 70±4 gray scale units. Chronic injuries repaired with suture and construct techniques had gray scale values of 58±5 and 65±4 gray scale units, respectively. Non-operative contralateral shoulders had an average brightness value of 95±6 gray scale units. Representative images from each treatment and control group can be seen in Figure 2.5.

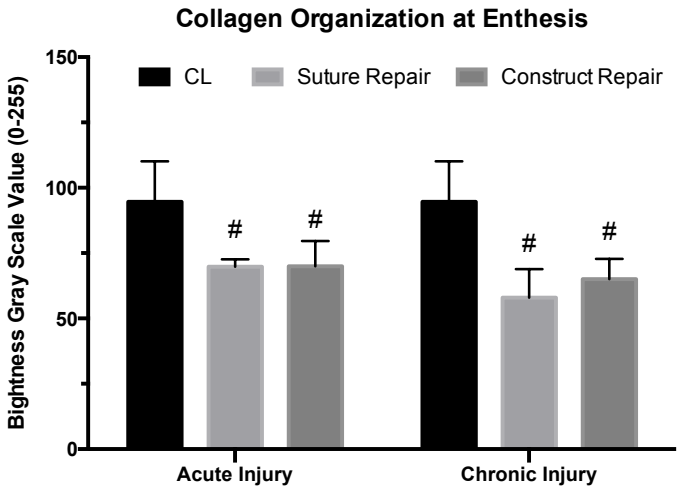

Figure 2.4 Collagen Organization at Enthesis Following Acute and Chronic Injury Repair. No significant differences were observed between acute and chronic injury groups. (#) Denotes statistical significance compared to contralateral (CL) shoulder (P<0.05). Data are shown as mean ± S.E. for each group.

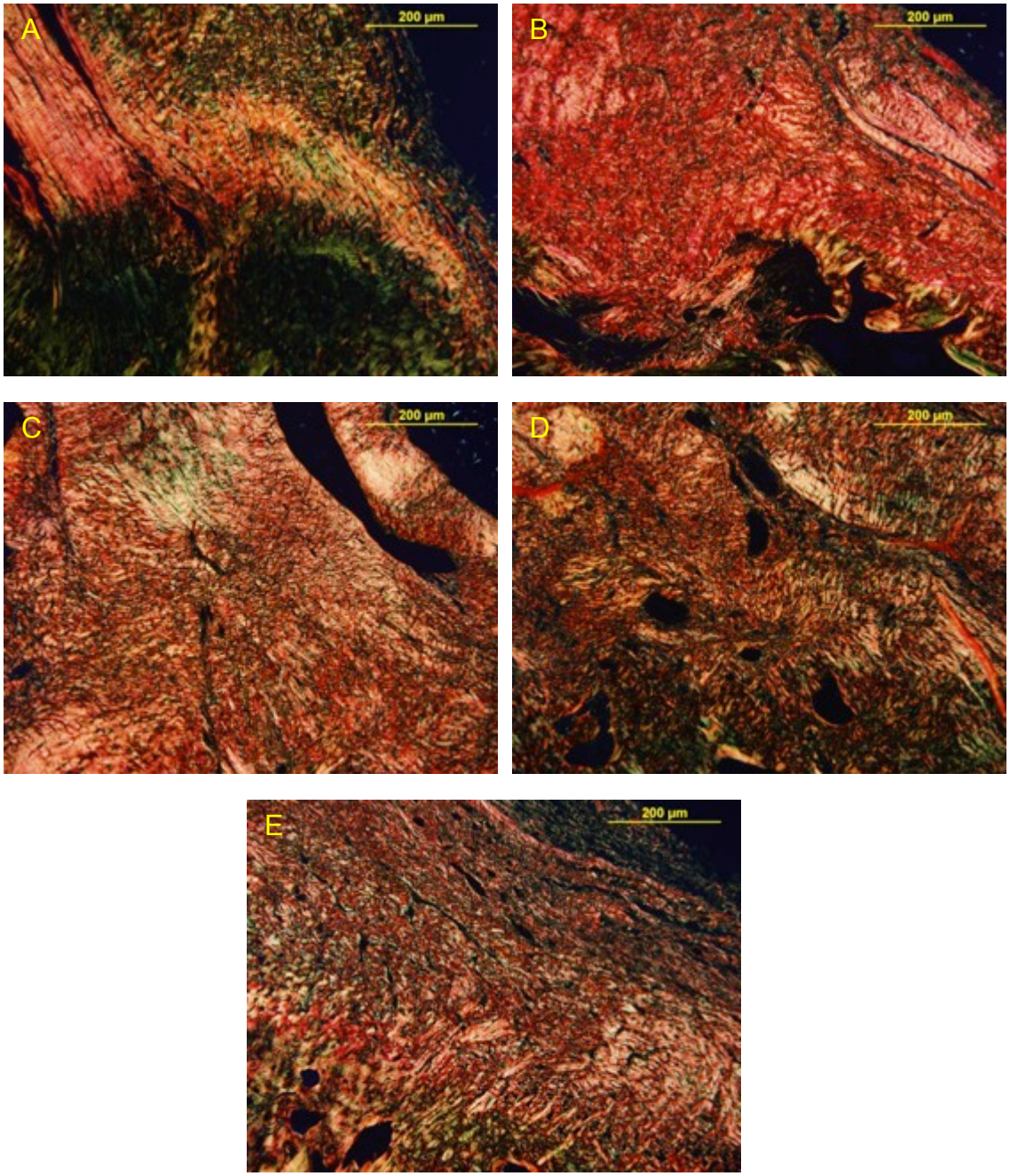

Figure 2.5 Representative Collagen Organization of Enthesis A) Contralateral shoulder, B) Acute suture repair, C) Acute construct repair, D) Chronic suture repair, and E) Chronic construct repair. Images are of picrosirius red stained sections under polarized light and imaged at X40 magnification.

The area of new fibrocartilage formation was evaluated at the tendon-bone interface by determining the area of metachromasia of safranin O stained sections. Five specimens were analyzed for each treatment group. Contralateral shoulders of the acutely and chronically injured animals were not significantly different and were combined for analysis. The enthesis, following suture and construct repair of acute and chronic injuries, had significantly less fibrocartilage area than the native contralateral enthesis (Figure 2.6). No significant difference in area of fibrocartilage formation was observed in acute injury suture or construct repairs. The area of fibrocartilage formation in the chronic injury group was significantly less in suture repaired specimens compared to both construct repaired specimens and unrepaired, contra-lateral shoulders. The total area of metachromasia, or area of fibrocartilage, for each treatment group was as follows: contralateral shoulders (109,905±5,095 μm^2), acute suture repairs (52,571±10,451 μm^2), acute construct repairs (67,063±11,455 μm^2), chronic suture repairs (11,272±6,707 μm^2), and chronic construct repairs (40,432±7,600 μm^2) (Figure 2.6). Representative images from each treatment and control group can be seen in Figure 2.7.

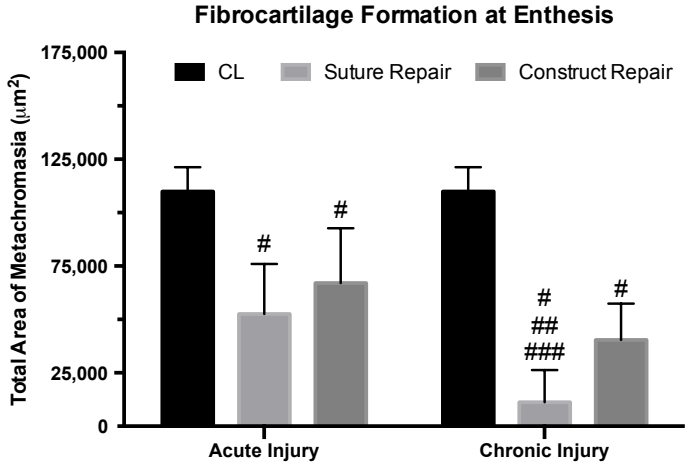

Figure 2.6 Fibrocartilage Formation at the Enthesis Following Acute and Chronic Injury Repair. Suture repair of chronically injured shoulders had significantly less fibrocartilage formation compared to both contralateral shoulder and construct repaired specimens. No significant differences were observed between acute and chronic injury groups. (#) Denotes statistical significance compared to contralateral (CL) shoulder (P<0.05). (##) Denotes statistical significance compared to acute suture repair (P<0.05). (###) Denotes statistical significance compared to chronic construct repair (P<0.05). Data are shown as mean ± S.E. for each group.

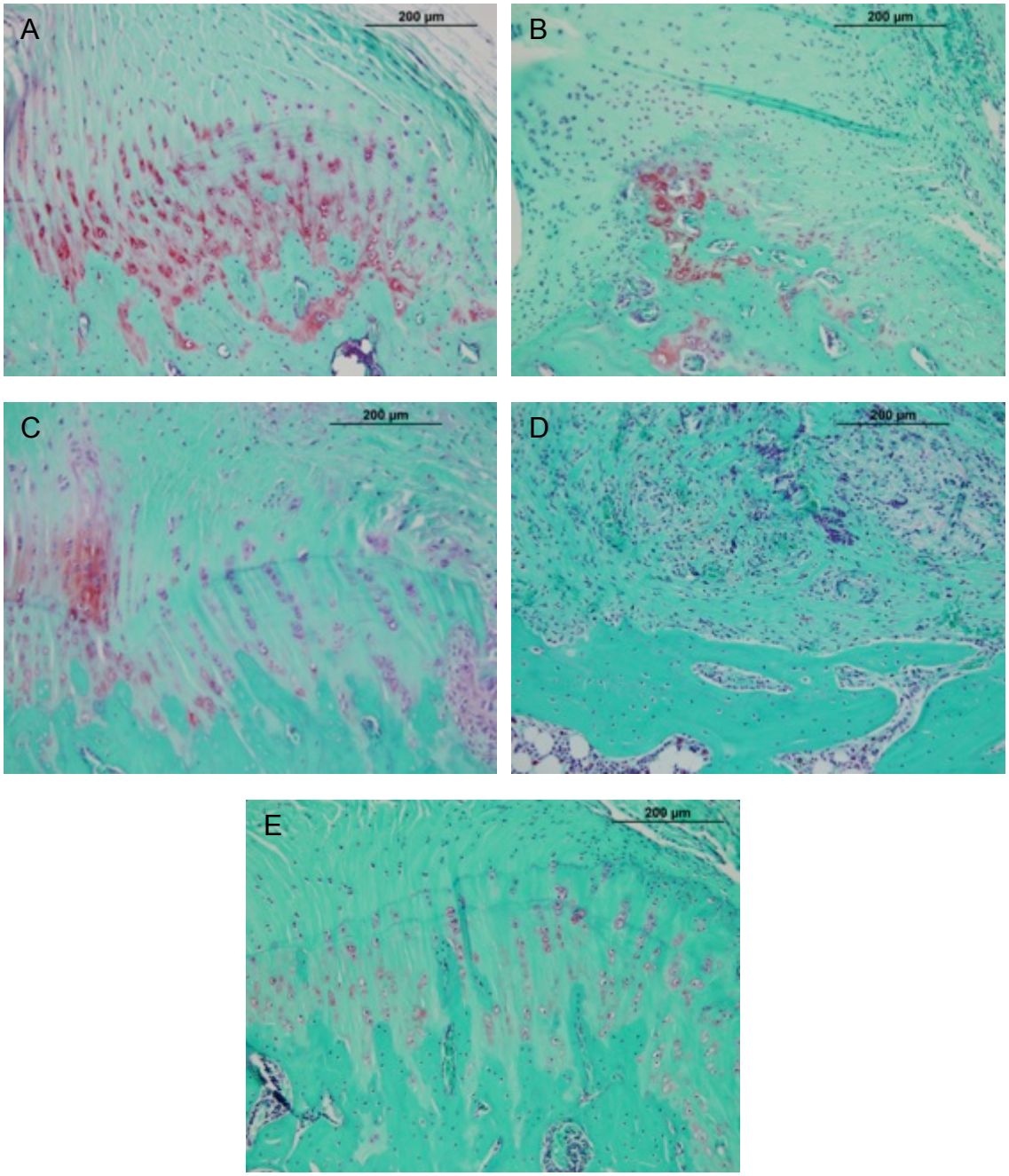

Figure 2.7 Representative Fibrocartilage Formation at Enthesis. Representative images of safranin O stained A) Contralateral, B) Acute Suture Repair, C) Acute Construct Repair, (D) Chronic Suture Repair, and E) Chronic Construct Repair sections. Area of metachromasia (depicted as red) in each image was outlined for semi quantitative analysis. Images are shown at X40 magnification.

H&E staining of the tendon-bone interface allowed for qualitative evaluation of the entheses repair. Acute and chronic tendon injuries repaired with suture had less area of fibrocartilage formation and fewer organized collagen fibers than both construct-repaired and contralateral shoulders. The attachment of tendon to bone utilizing our tissue constructs resembled a more organized, native appearance. Suture repaired shoulders in both acute and chronic injury models had a more abrupt, fibrous interface at tendon-bone transition site, especially in suture-repaired specimens of chronic injuries. Representative images from each treatment and control group can be seen in Figure 2.8.

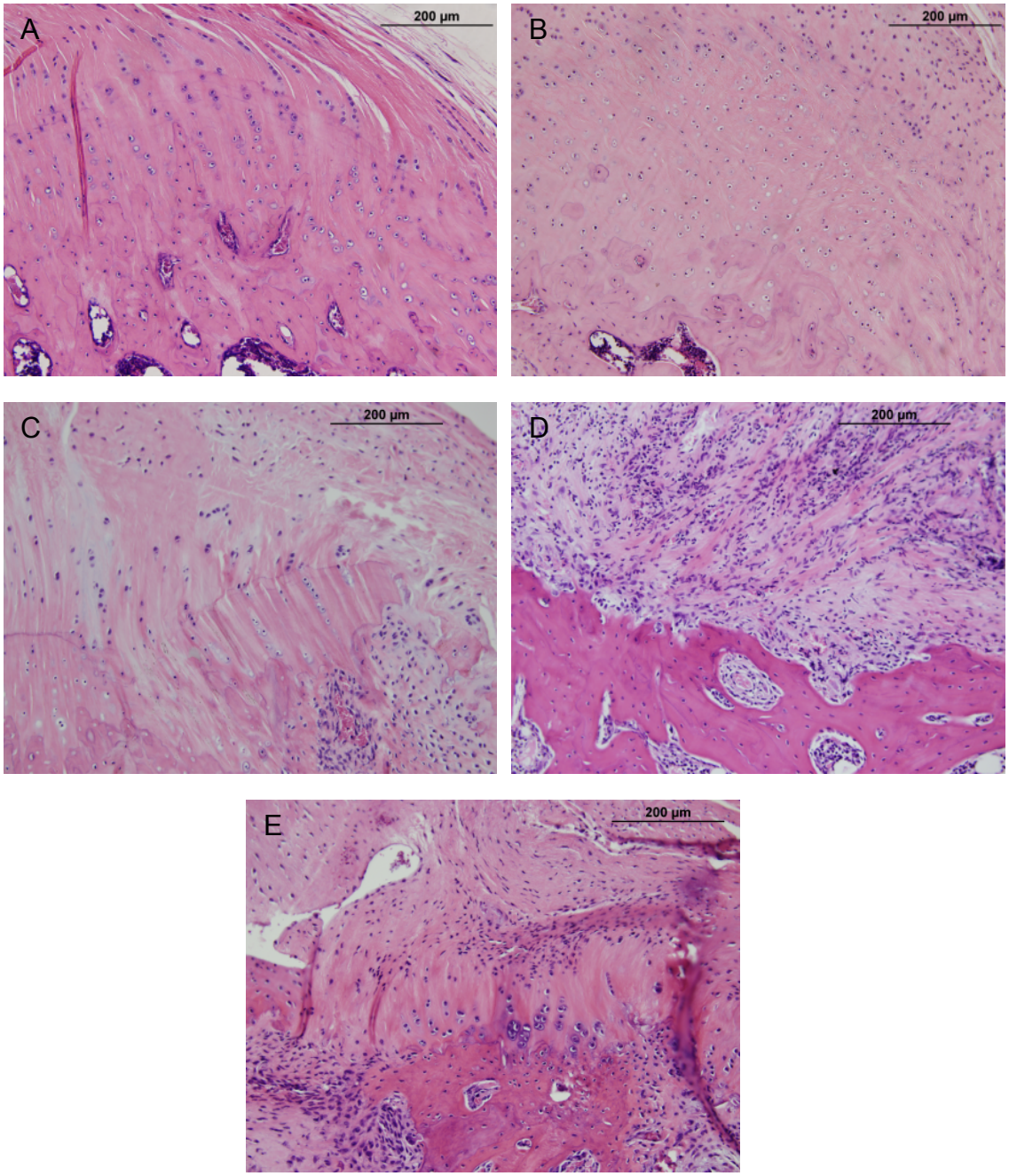

Figure 2.8 Representative Structure at Enthesis. Representative images of H&E stained A) Contralateral, B) Acute Suture Repair, C) Acute Construct Repair, D) Chronic Suture Repair, and E) Chronic Construct Repair sections. Suture repaired shoulders were more disorganized and fibrous than contralateral or construct repaired shoulders. Images are shown at X40 magnification.

2.4 Discussion

Tissue engineering to improve the architecture and structural integrity of the healing enthesis after rotator cuff repair offers future promise to improve outcomes in patients. Bone-like constructs, instead of tendon/ligament-like constructs, were used in this study based on their ability to specifically regenerate the tendon-bone interface in an ACL repair model. Future work involving the use of multi-phasic tissues (with both bone and tendon/ligament tissue) may further enhance the properties of the tendon mid-substance but was beyond the scope of this experiment. The objectives of this current study were to evaluate the efficacy of our scaffold-less tissue engineered tendon construct to regenerate the native tendon-bone interface of the supraspinatus following full-thickness acute and chronic injury in a rat model. Furthermore, we tested the hypothesis that tendon-bone repair utilizing our scaffold-less construct could strengthen enthesis healing and improve collagen organization and fibrocartilage formation compared to suture fixation alone.

In the acute injury repair model, our results demonstrate that there were positive effects with the utilization of our scaffold-less constructs. While no significant differences in structural mechanics were observed, failure occurred more frequently at the tendon-bone interface in suture-repaired, acutely injured shoulders. Histologically, qualitative differences in general morphology revealed more native histological architecture by 8 weeks post-operatively. In tendons with chronic injury, repairs utilizing our tissue engineered construct resulted in a more native-like enthesis. Despite similar biomechanical properties with load-to-failure testing, suture repaired specimens of chronic injuries failed more frequently at tendon-bone interface. However, the structure of the construct repaired enthesis appeared qualitatively more native-like in appearance and quantitatively more fibrocartilage was observed at the tendon insertion site compared to suture repairs.

The formation of fibrocartilage at the tendon-bone insertion site has an important role in the force transmission and energy dissipation between two tissues with vastly different properties. This complex interface is seldom recreated with current fixation techniques and often results in repair failure. The healing of the enthesis following repair is known to be influenced by mechanical cues. In separate studies performed by Galatz and Hettrich et al., complete removal of load following repair via immobilization and botulinum toxin application to supraspinatus muscles resulted in decreased structural properties and decreased ECM production at the tendon-bone interface [54,77]. As such, suture techniques that rely on rigid mechanical fixation of tendon to bone may impede signals that may be necessary for proper enthesis regeneration resulting in a more fibrous tissue interface. The unique ability of our initially compliant construct to sense and respond to local mechanical cues and biological factors has led to improved structure and fibrocartilage formation at the enthesis.

The biological composition of our graft may also contribute to repair of tendon-bone interface. Recent research has shown that application of MSCs, with the addition of appropriate growth factors, can enhance tendon-bone healing of the repair [70]. Our constructs are fabricated from MSCs and driven towards an osteogenic lineage, via the addition of previously described growth factors. As such, enthesis regeneration at a repair site may be due to the unique cellular and molecular signals provided by the cells of our construct that are necessary for facilitating the proper host-mediated response. Alternately, the implanted construct may be actively forming a new interface tissue *in vivo*. Current studies are underway to evaluate the origin of the regenerated enthesis tissue.

Although more successful at regenerating the enthesis than current suture techniques, the excessively high strains at the site of repair may have limited repair outcomes. High tensile loads, especially in chronically retracted tendons, can lead to elongation of the tendon, reducing overall muscle length and compromising shoulder function. Though the length of tendon following repair

was not evaluated in this study, gross morphological changes of the supraspinatus tendon and muscle were not observed. Nonetheless, due to the compliance of our tissue, the primary benefit of our construct may be initially biologic and a reliance on compositional properties of the graft until sufficient tissue mechanical development can occur. As such, initial load sharing at the repair site utilizing our construct as a biological in-lay may enhance repair outcomes.

There were several limitations to this study. Mechanical testing evaluated stiffness and load-to-failure of a single test. Cyclic loading, a more clinically representative measure, was not performed. Furthermore, material properties utilizing tissue level strains of the repaired tissue were not evaluated due to technical difficulties and may explain the lack of significant differences in mechanics despite histological differences in tissue composition and location of failure. Assessment of the material properties of the regenerated tissue (i.e. moduli) utilizing tissue level strains, rather than only geometric properties (stiffness and load at failure) of the tissue, may better evaluate the quality of the regenerated tissue independent of size. Additionally, the creation of a chronic supraspinatus injury in the rat may not be fully representative of the human condition. Healing in the rodent model is relatively robust and may not simulate the difficulties experienced in structure failure after large and massive repairs in human patients. Additionally, as this study focused specifically on enthesis regeneration, important components of rotator cuff injury specific to the tendon mid-substance and muscle such as muscle atrophy, fatty infiltration, quality of tendon, etc., were not evaluated.

In conclusion, repair of acute supraspinatus injuries in a rat model with engineered constructs more accurately recapitulated the appearance of the native enthesis but was not significantly different biomechanically compared to suture techniques. Utilization of scaffold-less constructs for repair of chronic rotator cuff injuries was found to reduce scar formation and increase the area of

fibrocartilage formation at the tendon-bone interface over suture-only repairs. Further investigation is needed to optimize the ideal tissue properties and surgical technique for encouraging maximum enthesis regeneration *in vivo*.

Chapter 3
Standardization of Existing Methodologies for Reproducible Construct Fabrication

3.1 Introduction

The previous chapter evaluated the use of scaffold-less tissue constructs for regeneration of the native tendon-bone interface following acute and chronic rotator cuff injury and repair. As with rotator cuff repair procedures, current ACL repair procedures also often fail to regenerate the native fibrocartilaginous enthesis and have been implicated in poor long-term outcomes and pre-mature graft failures. However, unlike repairs of the supraspinatus tendon that require re-attachment of the damaged tissue to its original insertion site, current strategies to repair the ACL replace the entire ACL complex within the knee. Current ACL replacement grafts are secured to bone tunnels drilled through the femur and tibia using interference screws, span the intra-articular space, and provide immediate knee stability. These ACL replacement grafts from cadaveric allografts or autografts from the patient's patellar tendon or hamstrings tendon have several disadvantages. The grafts often do not fully integrate with the native tissue within bone tunnel and fail to restore full function to the knee. Additionally, a mismatch of mechanical properties exists between the tendon replacement graft and the native ACL [105]. This mismatch of mechanical properties may play a role in the early onset of OA. As such, a multi-phasic graft capable of integrating with both bone tunnels and regenerating the native properties of the ligament mid-substance would be advantageous.

As described in Chapter 1, our lab has tissue engineered a compliant BLB graft consisting of viable ligamentous mid-substance tissue, osteogenic tissue at each end, and viable entheses in between. In both rat MCL and sheep ACL repair models the graft induces endogenous bone and ligament regeneration, rapidly develops biochemically relevant and biomechanically compatible interfaces with native tissue, and restores the native anatomy and function to the knee [105]. As an "off-the-shelf" allogeneic ACL graft, our tissue-engineered graft could eliminate donor site morbidity from autologous tendon harvesting and improve the structural and mechanical outcomes compared to current grafting techniques[105]. It is clear that utilization of this tissue engineering approach has tremendous potential to improve musculoskeletal tissue repair and regeneration.

A significant amount of work remains before we can use our current lab-based tissue engineering processes for large-scale clinical use. Our hands-on, labor intensive laboratory methods must be advanced to more efficient protocols capable of producing consistently uniform, reproducible constructs that meet the current industry regulations within the health care field. The commercialization of our BLB construct, specifically for ACL repair, will be used for the remainder of this thesis as an application-specific model for the translational process of tissue engineering products.

3.2 Background/Motivation

The Food and Drug Administration (FDA) regulates all engineered tissue and regenerative medicine products. The FDA oversees the pre-market approvals and conducts post-market surveillance of existing products. The focus of the FDA is to ensure the safety and effectiveness of new products through clinical trials and to oversee the manufacturer's processes validation in accordance with current good manufacturing practice (CGMP) regulations. Overall these regulations require exquisite definition and control of the product and fabrication process [177].

Failure to adequately transition from a labor-intensive laboratory process performed by expert technicians to an automated industrialized production method is a major hurdle in the translation of all current tissue engineering technologies. Though process validation may be performed in parallel with clinical trials, the consideration of designing a process that is compliant with existing FDA regulations is essential to avoiding late-stage product failures and costly product development cycles. Implementing FDA compliant technologies early in the research stage has the potential to shorten the duration of the FDA approval process and hasten the availability of our tissue-engineered grafts for widespread clinical use.

Tissue engineering products, in particular, are among the most complex products to manufacture[132]. Tissues are composed of various living cells and ECM components that are constantly changing and remodeling in response to environmental cues. Due to the inherent heterogeneity of cells, the FDA requires creation of tissue end product specifications and the demonstration of a consistent manufacturing process. As such, extensive work in the tissue engineering/regenerative medicine field is needed to design and implement novel, high-quality manufacturing systems capable of generating sufficient amounts of data needed to establish statistical confidences of variability, define product specifications, and demonstrate overall process consistency.

CGMP requires that each step of the manufacturing process be designed and confirmed such that in-process materials and the final-end product(s) are produced consistently and reliably, and meet their predetermined quality attributes. The manufacturer must evaluate the process performance and control batch-to-batch variability within the system. To ensure process consistency, in-process specifications must be established to monitor variability in the characteristics of process materials or end products. As described by CGMP regulations, “in-process specifications shall be derived from previous acceptable

process averages and process variability estimates where possible and determined by the application of suitable statistical procedures where appropriate" (See FDA Section 2.11.110(b)).

Therefore, as a first step for our technology, a robust, well-established manufacturing method must be designed at an early stage to provide information and knowledge about product reproducibility and to define the process to identify and control for variability. To eliminate or reduce the variability associated with our multi-step process, critical steps reliant on technician skill should be minimized or eliminated. In addition, the ability to systematically collect data during the process is critical to establishing baseline averages, to evaluating the sources, degree, and impact that procedural variation has on manufacturing process, and ultimately to determining the attributes of the end product. Only after process variability has been minimized, controlled, and properly characterized can in-process specifications be defined minimizing any remaining variation in proportion to the risk it represents to the process and final product. Once appropriate controls have been established, the process can be evaluated under CGMP compliant conditions to demonstrate that the commercial manufacturing process is capable of consistently producing a quality product. Additionally, from a manufacturing standpoint, understanding the process variation can lead to more efficient manufacturing systems that improve production volumes and reduce failure rates.

The process of obtaining FDA approval for products in the field of tissue engineering regenerative medicine is complex and the specific requirements for process validation and regulatory approval are not clearly defined. Due to the broad range of medical technologies being developed, new products are generally evaluated on a case-by-case basis. Thus, the specific information that is needed as part of an FDA regulatory submission to demonstrate sufficient process control is unknown. Guidance documents provided by the FDA outline the FDA's current thinking on various topics (including process validation) and

serve as useful guidelines for industry. These documents incorporate principles and approaches that manufacturers can use to validate manufacturing processes for human, animal, drug, or biological products under current CGMP regulations.

3.2.1 Current BLB Manufacturing Process

For the purposes of this study, I will focus exclusively on the fabrication of the ligament portion of our BLB construct, the region that replaces the damaged ACL tissue within the intra-articular space. The stiffness of this region directly determines the graft's ability to accommodate strain under normal knee loading and the fabrication of this region is currently the most difficult aspect of the BLB fabrication process to reproduce. Thus, the goal of this study is to design strategies to enhance construct production and to characterize the properties of the ligament region during fabrication. The methods developed here to establish a reproducible protocol for production of the ligament-region of the BLB graft will be useful as a guide for improving production of the bone-region in future research.

The original process used for BLB fabrication has been described by Ma et al., with slight modifications [104,105]. Briefly, the methods used in the Ma paper to harvest bone marrow for the fabrication of ligament tissue required the sacrifice of a donor animal, removal of the whole femoral bone, and extraction of the entire content of femoral bone marrow. Obviously, the removal of the entire femur and the extraction of the entire marrow contents is not a practical method for obtaining cellular material and should be replaced with more clinically relevant bone marrow aspiration techniques. In the previous fabrication process, the entire amount of extracted marrow was plated onto four polystyrene dishes and MSCs were isolated by their plastic adherence properties. This method of bone marrow extraction led to low primary MSC yields and often necessitated significant and unpredictable amounts of time in culture to achieve suitable cell quantities for passaging. The execution of these process steps at irregular intervals added an unnecessary variable to the protocol and reduced the overall

efficiency of the process. The previous methodology resulted in differences in the amount, cellularity, and composition of bone marrow collected for tissue fabrication. Standardization of the original isolation procedure was needed to appropriately evaluate variability between and within donor samples and recover reliable cell volumes at defined time points.

In addition to standardizing the bone marrow isolation methods, the MSC differentiation and expansion methods associated with our original BLB protocol also required improvement to obtain sufficient quantities of a consistent starting cell population prior to seeding. Existing methodologies induced an unknown amount of MSCs toward a fibrogenic lineage and passaged these cells every other day at a 1:3 liquid volume ratio until sufficient numbers of ligament cells were achieved. Failure to rigorously monitor the plate density to the desired 80% confluence mark between passages led to significant variability in the number of recovered cells. This error in cell number was exacerbated in successive passages. The recovery of low cell quantities during passaging led to a decrease in the number of constructs that could be fabricated, and reduced the overall efficiency of the process. Optimal culture conditions for passaging MSCs typically occur at 80% confluency [115]. High cell densities during passaging were typically indicative of a plate that was well beyond 80% confluence. The resultant cell-cell contact at these high cell densities may lead to changes in cell phenotype, genetics, and construct structure and function that can introduce significant variability into the manufacturing process. Thus, we determined that it was imperative to standardize the methodologies used to expand and induce the MSCs to ligament cells during passaging and to maintain the cells at each passage as close to 80% confluence as possible, to minimize cell-to-cell contact and provide adequate cell qualities for tissue fabrication. The establishment of set passage densities would allow for accurate predictions of appropriate times between passages necessary to obtain consistent starting cell numbers.

In addition to the issues associated with obtaining and expanding the MSC population to a consistent fibrogenic lineage, we recognized that our current

methodologies for fabricating 3D BLB constructs could also be improved. The process for capturing and constraining the spontaneously delaminating ligament monolayers into uniform cylindrical constructs, in particular, was unpredictable, technically challenging, led to a significant loss of constructs, and reduced the overall number of constructs produced. Briefly, in our original method, once a hyper-confluent monolayer was formed and a sufficient amount of extracellular matrix was produced, plates were switched to a low-serum medium and fed TGF-β to induce intercellular tension and spontaneous contraction of the monolayer. These resulted in the spontaneous delamination of the monolayer that facilitates the formation of a 3D cylindrical construct. During delamination, the monolayer had to be delicately transferred onto a syglard-coated plate and pinned. Constraint pins were applied to the monolayer and the delaminating tissue aligned along a singular axis of the pins allowing for the remodeling of the construct into a 3-D tissue (Figure 3.1).

The delamination process occurs spontaneously. The inability to continuously monitor and manipulate the tissue at the beginning of the delamination process led to the loss of a significant number of constructs. Failure to constrain the monolayers at an appropriate length before significant tissue contraction occurred resulted in tissues of an unsuitable length for use as a replacement graft (>6cm) (Figure 3.1). Additionally, variation in the placement of the pins often led to uneven tension during tissue contraction and resulted in construct thinning, abnormal construct geometry, and eventual failure in a substantial number of constructs (Figure 3.1).

Figure 3.1 *In vitro* Tissue Constructs A) BLB graft pinned at an appropriate length for use in ACL reconstruction. Suture integrated into the bone regions (ends) of the construct is applied immediately prior to surgery to introduce and anchor the construct within the knee. B) Ligament constructs manually formed. Variability in pin placement resulted in varied construct lengths and geometries rendering the tissue unsuitable for ACL reconstruction.

Our previously published data on the biological and mechanical properties of the BLB were of a relatively low sample size (n=3) and were derived from cells of a single donor animal. Thus, we have been unable to report the consistency and reproducibility of the fabrication process within and between multiple donor cell populations. Additionally, the meticulous and user-dependent steps of our construct formation process led to relatively few appropriately formed constructs suitable for implantation or *in vitro* evaluation. This overshadowing technician variability prevented the evaluation of construct variability with respect to size, mechanics, and histology, within and among different donor lots. Thus the second objective of this study was to design a novel tissue capture system to facilitate 3D construct delamination without technician manipulation.

3.3 Objective

The objective of this study was two-fold. First, a standardized bone marrow (BM) isolation technique and a reliable method for obtaining and expanding MSCs towards a fibrogenic lineage were needed. Second, following the production of a consistent cell population, a novel tissue capture system was needed to automate the capture and 3D formation of the construct. To complete these objectives, the old BLB fabrication process described above was changed to incorporate: Ficoll MSC cell isolation method to produce a well-defined starting

cell material from a clinically relevant bone-marrow aspiration, consistent passage densities to limit significant cell-cell contact known to alter cell phenotype and function, and a novel capture system to automatically capture the monolayer delamination and allow the formation of a 3D construct on the plate. We hypothesized that the incorporation of these changes would allow for the fabrication of more consistent and reproducible tissue constructs with defined end-product specifications and marginal variability. The information and knowledge gained from the addition of these methodologies will be useful in generating the large number of constructs needed to establish an acceptable baseline average and to statistically evaluate the process variation.

3.4 Methods

3.4.1 Preparation of Solutions and Media

We did not perceive the media and growth factors to be a significant source of variation in the fabrication process. Solutions used for cell processing were prepared as described in previous published work, with slight modifications [104,153]. Briefly, all media and solutions were prepared and stored at 4°C prior to use. Media were warmed in a heated water bath to 37°C before use for the culture of cells. Media were prepared, as described previously, with slight modifications [104,153]. Growth medium (GM) consisted of Dulbecco's Modified Eagle Medium (DMEM; Gibco, Rockville, MD, Cat# 10565-042) supplemented with 20% Fetal Bovine Serum (FBS; Gibco, Rockville, MD, Cat# 10437-028) and 2% antibiotic-antimycotic (Sigma, St. Louis, MO, Cat# A9909). Fibrogenic GM consisted of GM supplemented with only 600ng/ml bFGF, 0.13 mg/ml ascorbic acid-2 phosphate and 0.05 mg/ml L-proline. Differentiation medium (DM) consisted of DMEM supplemented with 7% Horse Serum Albumin (HS, Gibco, Rockville, MD, Cat# 16050-122) and 2% antibiotic-antimycotic. Fibrogenic DM consisted of DM, plus the addition of 0.13 mg/ml ascorbic acid-2 phosphate, 0.05 mg/ml L-proline, and 2 ng/ml transforming growth factor-beta (TGF-b; Peprotech, Rocky Hill, NJ, Cat# 100-21).

3.4.2 Preparation of a Novel Plate to Eliminate the Loss of Monolayers

To reduce the loss of monolayers during the delamination process, we fabricated a novel tissue culture plate designed to automatically capture the monolayers during delamination. This eliminated the need for time-consuming observation of monolayers and labor-intensive manual pinning of the plates. To accomplish this task we drilled two small holes (0.53 mm) through the culture surfaces of 100 mm tissue culture treated polystyrene plates (BD Falcon). Each hole was drilled 3 cm from the center of the plate and aligned axially. Stainless steel wire, 0.51 mm in diameter, was cut to approximately 1 cm in length. The wire pieces were bent at right angles approximately 6.35 mm from one end. The unbent ends of the pins were inserted into the drilled holes of the tissue culture plate until the bent end was flush with the exterior base of the plate. Using a silicone elastomer (Sylgard-102, McMaster-Carr), the pins were sealed in place between the base of the culture plate and an additional polystyrene lid that prevented leakage or damage during use. The elastomer was allowed to cure for at least 12 hours in an oven at 37°C. The end result was a tissue culture plate with two steel pins protruding from the culture surface 60 mm apart, termed a “pin plate” (Figure 3.2). The pin plates were disinfected with 70% EtOH, and UV treated (UV wavelength 253.7 nm) for at least 1 hour prior to use. The same fabrication methodology can easily be applied to tissue culture plates of various sizes. Plates 35, 60, and 150 mm in diameter could be fabricated with posts placed 1.5 cm, 2 cm, and 6 cm apart, respectively. Before the addition of cells, the plates were again sprayed with 70% EtOH, placed into a sterilized laminar flow hood, and rinsed with DPBS.

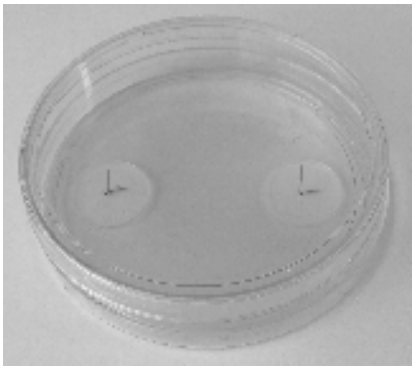

Figure 3.2 Novel "Pin Plate" Capture System. Shown polystyrene tissue culture dish is 100 mm in diameter. Distance between pins is 60 mm.

3.4.3 Bone Marrow Aspiration and Isolation Technique

To shift to a more clinically relevant method for obtaining MSCs, bone marrow was aspirated from the iliac crest of sheep using a Monoject Illinois needle (Sherwood Medical Company, St. Louis, Mo). With the animal under general anesthesia induced by intravenous propofol and sustained with inhalation of isoflurane in oxygen, bone marrow aspirates were collected using heparinized needles and dispensed into EDTA blood collection tubes (BD, San Jose, Ca) for processing. The marrow was passed through a 100 μm filter to remove solid debris before it was consolidated into a single 50 ml conical. An equivalent volume of DPBS was added to the bone marrow. Next, the diluted bone marrow solution was slowly added to a 15 ml layer of Ficoll-Paque™ Premium (GE Healthcare, Munich, Germany) contained within a separate conical and centrifuged (AccuSpin FR; Beckman Coulter Inc., Fullerton, CA) at 600 g for 30 minutes @ 25°C. Following centrifugation, the upper layer of the mixture containing plasma and platelets was discarded and the mononuclear cell (MNC) layer, containing the resident MSC population, was transferred into a new sterile conical. The cells were suspended in at least three times volume of DPBS and centrifuged at 500 g for 10 minutes. The supernatant was removed and an equivalent volume of ACK lysis buffer was added to the pellet volume to lyse any remaining red blood cells. The conical was then filled with DPBS and centrifuged at 400 g for 5 min. The supernatant was again removed and the MSC pellet was re-suspended in 20 ml of GM. Viable cells were counted via trypan blue

(Invitrogen) exclusion staining and a Countess automated cell-counting system (GE Healthcare). Viable cells were immediately plated at a 40,000 cells/cm^2 density to approximate the original protocol (approximately 80% plate confluency within 5-15 days).

3.4.4 Optimization and Standardization of a Protocol for the Expansion of MSCs

To optimize and standardize the methods for MSC cell expansion, the following protocol was established. First, the adherent MSC population was allowed to attach for 3 days before the plate was rinsed with DPBS to remove any remaining debris or contaminating non-adherent cell populations. Next, MSCs were induced towards a fibrogenic lineage and expanded to sufficient numbers by feeding fresh GM supplemented with 600 ng/ml bFGF every 2 days. Eight days after plating plate were approximately 50-80% confluent and the plate-adherent cell population was passaged.

Approximately 12 µl/cm^2 of trypsin-0.25% EDTA was added to the culture plate surface before the culture plate was placed into a tissue culture incubator at 37°C, 5% CO_2, and 95% humidity for 10 minutes. The trypsin was neutralized by the addition of GM comprised of 20% FBS. The cell suspension was removed from the tissue culture plate and centrifuged at a speed of 1500 rpm for 5 min. Following centrifugation, the supernatant was removed and the viable cells were counted in triplicate via trypan dye exclusion using a Countess automated cell counter. Cells were re-plated at a density of 5,000, 10,000, and 20,000 cells/cm^2 and passaged approximately every 48 hours to achieve the ideal plate confluency (80%) for successive passaging and minimizing cell-to-cell contact. At passage three, cells were collected and used for construct fabrication. Statistical analysis of recovered cell yields was performed with a one-way ANOVA and $P<0.05$ considered significant. Bartlett's test with $P<0.05$ was used to evaluate the equality of variances between groups.

3.4.5 Formation of Ligament Constructs

The protocol for the formation of the 3-D ligament tissue was not altered from previously published papers [105]. Briefly, cells were seeded onto 100 mm polystyrene pin plates at a density of 21,000 cells/cm^2. Fibrogenic GM was exchanged every other day for 8 days until a confluent monolayer was formed. At that time, the medium was replaced with fibrogenic DM and cultured another 5 days until spontaneous delamination occurred. The plates were kept in a tissue culture incubator at 37°C, 5% CO_2, and 95% humidity and DM was exchanged every 2 days. Following delamination, the tissues were maintained in fibrogenic DM and allowed to mature between the constraint pins for 2 weeks before analysis. Partially delaminated constructs were manually rolled upon pin plates to maintain consistent time in culture prior to mechanical and histological testing.

3.4.6 Mechanical Analysis

Mechanical testing of the tissue-engineered constructs was performed with a custom-built tensile testing system with a 2.5 N load cell (Applied Biosystems). Constructs were manually removed from pin plates and submerged in a warmed DPBS bath within the testing system. Construct ends were secured to the apparatus using two custom designed Velcro compression grips. The grips were incrementally lengthened to approximate the original length of the construct upon the pins of the culture dish. Sixty-micron diameter beads were painted onto the surface of the tissue for post analysis digital image correlation (DIC) to extrapolate the tissue-level strain during testing. The construct was loaded until failure occurred at a rate of 0.01/sec. Synchronized force and image recordings were complied from a Basler A102fc digital video camera using LabVIEW.

Cross-sectional area measurements were extracted from a microscope image captured immediately prior to loading. The image was imported into Image J and pixels calibrated to scale. Vertical lines were drawn at 10 randomly chosen regions along the length of the construct to account for sampling variation of the construct's diameter (Figure 3.3). Approximating the construct as a cylinder, the

cross-sectional area was determined and utilized for calculations of stress and subsequent data analysis. Statistical analysis of average construct diameters was performed via one-way ANOVA test with a $P<0.05$ considered significant. A Bartlett's test with $P<0.05$ was used to evaluate equality of variances between groups.

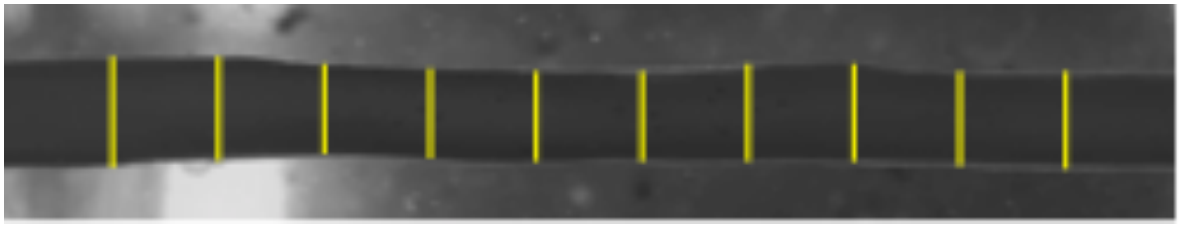

Figure 3.3 Determination of Construct Diameter. Image depicts the technique used for determination of construct diameter during mechanical testing. Lengths of 10 randomly spaced vertical lines were determined for each specimen tested.

Metamorph software was used for DIC and tracking. The tangent modulus over a strain range of 0.05-0.07 was determined by calculating the secondary slope of the nominal stress (load/cross-sectional area) versus nominal strain (change in separation of image data/ initial separation) response curve. Statistical analysis was performed via one-way ANOVA with $P<0.05$ considered significant. A Bartlett's test with $P<0.05$ was used to evaluate equality of variances between groups.

3.4.7 Histological Analysis

The constructs used for histological analyses were immediately fixed in 4% paraformaldehyde (PFA) for 1 hour while secured to pin plates. The fixative was replaced with a 15% sucrose solution for 1 hour at 4°C followed by a 30% sucrose solution overnight (>12 hrs). The constructs were then transferred into TBS medium, frozen over dry ice, and stored at -80°C until needed. Samples were sectioned with a cryostat to obtain 12 μm longitudinal sections that were adhered to Superfrost Plus microscopy slides until used for staining. The general morphology of the tissue sections was analyzed with H&E staining. Picrosirius red staining under polarized light was used to detect collagen birefringence within

the sections. Birefringence under identical imaging parameters is indicative of collagen alignment. All tissue sections were imaged at x10 magnification using an inverted light microscope (Nikon 23500).

Immunofluorescent staining with specific antibodies was performed to detect the presence of collagen type I within the engineered tissues. Frozen sections were fixed with ice-cold methanol for 10 min and subsequently rinsed 3 times with Phosphate Buffered Saline (PBS). Sections were blocked for 30 min with PBS-0.05% Tween20 (PBST) containing 20% calf serum (PBST-S) at room temperature. Sections were incubated overnight at 4°C with the primary antibodies in PBST-S. The concentration of rabbit anti-rat collagen type 1 (Abcam) was 10 mg/ml. Sections were incubated at room temperature for one hour with Cy3-conjugated anti-mouse or anti-rabbit antibody (Jackson ImmunoResearch Lab., West Grove, PA). Nuclei were stained incubation with a DAPI solution (Sigma, St. Louis, MO) in PBST for 5 min. The sections were examined and photographed with a confocal microscope (Olympus A) with dual excitation wavelengths of 488 nm and 568 nm.

3.5 Results

3.5.1 Bone Marrow Aspiration and Isolation Technique

To standardize the collection and isolation of our initial MSC population, a Ficoll density centrifugation technique was used to isolate the mononuclear cell fraction from a clinically relevant bone marrow aspiration harvested from the iliac crest of sheep. Comparative analyses of cell yields (cells/cm^2) isolated from four different BM donors are shown in Table 1**.** The plastic adherent MSCs were recovered following 8 days in culture. The coefficient of variance (standard deviation/mean) of MNCs and recovered MSCs was 28% and 74%, respectively. The relatively high variability between donors observed among MSCs recovered following 8 days in culture, suggested differences in BM composition or MSC growth. Cells isolated from donors 2-4 visually appeared less than 80% confluent during

passaging while the MSCs recovered from donor 1 were approximately 85% confluent at equivalent time points. Nonetheless, MSCs recovered from each donor were subsequently expanded and used for construct fabrication as described above.

Table 1 Comparative Analysis of MSC Yields

Donor #	Sex	BM Aspiration Volume (ml)	MNC Cells	MNC Yield (cells/ml BM)	Seeding Density (cells/cm^2)	MSC Yield (cells/cm^2)
1	F	10.0	1.1E08	1.1E07	4.0E04	4.4E04
2	F	30.0	2.2E08	7.2E06	4.0E04	9.5E03
3	F	7.0	5.1E07	7.3E06	4.0E04	2.5E04
4	F	14.0	8.3E07	6.0E06	4.0E04	9.7E03
Average	N/A	15.3	1.2E08	7.9E06	N/A	2.2E04
S.D.	N/A	10.2	7.1E07	2.2E06	N/A	1.7E04
C.V.	N/A	67%	62%	28%	N/A	74%

3.5.2 Expansion of MSCs with Standardized Passage Densities

The ability of MSCs cultured in fibrogenic media to form 3D constructs following expansion at various passage densities (5,000, 10,000, and 20,000 cells/cm^2) was evaluated. The confluency of the plates and number of viable cells recovered at each passage was recorded. Cells were utilized for construct formation following passage 3. Representative images of each plating density immediately prior to passaging are shown in Figure 3.4. Passaging at 5,000 cells/cm^2 yielded approximately 80% plate confluence every other day with minimal contact between cells. Passaging at densities of 10,000 cells/cm^2 and 20,000 cells/cm^2 resulted in plates approximately 90% and 100% confluent at equivalent time points.

Following passage 3, the cells from each group were seeded onto polystyrene tissue culture dishes at a plating density of 21,000 cells/cm^2. At this plating density, cells achieved 100% confluence within 2 days with a hyper-confluent monolayer observed following 8 days in culture (Figure 3.4). Monolayers successfully delaminated by day 15 of the fabrication protocol. As no apparent differences in the cells' ability to form a 3D construct were observed among cells passage at different densities, the 5,000 cells/cm^2 passage density was utilized

for all future experiments. This density maximized the potential cell yields and established a consistent cell expansion protocol for construct formation.

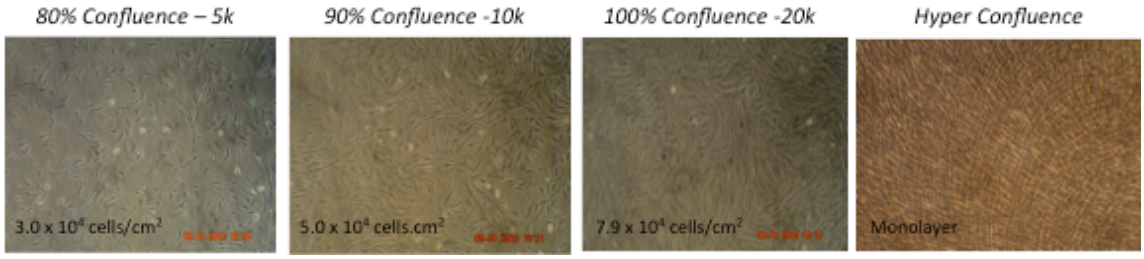

Figure 3.4 Average Cell Yield and Plate Confluence. A-C) Average cell yield/cm^2 and representative confluence at 5k, 10k, and 20k cells/cm^2 passage densities, and D) Plate confluence following plating and 8 days of culture.

3.5.3 Reproducibility of MSC Expansion Protocol

Cells isolated from each of the four donors, as described in 3.5.1, were seeded onto 150 mm tissue culture plates, passaged at a 5k cells/cm^2 density every 48 hours, and fed GM supplemented with 600 ng/ml FGF-b. Averaged cell yields/cm^2 from all donors, at each passage, were recorded as mean ± S.E. and shown in Figure 3.5. Representative plate confluences described in Figure 3.4 are plotted for each passage in Figure 3.5. Plates did not exceed 80% confluence at any passage time point, but the cell density was greatest following passage 2. Recovered cells at each passage were not significantly different between donors. The relative variability (standard deviation/mean) of cell yields at each passage, for each donor, was approximately 34±14% indicating a moderate level of variability between donor groups.

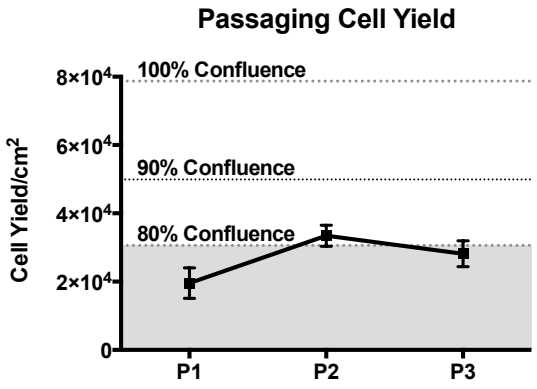

Figure 3.5 Cell Yield Following Passaging. Data represents average cell yield/cm^2 ± S.E.

3.5.4 Fabrication of Ligament Constructs Utilizing Standardized BLB Protocol

Having standardized the seeding and passage densities optimal for expansion, MSCs from each of the four donors were seeded onto the custom 100 mm pin plates and cultured in fibrogenic GM for 8 days until a confluent ligament monolayer was formed. The GM was then replaced with DM and the monolayer was cultured for an additional 5 days. The constructs began to spontaneously self-delaminate approximately 4-5 days following the switch to DM, or 13 days from the initial plating of MSCs. The delaminating monolayer was captured on the posts of the pin-plates and created a uniform 3D ligament construct 6 cm in length (Figure 3.6A). The constructs were allowed to condense and mature on the posts for 2 weeks and formed a uniform construct diameter of approximately 0.9±0.1 mm (mean ± S.D.). Average construct diameters for each donor, determined from images taken during mechanical testing, are shown in Figure 3.6B. No significant differences in average construct diameter were observed between donors. Additionally the standard deviation within each group was not significantly different among groups. The average coefficient of variation for construct diameters within each batch of constructs was 16±4% and not significantly different between donors indicating that the construct diameters were uniform and reproducible within and between donor groups.

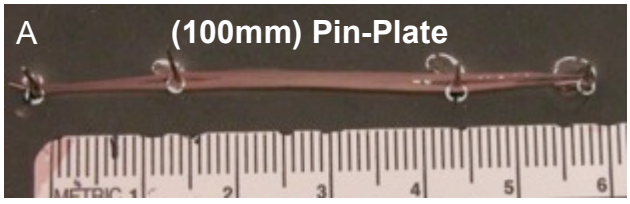

Length: 60mm Width: ~2mm @ 1 week

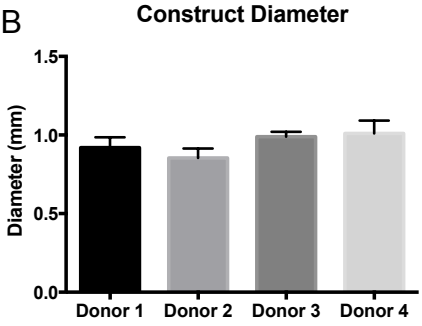

Figure 3.6 Ligament Construct Formation A) Construct captured via pin plate at 1-week post-delamination and B) Construct diameter 2 weeks following delamination. Data are represented as mean ± S.E. for each donor.

3.5.5 Mechanical Analysis of Constructs

Following measures of diameter, the mechanical properties of the constructs were determined from a minimum of 6 samples. Overall, constructs had average tangent moduli of 2.3±1.1 MPa within a physiologic strain range of 0.05-0.07. The tangent moduli (shown as mean ± S.D.) of the constructs fabricated from each respective donor are shown in Figure 3.7. The average coefficient of variation within each batch of constructs was 26±6% and was not statistically different among donors. The relative variability of the tangent modulus among all donors was relatively high (50%) and likely attributable to the mechanical properties of constructs fabricated from donor 1 cells. The tangent moduli of the constructs fabricated from cells of donor 1 were significantly stiffer (about two-fold greater) than constructs engineered from cells obtained from the other three donors. Significant differences in tangent moduli were not observed between constructs fabricated from donors 2, 3, and 4.

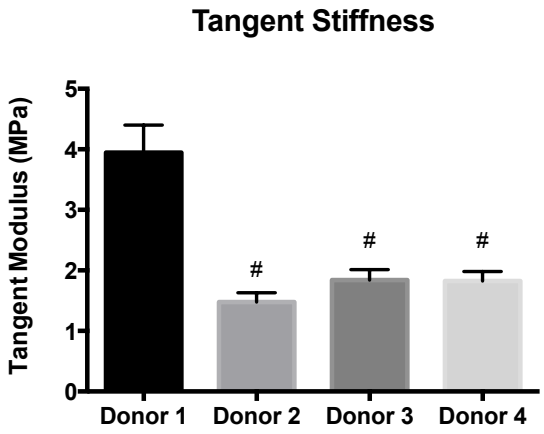

Figure 3.7 Construct Mechanics. Data are presented as mean ± standard error. (#) denotes significance compared to donor 1.

3.5.6 Construct Histology

Following mechanical testing, the constructs were frozen and saved for histological analysis of tissue properties. Representative images of constructs fabricated from each donor are shown in Figure 3.8. H&E staining for general morphology showed nuclei present throughout the construct. The collagen fibers were more axially aligned on the periphery of constructs from donors 2-4, with

relatively amorphous tissue in the center. Increased birefringence of collagen tissue was observed using picrosirius red staining and polarized imaging methods and suggests an increase in collagen fiber alignment in donor 1 constructs versus constructs of other donor groups. Antibody staining of type 1 collagen and DAPI showed that the ECMs of all donor constructs were comprised of primarily type 1 collagen and contained viable nuclei throughout. Tissue compositions and structures from this study were comparable to previous published works evaluating morphology of engineered ligament constructs.

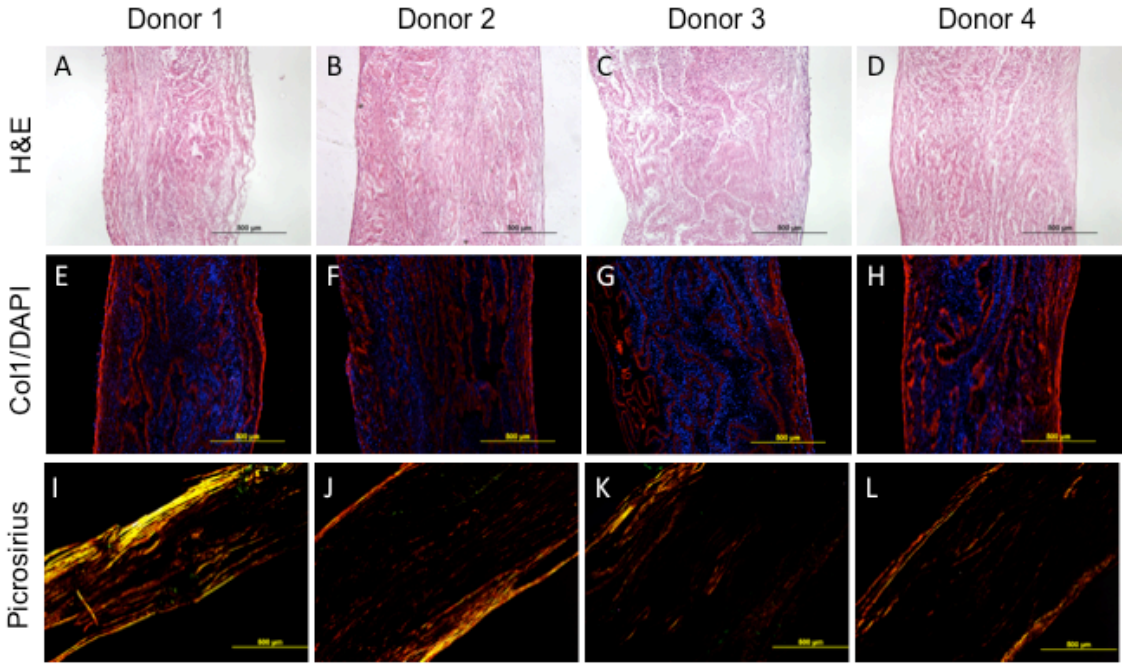

Figure 3.8 Histological Staining of Ligament Constructs Top Row: H&E of general morphology for all respective donors, Middle Row: Picrosirius Red staining imaged under polarized light (yellow/red). More collagen alignment was present in constructs from Donor 1. Bottom Row: Collagen type 1 (red) /DAPI (blue) immunostaining. All images were taken at X40 magnification. Scale bar = 200 µm.

3.6 Discussion

The overall goal of this study was to implement a standardized process to fabricate reproducible and uniform tissue constructs. Creation of such a process is critical for evaluating manufacturing consistency and for identifying and controlling sources of variation within the manufacturing system. The utilization of a non-terminal bone marrow aspiration method and Ficoll density gradient

isolation technique allowed for a consistent number of plastic-adherent MSCs to be isolated from a known amount of starting material. Additionally, considering multiple aspirations can be performed from a single donor, these methodologies greatly improve the amount of cells and the number of resultant constructs that can be fabricated from a given BM donation.

As the new BLB fabrication method can be performed from a routine bone marrow aspiration, commercial manufacturing can be performed as an autologous or allogeneic process. An autogenic manufacturing process would treat each graft as a patient-specific product. While the risk of immune rejection is eliminated with autogenic grafting, the variation between the starting cell sources obtained from patient specific bone marrow aspirations can lead to large variations in the tissue-engineered end products and make it difficult to meet the established manufacturing process controls and end-product specifications necessary to demonstrate the end products are acceptable for use. In contrast, an allogeneic process, while having some risk of immune rejection, would allow for many constructs to be made from a single well-characterized donor source and is a more commercially viable approach for manufacturing our grafts.

Although the use of the Ficoll isolation technique improved upon our existing methodology by providing an increased number of adherent MSCs, significant variability still existed in the resultant cell isolates from each donor. Despite each plate having an equivalent numbers of mononuclear cells seeded initially onto the cell culture plates (40,000 cells/cm^2), the cell yields following 8 days of culture were significantly different. This finding is consistent with the work of other researchers that have demonstrated variability in MSC yields even between two aspirations taken from the same donor during the same procedure [28]. This finding suggests that the initial plating density may not be critical for isolating a well-defined cell population[119] and that amplification of cells with successive passages may be sufficient to expand and isolate a purified MSC source. However, even if a purified MSC population can be expanded through passaging, characterization

of this population will be required by the FDA to confirm the degree of purity and identity of the cell population and to evaluate the variability related to differentiation potential, growth rates, etc. that may exist between cells obtained from different donors or the same donor at different time points.

We found that the newly established passage density of 5,000 cells/cm^2 consistently expanded the isolated cell populations *ex vivo* to 80% confluence, and prevented over confluence that can potentially alter the cells' phenotype. Recent work suggests that lower passage densities may reduce population doubling times of MSCs [119]. Thus, future work investigating the optimal parameters for maximizing cell yields in the shortest amount of time will be beneficial to improving our process efficacy and reducing overall costs.

The fabrication of individual constructs utilizing our novel pin-plate design has significantly streamlined the manufacturing process. The rate of success for capturing and constraining the delaminating monolayer to an appropriate length significantly improved from about 30% with the old protocol to 100% with the novel pin-plate approach. In a few constructs, the contraction of the tissues around the pins post-delamination, led to very thin constructs that tore off the pins. Future studies will need to investigate factors that influence tissue roll-up including growth factors, pin locations, and time in culture, to improve the longevity of our 3D construct fabrication process.

The use of the pin-plates decreased labor and eliminated the variability associated with using a technician. This allowed for more accurate evaluation of variability between and within constructs engineered from different cell populations. Additionally, because a technician is not required to transfer monolayers to a new plate and manually constrain them with pins, a single technician can fabricate many more constructs in the same amount of time. The increased ability of the grafts to survive *in vitro* will be critical for increasing the sample sizes per batch required to adequately characterize the resultant tissue.

The rate-limiting step of the construct manufacturing process now shifts to our ability to efficiently exchange and add media to each plate. Therefore, future experiments were designed to include an automated bioreactor system, capable of feeding multiple plates at once.

The relative variability in the average tangent modulus of engineered constructs was relatively high (~50%). This was in part due to the significantly higher modulus of construct fabricated from donor 1 cells compared to those made from cells of the other donors. Exclusion of donor 1 constructs from analysis of BLB mechanics shows that variability among donors is greatly reduced with an average tangent modulus of 1.7±0.2 MPa and a relative variability of across all donors of 12%. While general morphology was similar across all groups, donor 1 qualitatively exhibited more aligned collagen as seen in polarized images of picrosirius red staining. This increase in collagen alignment may have led to increased mechanics of these tissues.

While ECM variability may explain the mechanical differences of our constructs, the source of this variation is unknown and likely related to variations in the initial cell populations obtained from each donor. To control for this variation, further identification and characterization of the cell population immediately prior to plating is needed to establish a purified starting population required for construct fabrication. While it may be impossible to completely eliminate heterogeneity within the starting cell population, the identification of specific cell properties or ranges of cell properties indicative of successful end-product performance, will be useful for improving process efficiency and construct quality. Defining acceptable cell criteria will also be important for CGMP compliant process validation that will require the identification and control of variation with the manufacturing procedures.

Despite differences observed in final construct properties among donor cell populations, significant differences in cell yields during passaging were not

observed. Alternative methods for characterizing cells during the construct fabrication process, such as relative gene expression analysis, may be needed to identify additional sources of variability that may exist between donor populations. Additional information about the donor (health history and age of the animal), may also be useful in identifying sources of variations that can influence the process results. In addition to adequate cell characterization, the identification of suitable construct properties and specifications, indicative of the efficacy of tissue regeneration *in vivo* is a significant challenge in the field of tissue engineering. Systematic data collection of much larger sample sizes within a tightly controlled, well-characterized manufacturing system is needed to help identify new *in vitro* targets that are more representative of the construct's therapeutic effect *in vivo*.

In conclusion, the novel methods described in this chapter have led to a standardized process for fabricating uniform and reproducible constructs. Future studies designed to optimize our process will concentrate on investigating plating densities, expression of ligamentous markers, and construct mechanics. Additionally, our newly introduced methods demonstrate the standardization of only the ligament part of the BLB manufacturing process. Cells grown under osteogenic culture conditions may have vastly different growth rates and properties. Thus, we will need to develop custom protocols to standardize passage densities, culture time, and growth conditions to optimize their osteogenic potential *in vitro*.

Chapter 4
Characterization of a MSC Population Required for Scaffold-less Construct Fabrication

4.1 Introduction

Despite the standardization of our MSC isolation and expansion methodologies, the mechanical properties of constructs fabricated from the bone marrow obtained from different donors varied. This variation was likely attributable to subtle differences in the starting cell populations of the extracted MSCs. Thus, it is necessary to further define and control the starting cell population in order to validate our manufacturing process, ensure a more consistent and well-defined end product, and comply with current CGMP regulations. Additionally, to improve the translational applications of our BLB technology, the ability to produce human derived constructs using our current fabrication method should be evaluated.

Within our current ligament manufacturing protocol, MSCs cultured in fibrogenic media attach to, proliferate, and differentiate towards a tendon/ligament-like lineage over successive passages before being seeded to form a self-delaminating monolayer. However, extensive characterization of these cells immediately prior to final seeding has not been performed and requires sufficient analysis to evaluate and define the composition, function, and ligamentous differentiation of this starting MSC population.

Human MSCs (hMSCs) have been shown to differentiate into a variety of tissues including tendon, bone, muscle, and fat. However, cell surface similarities between MSCs and tendon fibroblasts and the lack of a specific tendon marker

make characterizing the differentiated tendon phenotype difficult. The use of gene expression data can be used to describe differences in the regulation of tendon-related ECM production even though they are not directly indicative of protein quantity. Work by several authors has utilized a combination of gene targets, including Col-1, Col-3, TenC, and scleraxis, to identify induction of MSCs toward a tendon-like lineage [27,183,185]. Scleraxis, although expressed in other cell types such as osteocytes and chondrocytes, is considered highly specific for ligament differentiation and believed to also regulate tenomodulin and Col-1 expression. The expression of Runx 2 and alkaline phosphatase (ALPL) is commonly associated with differentiation to an osteogenic lineage and can be used as a negative control to confirm the commitment towards ligament versus bone.

The characterization of human MSCs is not trivial. MSCs isolated from bone marrow aspirations have been shown to be few in number with roughly 1:10,000 nucleated cells attaching to the culture dish [30]. Additionally, contamination of the MSCs with plastic adherent hematopoietic debris complicates the isolation of a purified MSC population. As such, successive expansion of the extracted MSCs is required to amplify and purify cells for subsequent characterization assays. In addition to their plastic adherence properties, MSCs are characterized by leptin receptors (CD45, 95, 105) and their ability to differentiate towards multiple lineages. Due to the increasing use of bone marrow derived MSCs in tissue engineering applications and regenerative cell therapies, several companies and researchers have begun investigating strategies for large-scale MSC production using CGMP compliant conditions. The use of sophisticated methods of manufacturing and characterization that are in accordance with international standards for MSC identification (i.e. plastic-adherence, cell surface markers, and differentiation potential) and allow for a well-defined cell population to be produced, are well beyond the capabilities of our laboratory.

Fortunately for us, well-defined MSCs are commercially available from companies such as Lonza and Rooster Bio. The utilization of these MSCs eliminates a significant part of the manufacturing process that involves the expansion and characterization of a consistent MSC starting population. It eliminates the extensive testing required to identify and describe the composition and phenotype of MSCs isolated with our current techniques. Additionally, the time saved by utilizing a ready-made, purified cell source would shorten fabrication time and improve the overall process efficiency. However, we have not tested the ability of an undifferentiated MSC population to differentiate to tendon-like lineage and directly form a 3D construct via our existing manufacturing protocol.

The objective of this study was therefore to utilize a commercially available and well-characterized hMSC population as our starting material and evaluate the ability of the hMSC to differentiate to tendon and form a 3D construct using our current BLB fabrication process. If successful, this will expedite the translational application capabilities by identifying a clinically relevant, regulatory compliant, pre-manufactured starting material for ligament/tendon construct fabrication. The characterization of the ligamentous MSC lineage throughout the ligament fabrication process via gene expression will be used to establish process validation criteria of the in-process intermediates, and will more accurately define the specifications and properties of our graft.

4.2 Methods

4.2.1 Formation of Ligament and Bone Constructs from hMSCs

First, human MSCs (Lonza and Rooster Bio) were removed from liquid nitrogen storage and placed in a 37°C water bath. Immediately following the thawing process, the entire volume of cells and media was transferred to a sterile 15 ml conical containing at least 3 times the volume of warmed GM. Next, the cell suspension was centrifuged at 1500 rpm for 5 min at 37°C. The supernatant was

aspirated and remaining cells were re-suspended in fresh GM and counted. Viable cells were seeded onto sterile polystyrene tissue culture plates at a density of 21,000 cells/cm^2. Plates were immediately induced towards bone and ligament linages through the addition of osteogenic and fibrogenic media, respectively. Both hMSCs manufacturers provided extensive characterization of the starting cell populations. De-identified characteristics of the donor and lot information of cells are described below in Table 2.

Table 2 Donor and Lot Details of Cells Used for Construct Formation

Manufacturer	Patient Sex	Patient Age	Lot #	Passage Frozen
Lonza	Male	23	056	P2
Rooster Bio	Male	30	007	7.2 Pop. Doubling
Rooster Bio	Female	33	012	7.6 Pop. Doubling

At various defined stages of our fabrication process, cells and tissue were harvested for subsequent qPCR analysis at 0, 4, 8, and 12 days. These time points correspond to the initial plating, growth phase, differentiation phase, and 3-D roll-up phase of the self-delamination tissue fabrication process, respectively. An additional 3 constructs were fabricated and allowed to remain in a 3D configuration *in vitro* until day 15 for subsequent mechanical and histological analyses of the formed 3D tissue. A diagram of the experimental set-up and sample size for each lot of donor cells is shown in Figure 4.1.

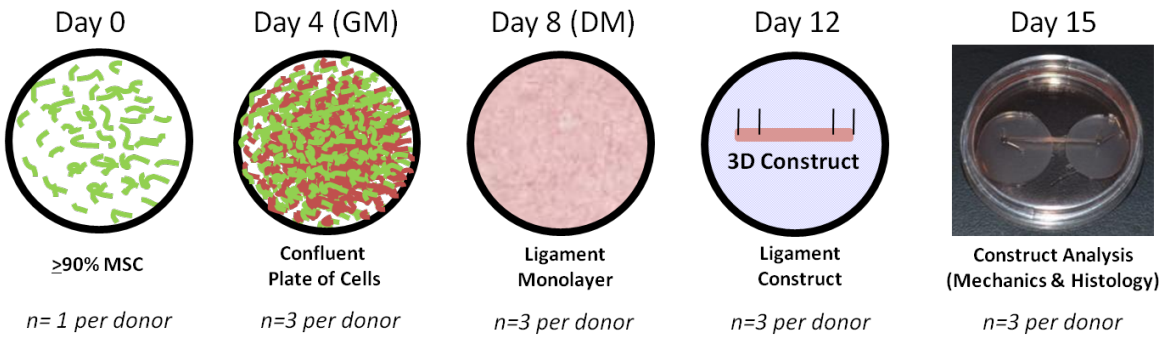

Figure 4.1 Experimental Design for hMSC Construct Analysis. Temporal gene expression was analyzed at day 0, 4, 8, and 12 time points that corresponded to various aspects of the construct manufacturing process. Mechanical and histological analyses were performed exclusively on day 15 (3 days following roll-up) constructs.

4.2.2 Cell and Tissue Preservation for RNA Extraction

Isolation of ribonucleic acid (RNA) was performed on cell and tissue isolates, at 0, 4, 8, and 12 days. Day 0 cell suspensions, directly from the manufacturer, were immediately placed in a 2 ml cryovial and centrifuged at 1500 rpm for 5 min at 25°C. Following centrifugation, the supernatant was removed and the cryovial was submerged in liquid nitrogen for a minimum of 30 seconds to freeze the resultant cell pellet. Cells and tissue recovered at 4, 8, and 12 day time points were first trypsinized from the culture surface, before being placed into 2 ml cryovials and centrifuged at 1500 rpm for 5 min at 25°C. Following removal of the supernatant, the resultant cell/tissue concentration was frozen in liquid nitrogen for at least 30 sec. All cryovials were stored at -80°C following freezing until required for further processing.

4.2.3 Histological Analysis of Tissue Constructs

Histological analysis of the constructs was performed to investigate the general morphology and distribution of collagen and mineral within the constructs. Methods for histological and immunohistochemical staining have been described previously in section 3.4.7. Briefly, at 3 days post 3D construct formation (day 15), constructs were rinsed with phosphate buffered saline (PBS, Sigma-Aldrich) and flash frozen in tissue freezing medium. Sample sections (10 μm, Milipore Cryostat) were prepared for histological and immunohistochemical analyses.

Tissue structure and collagen distribution were determined using H&E and collagen-1/DAPI immunohistochemical staining, respectively. Deposition and distribution of calcified mineral was determined with Alizarin Red S staining [130].

4.2.4 Gene Expression Analysis

Total cellular RNA was isolated by lysis in Trizol (Qiagen) followed by a one-step phenol chloroform-isoamyl alcohol extraction. RNA isolation was performed on undifferentiated MSCs (n=1 sample, per donor) and cells harvested at days 4, 8, and 12 of the BLB fabrication process (n=3 samples, per time point and donor) by using a miRNeasy Kit (Qiagen) and treating with DNase I (Qiagen). Osteogenic constructs were simultaneously fabricated and evaluated at equivalent day 4, 8, and 12 time points (n=1 sample, per time point and donor). The amount and integrity of RNA were quantified using a bio-analyzer system (Nanodrop 2000). A total of 200 ng of RNA was reverse-transcribed using an RT^2 HT First Stand kit (Qiagen). The amount of cDNA in each sample was analyzed using a Nanodrop system, and 200 ng of the cDNA template was used for each qPCR reaction. The cDNA was amplified in a CFX96 real time thermal cycler (BioRad) using a Taqman gene expression assay kit. The level of expression of mRNA transcripts of each target gene was calculated as $2^{-(dCt)}$ and normalized to GAPDH using methods of Schmittgen and Livak [94]. A list of TaqMan® Gene Expression Assays used in this experiment is shown in

Table 3. The qPCR reactions were run in duplicate and results are presented as averaged target gene expression (mean ± standard error) normalized to GAPDH for all donors.

Table 3 TaqMan Gene Expression Assays (Applied Biosystems) used for qPCR

Gene Symbol	Gene Name	Assay ID
GAPDH	Glyceraldehyde-3-Phosphate Dehydrogenase	HS02758991_g1
COL1A1	Collagen I – α1	Hs00164004_m1
COL3A1	Collagen III - α1	Hs00943809_m1
TNC	Tenascin C	Hs01115665_m1
SCXA/B	Scleraxis	Hs03054634_g1
RUNX2	Runt-related transcription factor 2	Hs00231692_m1
ALPL	Alkaline phosphatase	Hs01029144_m1

4.3 Results

4.3.1 Formation of Human Bone and Ligament Constructs

We successfully fabricated three-dimensional bone and ligament constructs utilizing undifferentiated MSCs using our current BLB fabrication protocol. The hyper-confluent monolayers successfully self-delaminated and were successfully captured on the custom 35 mm pin plates, with pin anchors set 20 mm apart (Figure 4.2). The constructs remained intact on pins for 3 days post roll-up and then were harvested for mechanical and histological testing.

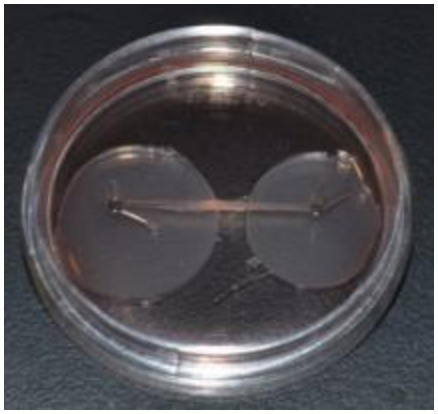

Figure 4.2 hMSC Ligament Construct. Dimensions of 3D tissue are approximately 20 mm x 0.5 mm x 0.5 mm

4.3.2 Mechanical Properties of Ligament hMSC Constructs

Ligament constructs were mechanically tested utilizing a custom built tensiometer as described earlier. Briefly, the constructs were removed from pins and tested 3 days following formation of a 3D construct. The stress vs. strain data for each sample are shown in Figure 4.3. Strain data were obtained through digital image correlation of markers on the tissue and calculated using methods described in section 3.4.6. The maximum tangent modulus was calculated for each sample by computing the slope of the nominal stress vs. nominal strain curve. The mean tangent modulus was 12.0 ± 0.2 kPa. No significant differences in the mechanical properties of the tissues were observed between cell lots (n>2 per donor). Due to the limited number of bone samples, the bone constructs were not mechanically analyzed.

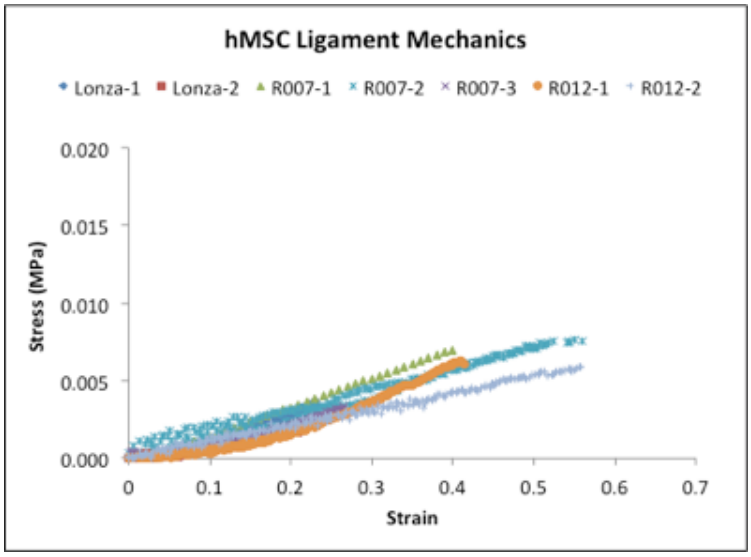

Figure 4.3 Mechanics of hMSC Ligament Constructs. All tests are shown until failure.

4.3.3 Characterization of the Human-Derived Tissue Constructs

Morphologically the constructs were similar in appearance to previously described constructs derived from ovine cells. The constructs were composed primarily of Col-1 with viable nuclei present throughout the tissue (Figure 4.4B). The H&E staining showed that the constructs were composed of relatively amorphous tissue with more highly aligned collagen regions observed on the

periphery of the tissue (Figure 4.4A). Alizarin red staining showed no calcified mineral present within ligament constructs (Figure 4.4C). However, alizarin red staining of bone constructs did confirm the presence of a small amount of calcified mineral (Figure 4.4D). Differences in the gross morphology and distribution of Col-1 between engineered bone and ligament constructs were not observed. Morphological differences between constructs derived from separate donor populations were also negligible.

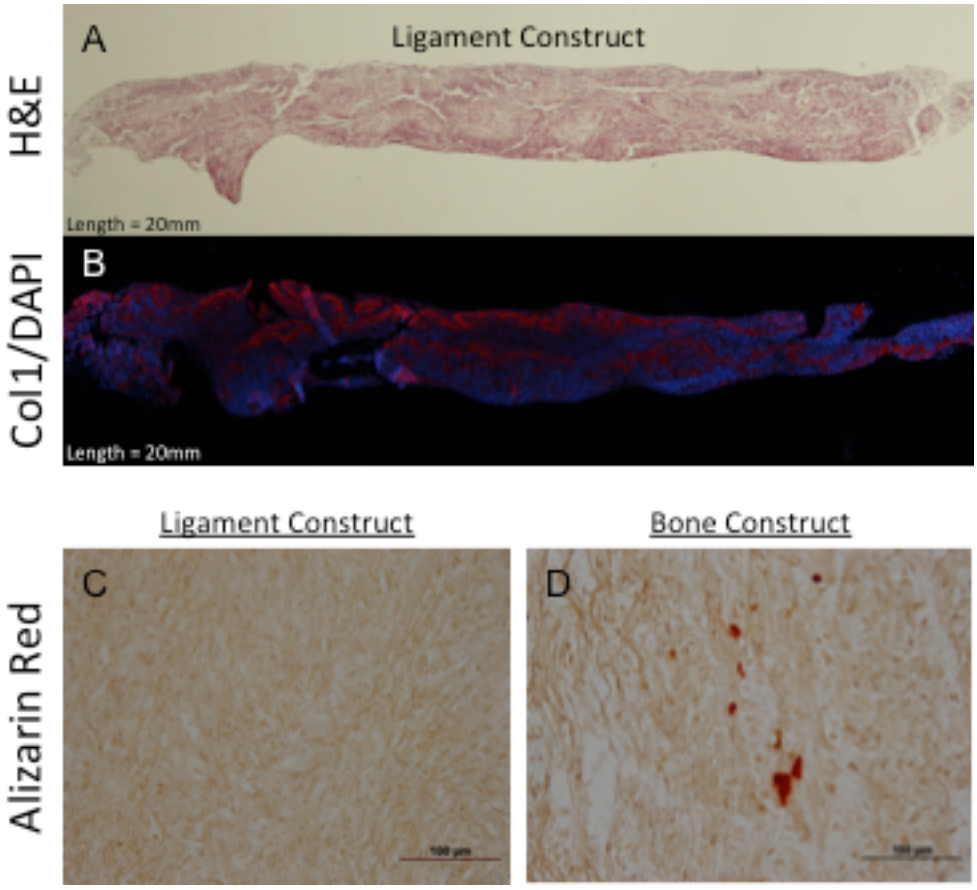

Figure 4.4 Histology of Human-Derived Constructs A) H&E (X4), B) Collagen-1/DAPI immunostaining (X4), C) Alizarin staining (X40) of ligament constructs, and D) Alizarin staining of bone construct (X40)

4.3.4 RT-PCR Results

Gene expression relative to GAPDH expression was analyzed via quantitative PCR (qPCR) for all tissue samples. Average gene expression was determined by combining analysis across all donor cell populations. Expression of genes

typically associated with tendon and bone differentiation was analyzed and compared over time in culture (days 0, 4, 8, and 12) and is shown in Figure 4.5. Relative gene expression of tendon differentiation markers Col-1, Ten-C, and Scx were significantly increased at day 8 compared to undifferentiated MSC starting cell populations. While the expression of Col-3 was increased by day 8 (P=0.07), the increased expression was not significant until day 12. The expressions of ligament markers Col-1, Ten-C, and Scx peaked at day 8 before dropping at day 12 to undifferentiated (day 0) expression levels. Additionally, expressions of Runx-2 and ALPL within our ligament constructs were significantly less at days 8 and 12 compared to undifferentiated MSC populations. The down-regulation of these bone-specific markers at day 8 and 12 time points further confirms the induction of the MSCs towards a tendon/ligament lineage.

The average relative gene expression of bone constructs was also evaluated (qPCR) at days 0, 4, 8, and 12 of culture (Figure 4.6). Expression of Col-1 and Col-3 increased with increased time in culture with approximately a two-fold increase compared to the undifferentiated MSC expression levels at day 0. The increase in Col-1 and Col-3 markers is consistent with an increased production of ECM material necessary for 3D tissue formation. As expected, significant increases in the expression of ligament-specific markers Ten-C and Scx were not observed in MSCs induced to an osteogenic lineage. Conversely, expression of bone-specific markers Runx 2 and ALPL did increase over time in the MSCs induced to an osteogenic lineage.

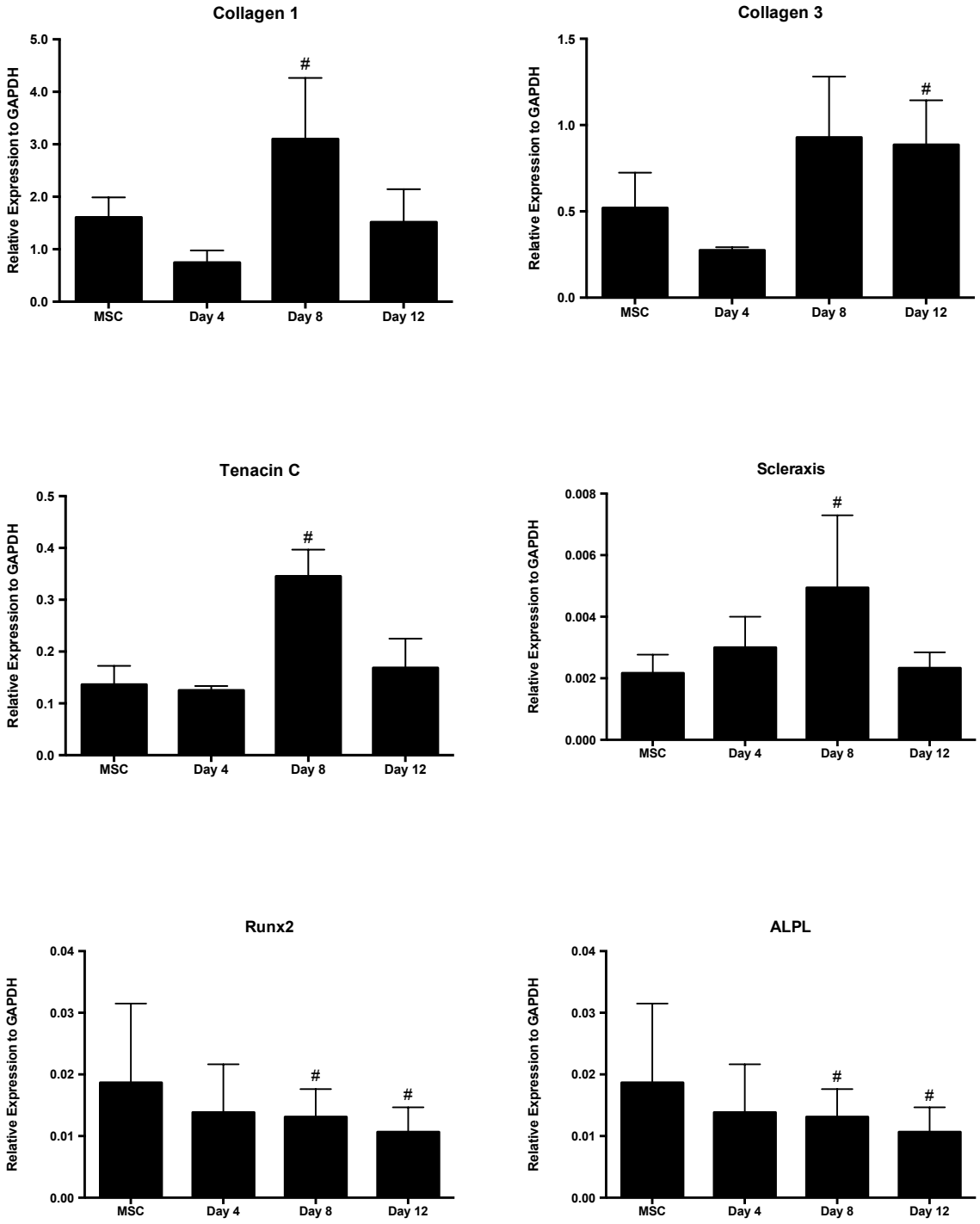

Figure 4.5 Relative Gene Expression of hMSC Ligament Constructs. (#) denotes significance with respect to undifferentiated MSCs.

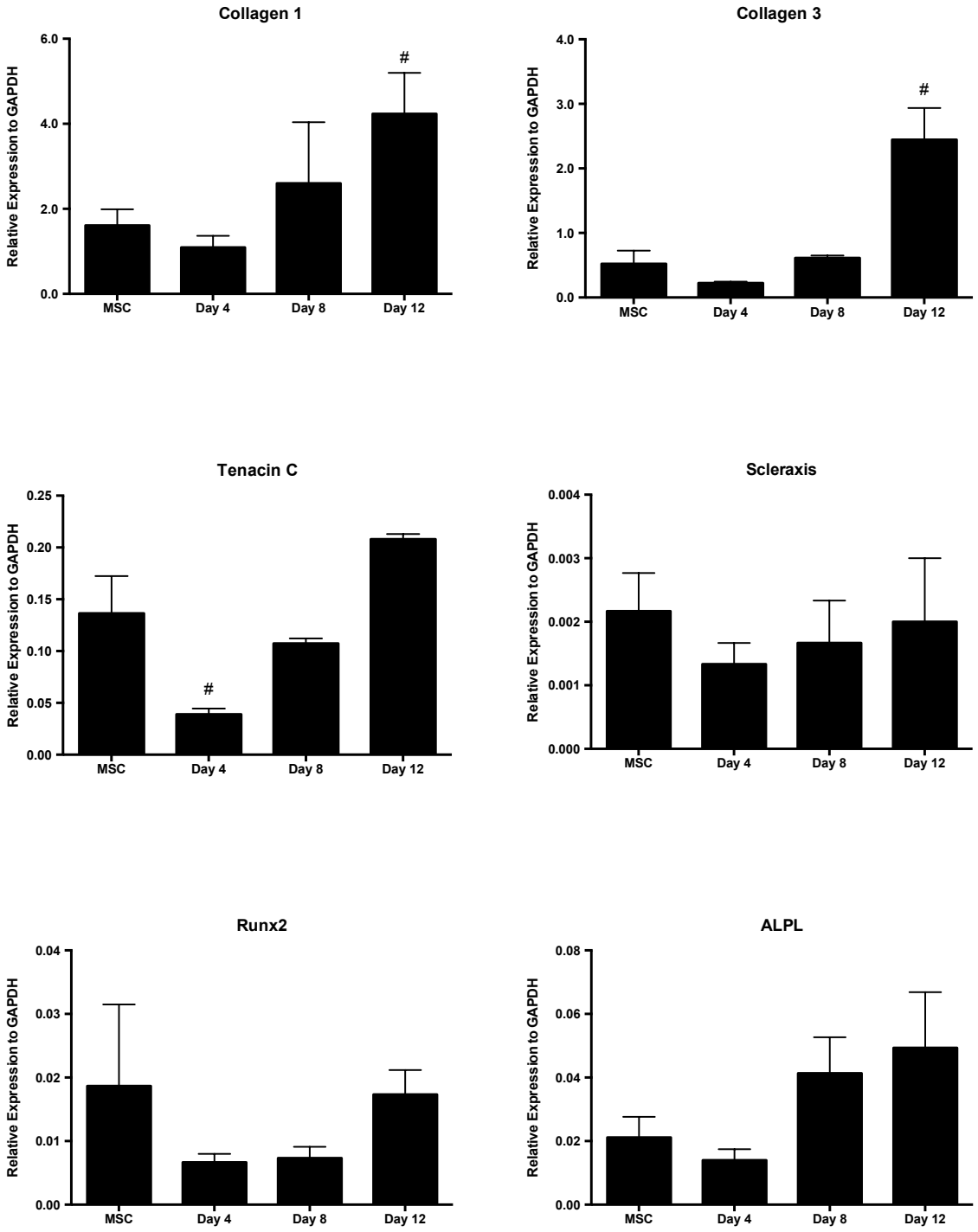

Figure 4.6 Relative Gene Expression of hMSC Bone Constructs. (#) denotes significance with respect to undifferentiated MSCs.

4.4 Discussion

The results of this study validate the use of our manufacturing process to engineer 3D tendon and bone constructs starting from a well-characterized commercially available cell source. Both tendon and bone tissues, fabricated directly from an undifferentiated MSC population and expanded to ligamentous or osteogenic lineages during the fabrication process, successfully formed 3D BLB constructs. The prevention of the labor intensive cell passaging steps in this newly developed manufacturing protocol reduces construct fabrication time by removing the need to define and characterize specific tendon and bone cell populations prior to use within our system and eliminating the need for continual monitoring by a highly trained technician.

The ability of MSCs to differentiate towards a ligament phenotype in culture was demonstrated through the analysis of gene expression data normalized to GAPDH. No significant changes in relative gene expression were observed between undifferentiated MSCs and MSCs induced to a ligamentous lineage for 4 days. However, following 8 days in fibrogenic media, the cells recovered from the confluent monolayer had a higher gene expression of ligament-specific markers of Col-1, Col-3, TenC, and Scx compared to the undifferentiated cells. Expression of bone-specific markers Runx2 and ALPL were also down-regulated at the 8-day time point. Within our fabrication process, the day 8 time point is believed to be associated with an increased synthesis of ECM as the cells form a confluent monolayer with sufficient matrix integrity to allow for self-delamination.

Following peak ligament-specific gene expression at day 8, the average expressions of Col-1, TenC, and Scx in cells cultured for 12 days were reduced to levels observed in the undifferentiated MSCs. Following the formation of a 3D construct at day 12, the protein synthesis of the cells may have switched from high rates of ECM synthesis to maintenance of existing ECM. It is important to note that gene expression is not always indicative of protein expression. In fact,

despite the finding that gene expression at 12 days was equivalent to that of undifferentiated MSCs, the overall amounts of tendon proteins within the developing tissue may have been increased. Histological staining with Col-1/DAPI confirmed a high abundance of Col-1 within the tendon portion of the constructs despite a decrease in relative gene expression of Col-1 at day 12.

MSCs cultured in osteogenic media demonstrated a decrease in ligament-specific makers and an increase in bone-specific markers (Runx-2 and ALPL) with time. Histologically small amounts of mineral were seen within the bone-differentiated engineered tissue. However, the relatively small amount of mineralization suggests that additional time *in vitro* may be required to elicit more substantial bone-like phenotypical changes in the bone region of the engineered tissue.

The earliest time point suitable to correlate the mechanics of our 3D tissues with gene expression immediately following delamination (day 12), was at three days following roll-up (or day 15 of fabrication process) because mechanical analysis of the material properties of our tissue requires accurate construct dimensions. Tissue monolayers immediately following delamination are amorphous and require sufficient time in culture to contract and uniformly align between the two constraint pins. Evaluation of the constructs before a uniform diameter had been established would have yielded inaccurate mechanical results. The moduli of our constructs at this three-day time point were significantly more compliant than previously reported tissue properties described in Chapter 2. This suggests that significant changes in ECM structure and composition may occur within tissues with increased time in culture.

While the average relative gene expression with time in culture was similar between hMSC donors, the degree of relative gene expression varied. Despite these differences between groups, observable changes in construct histology or mechanics were not observed. However, more detailed assays looking at protein

content within our constructs may be needed to further characterize ligamentous differentiation and construct properties among donor samples.

Continued evaluation of our fabrication process utilizing a well-defined cell population is needed to identify and control sources of variation within the manufacturing system. The use of standardized markers of gene expression may provide suitable specification necessary to demonstrate production consistency and graft effectiveness *in vivo*.

In summary, use of characterized, undifferentiated, bone marrow derived hMSCs is an acceptable starting cell population for the fabrication of scaffold-less constructs. As these MSCs are capable of differentiating towards both ligamentous and osteogenic lineages during the construct formation process, significant time associated with expansion and characterization of a pre-differentiated tendon or bone-like MSC population can be eliminated. Additionally, sufficient quantities of these well-characterized cells can be readily obtained from CGMP compliant manufacturers, making them an ideal input material for our translational manufacturing process.

Chapter 5
Bioreactor Manufacturing of Multi-Phasic Tissue Constructs

5.1 Introduction

In addition to establishing a robust protocol capable of producing uniform constructs reproducibly, significant hurdles remain with respect to commercial manufacturing of an engineered product. Transitioning the laboratory concept/methods into a well-characterized medical product/process is a significant challenge, commonly underestimated by researchers in tissue engineering and regenerative medicine fields. In addition to meeting regulatory requirements to ensure consistency and safety of any product, the manufacturing system must be scalable and cost-effective to be sufficiently economically viable to displace current treatment options. Addressing manufacturing issues related to quality control, cost-effectiveness, and large-scale production early in the research stage, can overcome problems that typically slow development, limit investment, and escalate costs limiting the clinical translation and availability of the treatment to patients in need.

5.2 Background/Motivation

Despite significant advancements in the field of tissue engineering, relatively few products have realized commercial success as tissue substitutes [22,102,103]. Several challenges still remain for translating tissue-engineering technologies from bench to bedside. In addition to demonstrating clinical effectiveness, cost-effective manufacturing processes are needed that comply with the current

quality and safety regulations [1,175]. Failure to adequately consider the likely cost of manufacturing early in the developmental stage has been recognized as a limiting factor for commercial success of technologies in the field [5]. Traditional manual laboratory tissue culture techniques are often not economical at large clinical scales and have inherent variability and contamination risks. However, due to their widespread use, simplicity, minimal development time, and low initial costs, these processes are still used to rapidly advance into clinical trials and the marketplace [24,38].

For example, Carticel™, recently acquired by Aastrom Biosciences, Inc. (Ann Arbor, MI), is an autologous cell transplantation product used to repair articular cartilage injures in the knee. Carticel™ is manufactured via manual techniques performed by trained technicians in a serologic clean room. Briefly, cells are isolated from the patient and expanded on tissue culture flasks to a sufficient number needed for therapeutic use [110]. This process requires a large number of manual labor-intensive manipulation steps. A manual process, though perhaps more feasible and economical on a small-scale during early process development, is generally regarded as high risk due to the increased potential for contamination [112,132]. Additionally, inherent differences in processing techniques between individuals, especially with technically challenging methods, can lead to process inconsistencies and end product variability [177]. Furthermore, as production demand increases, scale-up will require multiple manual processes to be performed in parallel, requiring additional technicians and generating substantial labor costs. As a result, the overall cost of production of such products tends to be high and can limit clinical success when the cost-benefit of the product is evaluated against competing and often simpler therapeutic strategies [133]. The risk of commercial failure can be greatly reduced by considering the economic viability of the product throughout the developmental process [176,178]. Automating manual tissue-culture processes through the use of bioreactor systems can provide a means to standardize the culture process, tightly control culture environment, remove user-dependent operation, and

establish a cost-effective tissue manufacturing process to meet large-scale clinical demand [24,175].

Automated bioreactors have long been used in tissue-engineering manufacturing and typically involve streamlining traditional 2D cell culture processes (cell selection, expansion, differentiation, etc.) [65,131,173]. While important, these cell manufacturing processes are often only the starting point for many tissue engineering strategies that utilize well characterized cell populations for tissue growth. Thus there is a need to foster automated bioreactor-based systems fit for the development of reproducible 3D engineered constructs. A closed, standardized, and operator-independent bioreactor system would have the potential to ensure safety and regulatory compliance and enable cost-effective, large-scale, *in vitro* tissue production [1,151].

Recently, Advanced Tissue Sciences developed an automated system for large scale manufacturing of their human fibroblast derived dermal substitute, Dermagrat™ (currently manufactured by Organogenesis, Inc. (Canton, MA)). Dermagrat™ consists of living cryopreserved allogeneic dermal fibroblasts seeded onto a bio-absorbable polyglactin mesh scaffold used for treatment of chronic skin wounds such as diabetic foot ulcers [109]. The entire manufacturing is performed in a closed bioreactor bag, eliminating user-dependent variability and shielding the culture process from risk of contamination. The bag also serves as a transport container. Following injection of cells into the system, the bioreactor is only externally manipulated until the graft is thawed and utilized in the operating room.

In addition to minimizing contamination risk, a closed bioreactor system can precisely control and maintain the tissue culture environment. Tissue growth and development is highly responsive to environmental factors (pH, temperature, nutrient concentration, etc.), and as such, the entire fabrication process is critical to the integrity of the final product and must maintain a high level of control to meet the rigorous current good manufacturing practice (CGMP) standards

required by the Food and Drug Administration (FDA) to ensure tissue safety and manufacturing consistency (Code of Federal Regulations, CFR 21).

The current BLB open manufacturing process is a labor-intensive one consisting of a multiple steps in an open-environment, to manually combine several tissue phases and form the multi-phasic graft. This labor-intensive process significantly limits the technician's BLB manufacturing capacity and is one of the greatest factors impacting cost of production with scale.

Current automated bioreactor systems for 3D tissue fabrication are product specific and/or not commercially available. As no bioreactor currently exists for the fabrication of our unique BLB construct in a single vessel, a novel bioreactor must be developed. As with current automated manufacturing systems, the bioreactor design should be user independent, only externally manipulated, sterile, and scalable. It must also recreate the unique multi-step formation process incorporating bone and ligament tissues engineered from distinctive cell populations into a single construct. As such, the current protocol developed in Chapter 3, consisting of Ficoll isolated cells, standardized passage density, and a novel pin-plate method for capturing spontaneous monolayer delamination, must first be modified as it still includes several technician dependent steps limiting the automation and scale of the process.

Firstly, the protocol for BLB fabrication described in Chapter 3 requires the simultaneous culture of bone and ligament monolayers. A trained technician, in a separate tissue culture plate, performs the combination of these distinct tissue types following their delamination. To facilitate formation of a single BLB construct within a single-closed vessel, the formation of the BLB construct must occur sequentially within the same chamber. Secondly, to engineer BLB constructs of sufficient size (>4 cm diameter) for use as an ACL graft replacement, at least four constructs must be manually transferred by a technician into a new plate and aligned in parallel to allow fusion of the grafts

with each other to form a single uniform construct. This labor-intensive step of the fabrication process must be eliminated to facilitate construct fabrication within a closed, hands-off bioreactor system. The utilization of larger tissue culture plates with increased surface area may allow for larger monolayers and resultant 3D construct diameters following delamination. Thirdly, for the sequential formation of bone and ligament tissue within a single vessel, the timing of cells introduced into both the bone and ligament fabrication process will have to be modified. To maintain a consistent starting cell population for tissue formation as determined in Chapter 3, bone and ligament cells must be expanded and cryogenically preserved at appropriate time points (passage 3 for ligament and passage 4 for bone). The efficacy of cryogenically recovered cells in forming a robust, self-delaminating monolayer and BLB construct has not been evaluated by our laboratory. The utilization of a cryogenically preserved allogeneic cell line will also allow for a consistent and well-characterized population of cells to be used for all experiments and will eliminate donor variability between tissues. Following these process changes, the BLB manufacturing protocol will be replicated in a closed, automated bioreactor system, resulting in a continuous multi-tissue constructs without any internal manipulation by the technician. As no such system currently exists, the goal of this study was to design, build, and test a novel automated bioreactor to fabricate a single ACL graft in a closed-system chamber.

To minimize contamination and technician variability, and to provide economy of scale, the bioreactor was designed to be closed, automated, modular, scalable, and to require minimal external manipulation. Bioreactor success was measured by the ability of the user to form a BLB construct without opening the bioreactor or manually manipulating the tissue. Bi-phasic structure of the construct was confirmed by chromosomal detection of bone cells (male) within expected areas of the construct. BLB construct structure and function were evaluated histologically (H&E, picrosirius red, alizarin red) and mechanically (tangent modulus, extensibility) at 1-week, post-3D construct formation. The histological

and mechanical properties of the current BLB fabrication process were used as the standards for comparison, since the current protocol described in Chapter 3 generates ACL grafts that effectively regenerate ligament *in vivo* (data not shown).

5.3 Significance

This study addresses the significant manufacturing and bioprocessing challenges inherent to the commercialization and translation of tissue engineered products from laboratory to clinic. In addition to demonstrating clinical efficacy and meeting regulatory standards, new tissue engineered products need to be cost-effective manufacturing processes to deliver the cost-benefit ratio needed to compete with alternative therapeutic options. Automated, closed bioreactor systems can provide the means for the development of standardized, cost-effective, and safe manufacturing of engineered tissues for clinical applications. Current bioreactor systems for 3D tissue fabrication are highly product-specific and often not commercially available. Therefore, a novel bioreactor design is required for sterile BLB graft fabrication and can fill an important knowledge gap in the field. The development of an automated manufacturing system during an early research stage has the potential to significantly lessen the technical, regulatory, and commercial barriers that tissue-engineering technologies are likely to encounter in the future pre-market stages. This development may also serve as a model or platform for other tissue systems or tissue-engineering technologies to streamline their associated laboratory processes into safe, reproducible, suitably scaled tissues for clinical studies.

5.4 Experimental Design

The development and design of a novel bioreactor culture system for closed, automated BLB manufacturing can be divided into two steps. The first step is to eliminate the manual steps associated with the current BLB fabrication processes. In particular, the user-dependent combination of separate bone and

ligament tissues into a single vessel and the fusion of multiple BLB constructs to achieve one construct with a diameter of suitable size for ACL reconstruction, must be eliminated. The second step is to design and validate a closed, automated, bioreactor system to recreate the adjusted manufacturing protocol.

Process methodologies were performed utilizing ovine-derived cell populations due to the large amount of knowledge associated with their ability to form a multi-phasic BLB construct. To eliminate timing issues associated with the sequential formation of multiple tissues, cryopreserved cell populations were used to form multi-phasic BLB constructs. Male and female cell populations were used to make bone and ligament tissues, respectively, to confirm the co-culturing of multiple tissue types following construct formation.

5.5 Step 1: Elimination of Manual BLB Manufacturing Processes

Previously described methods for BLB fabrication require the simultaneous culture of bone and ligament monolayers in separate culture dishes. Forming the actual multi-phasic BLB graft requires the timed, manual transfer of two 3D bone constructs onto a confluent ligament monolayer prior to the monolayer's delamination. The delicate timing and difficulty associated with manually performing this process make it difficult to replicate in a closed bioreactor design. The sequential preparation of bone and ligament tissues in a single culture vessel would greatly eliminate the technical complexities of this process and simplify the bioreactor design. However, the ability to form a confluent, spontaneously delaminating ligament monolayer from a single fibrogenic cell suspension while in the presence of pre-formed bone constructs had not been evaluated by anyone to the best of our knowledge.

The current process of BLB construct fabrication requires the manual combination and fusion of multiple 3D BLB constructs to form a construct of suitable diameter for use as a graft in ACL reconstruction. Again, from a design

perspective, it would be advantageous to eliminate this manual combination step and fabricate a single construct of sufficient size for implantation within a single vessel. The inclusion of these protocol changes to the current BLB fabrication process will simplify the design of a closed, “hands-off” bioreactor system.

5.6 Methods

5.6.1 Isolation of MSCs

Bone marrow was aspirated from the iliac crest of sheep using a Monoject Illinois needle (Sherwood Medical Company, St. Louis, Mo) with the animal under general anesthesia induced by intravenous propofol and sustained with inhalation of isoflurane in oxygen. A minimum of 15 ml of bone marrow volume was collected using heparinized needles and dispensed into EDTA blood collection tubes (BD, San Jose, Ca.) for processing.

The marrow was filtered through a 100 mm filter to remove solid debris and consolidated into a single 50 ml conical. An equivalent volume of Dulbecco’s Phosphate-Buffered Saline (DPBS) pH 7.2 (Gibco BRL Cat# 14190-144) was added. The marrow solution was slowly added to a 15 ml layer of Ficoll-Paque Premium (GE Healthcare, Munich, Germany) contained within a separate conical and centrifuged (AccuSpin FR; Beckman Coulter Inc., Fullerton, CA) at 600 g for 30 minutes at 25°C.

The upper layer containing plasma and platelets was discarded, and mononuclear cell layers containing the MSC population were transferred into a new sterile conical. The cells were suspended in at least three times their volume of DPBS and centrifuged at 500 g for 10 minutes. The supernatant was removed, and an equivalent volume of ACK lysis buffer was added to the pellet volume, lysing any remaining red blood cells. The conical was filled with DPBS and centrifuged at 400 g for 5 min. The supernatant was again removed, and the MSC pellet was re-suspended in 20 ml of growth medium (GM; DMEM

supplemented with 20% FBS and 2% ABAM). Cells were counted utilizing a Countess automated counting system and immediately plated at a density of 40,000 cells/cm^2 in a 150 mm tissue culture dish.

5.6.2 Expansion and Cryopreservation of MSCs

The adherent cell population was allowed to attach for 3 days before the plate was rinsed with DPBS to remove any remaining debris or contaminating non-adherent cell populations. Following plating, cells were immediately cultured towards either an osteogenic or ligamentous lineages. Osteogenic growth medium consisted of GM supplemented with 600 ng/ml basic fibroblast growth factor (bFGF; Peprotech), and 400 ng/ml dexamethasone (dex; Sigma-Aldrich). Ligamentous growth medium consisted of GM supplemented with only bFGF. Plates were fed either bone or ligament medium every other day. At approximately 50% confluence, the plate-adherent MSC populations were trypsinized (trypsin-0.25% EDTA), combined into a single conical, and passaged at a density of 5,000 cells/cm^2 every other day. Following passage three, ligamentous derived MSCs (ligament cells) were trypsinized and cryogenically preserved. MSCs induced to an osteogenic lineage (bone cells) were passaged and cryopreserved after passage four. Cells were cryogenically preserved at a concentration of $5x10^6$ cells/ml in GM+10% DMSO (Sigma-Aldrige). One ml volumes were aliquoted into 2 ml cryovials (Nalgene) and slowly frozen (approximately 1°C/hr) overnight to -80°C. The vial was then transferred into a liquid nitrogen freezer for long-term storage.

5.6.3 Thawing and Plating of Cells

As needed, cells were removed from liquid nitrogen storage and placed in a 37°C water bath. Immediately after the medium turned to liquid, the entire volume of cells and medium was transferred to a sterile 15 ml conical containing at least 3 times their volume of warmed GM. The cell suspension was centrifuged at 1500 rpm for 5 min at 37°C. The supernatant was aspirated and remaining cells were re-suspended in fresh GM and counted. Cell viability was assessed with trypan

blue dye (Life Technologies). Recovered cells utilized for tissue formation contained greater than 90% viable cells. Cells were seeded onto sterile polystyrene tissue culture plates at a viable cell density of 21,000 cells/cm^2. Bone plates were fed GM supplemented with 400 ng/ml dex, 13 mg/ml ascorbic acid, 5 mg/ml L-proline, and 600 ng/ml bFGF. The ligament medium was similar to the GM, lacking only the dex.

5.6.4 Preparation of Bone Constructs

Bone cells were first seeded onto 8-well rectangular tissue culture treated polystyrene plates (NUNC Plastics) modified with two metal posts aligned longitudinally and centered within the plate 15 mm apart (Figure 5.1A). Medium was changed every 2-3 days. Cells became confluent after approximately 12 days. After 5 days in culture, the dishes had become hyper-confluent, forming a monolayer sheet consisting of cells and cell-generated ECM. At this time, the medium was switched to differentiation medium (DM; supplemented with 7% HS and 2% ABAM) supplemented with 10µl/ml dex, 10µl/ml ascorbic acid/proline, and 20µl/ml TGF-B. After approximately 1-2 days in culture, spontaneous de-lamination of the monolayer occurred. The capturing of the shrinking monolayer between the two constraining posts formed 3D cylindrical bone constructs.

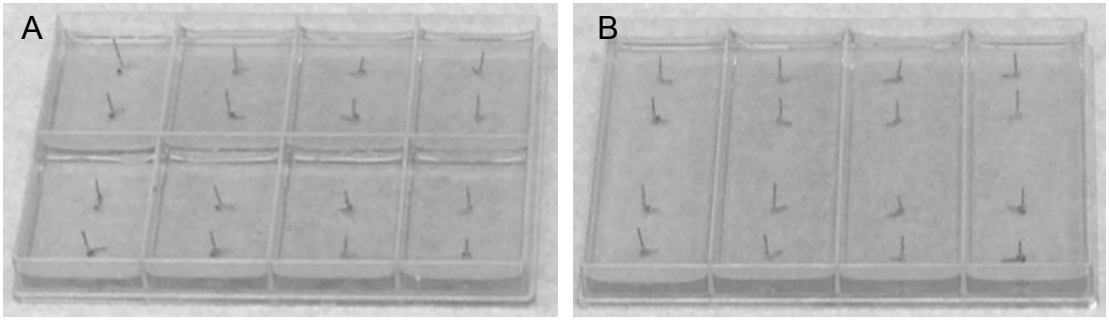

Figure 5.1 Custom Pin Plates A) 8-well Bone Plate, and B) 4-well Ligament Plate. The locations of the posts were precisely aligned between the bone and ligament plates, facilitating the efficient transfer of uniform bone constructs onto ligament plates.

5.6.5 Preparation of Ligament Culture Plates

Bone constructs were transferred at fixed length onto identical post locations in a sterile 4 well-rectangular tissue culture treated polystyrene plate (NUNC Plastics)

(Figure 5.1B). The arrangement of the wells identically matched to 8-well bone plates to ensure each ligament well had two bone constructs separated by a 30 mm distance centered along the long axis of the well. Ligament cells were seeded into each well at a density of 21,000 cells/cm^2. Cells became confluent within 1-2 days and formed a hyper-confluent robust monolayer after 8 days in culture. Cells were fed ligament GM every 2-3 days. After 8 days, the medium was switched to ligament DM that induced the spontaneous delamination of the monolayer within 3-5 days.

5.7 Results

5.7.1 Sequential Formation of BLB Constructs Within Single Vessels

Monolayers derived from both bone and ligament cryopreserved MSC lineages successfully formed and spontaneously delaminated, demonstrating the ability of cryogenically preserved cells to form BLB grafts. Additionally, seeding of ligament cells following transfer of bone constructs to the ligament culture surface did not interfere with ligament monolayer formation and resulted in the successful co-culture of ligament and bone required for BLB formation. The delaminating ligament monolayers fully surrounded the bone constructs, capturing them within the newly formed BLB construct (Figure 5.2). The diameter of the ligament region was noticeably thin (0.3$\pm$0.1 mm, n=5) with approximately half of the constructs failing in the ligament mid-substance after 2 weeks. The results demonstrate the ability to form a BLB sequentially in the same dish by first adding bone constructs and then seeding ligament cells.

Figure 5.2 BLB Delamination. Bone regions were captured and surrounded by delaminating ligament monolayer. The culture surface for each of the 4 wells is 21.8 cm^2.

5.7.2 Formation of Large Diameter Tissue Constructs

Larger pin plates were fabricated utilizing 150 mm tissue culture plates, with a culture surface area of 182 cm^2, and two metal posts located 50mm apart centered and aligned uni-axially. As a control, 100 mm pin-plates, with a culture surface area of 82 cm^2, were also fabricated as described in Chapter 3. Plates were UV treated for at least 1 hour, sprayed with 70% ETOH, and rinsed with approximately 20 ml DPBS prior to use. Ligament cells were seeded onto 100 mm and 150 mm pin-plates and grown into a confluent monolayer, and spontaneously delaminated into a 3D construct. Construct diameters were compared at a one-week time point following delamination, as shown in Figure 5.3. The 100 mm pin-plate formed a construct approximately 2 mm in diameter (n=3) while constructs fabricated in the 150 mm pin-plates formed constructs about 5 mm in diameter (n=3). Pin locations were identical in each of the plates.

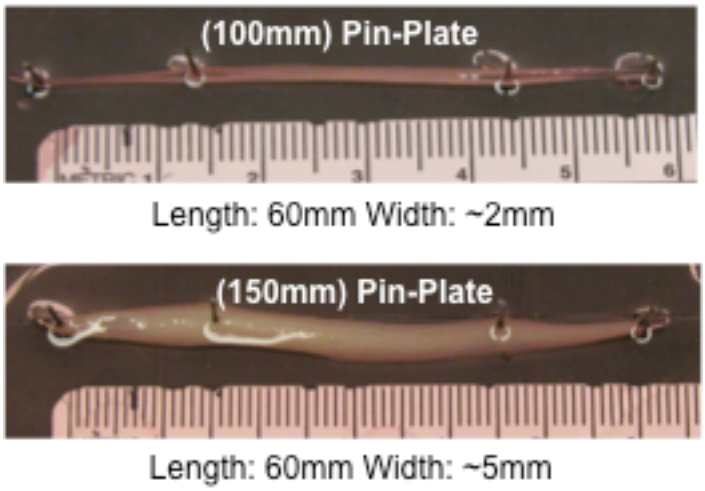

Figure 5.3 Pin Plate Construct 1 Week Post Delamination. Top: Construct fabricated on 100 mm plate. Bottom: Construct fabricated on 150 mm plate

5.8 Discussion

Adding ligament derived MSCs to individual wells, containing strategically placed pre-formed 3D bone constructs, formed a BLB construct. This is in sharp contrast to previous methodologies that require the combination of 3D bone constructs onto confluent ligament monolayers to form the multi-phasic tissue. The results demonstrate the feasibility of forming BLB constructs within a single well by sequentially seeding cryogenically preserved bone and ligament cells. This process adaptation eliminates the need for technicians to combine bone and ligament tissues to form a BLB. As cells instead of 3D tissues are input into the system, the process can easily be performed sterilely. The elimination of technician dependent steps allows for the process to be automated and performed in a closed system, which is essential for use within a bioreactor.

The use of cryogenically preserved allogeneic cells also allows for large-scale expansion of cells that can be well characterized and used as needed for graft fabrication. This is a significant advantage for process scalability compared to fresh cells, as the starting cell population can be screened and evaluated before investing time and resources into large volume construct production. The regulatory perspective requires a well-defined starting cell population. Utilization

of allogeneic cells has the advantage of performing this characterization only once. Autogenic cells must be characterized for each donor significantly increasing the economy of scale and limiting the commercialization potential.

The fabrication of larger diameter grafts formed on the 150 mm plates compared to 100 mm plates reveals the ability to control graft size through the manipulation of culture surface area. This process eliminates the need for manual fusion of multiple constructs by a technician, again, a technician-dependent step that can impede the development of efficient, automated manufacturing processes, suitable for bioreactor incorporation. Further evaluation of the change of construct diameter, passive construct tension, and tissue mechanics must be evaluated further. The described methods demonstrate essential protocol adaptations that were needed to facilitate fabrication of BLB constructs within single well, closed, bioreactor systems. The following sections will describe the development of that system.

5.9 Step 2: Bioreactor Development

5.9.1 Bioreactor Design

Following the removal of user-dependent steps from the fabrication process, the end multi-phasic tissue graft must be replicated within a closed bioreactor system. As no current bioreactor system exists, a novel device must be designed, fabricated, and tested to confirm that a viable multi-phasic BLB graft can be fabricated by user-independent methods within a closed system. The bioreactor device shown in Figure 5.4 below was designed based on the following design elements and performance requirements.

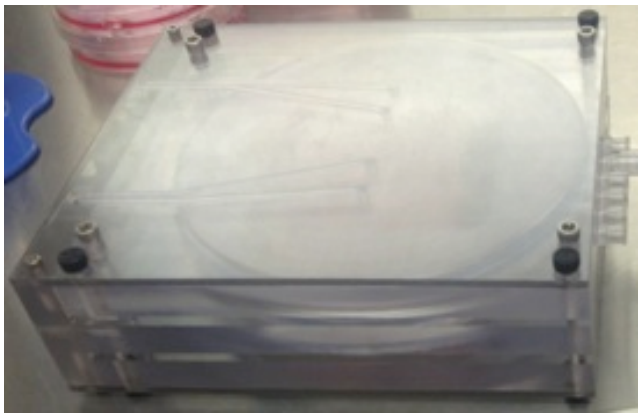

Figure 5.4 Flip Plate Bioreactor System. Approximate dimensions are 7 in x 6 in x 2 inches.

5.9.2 Bioreactor Design Criteria

- Minimizes Contamination Risk
    - Closed system – completely "hands-off" internal manipulation, beginning with the injection of starting material and ending with final construct formation
    - Potential for inline monitoring and media sampling
    - Container suitable for construct preservation, packaging, and shipping
    - Consists of FDA compliant materials that are capable of being easily sterilized (autoclavable, ethylene oxide)
        - Or the use of disposable elements that can be replaced if they come into contact with cell, media, or wastes
- Eliminates Manual, User-Dependent Processes
    - Automated – capable of being controlled without no reliance on a technician
    - Only external manipulation
        - Eliminates user variability and construct consistency
    - Simple to use, easy to operate, and the construct is exposed only when needed for patient use
- Scales Economically
    - Automated – reduce manufacturing time and increase capacity

- Modular – capable of incorporating multiple cartridges into larger centrally controlled unit
- Small - Relatively small overall volume to minimize required space.

5.9.3 Performance Requirements of Bioreactor

- Replicate Current Self-delaminating BLB Fabrication Process
  - Cells, media, nutrients can be added and waste removed on a regular basis
  - As suture will be primary method of introducing during ACL repair surgery, suture must be made available and easily integrated into construct.
- Form a Continuous Multi-phasic BLB Construct within a Single Device

5.9.4 Cell-Culture for Use in Bioreactor

Bone and ligament MSC populations were isolated, expanded, and cryogenically preserved as described in section 5.6. For use within the bioreactor, bone cells were fabricated from male ovine bone marrow while ligament cells were derived from female ovine bone marrow. The use of gender-specific cell populations allowed for identification of male cell migration between bone and ligament regions and verification of co-culturing of two distinct cell populations within a single BLB graft.

5.9.5 Flip-Plate Bioreactor Design Summary

The final bioreactor design, termed a “Flip-Plate”, consists of an enclosed chamber, multiple monolayer growth modules, a suture capture system for constraining the monolayers during delamination and maturation, and a mechanism for enabling tissue co-culturing through magnetic translation of tissue. The Flip-Plate bioreactor can be used for the fabrication and co-culture of multiple tissue types. As an example, the use of this device for the creation of a BLB construct will be described.

BLB constructs are made from MSCs differentiated to osteogenic and fibrogenic lineages and integrated within the bioreactor to form a continuous multi-tissue construct with sufficient structural integrity and mechanical compliance to withstand physiological loading when used as a graft for ACL repair without the inclusion of exogenous scaffolding. As the culture surface of the bioreactor could not be visualized under a microscope, ligament only and bone only constructs were fabricated on 100 mm and 60 mm pin plates, respectively, and used as process controls. BLB constructs formed within the bioreactor were evaluated histologically and mechanically and compared to manually fabricated bone and ligament tissues. The details of one or more aspects of the Flip-Plate device are described in the accompanying drawings and descriptions below. Other features, objectives, and advantages of the invention will be apparent from the detailed description and drawings.

5.9.6 Detailed Flip-Plate Design and Description of Use

Referring to Figure 5.5, cell differentiation, monolayer growth, capturing, and co-culturing required to make the BLB are accomplished in **bioreactor 40**. Though this bioreactor is designed for the fabrication of scaffold-free BLB tissue constructs, other cell types (i.e. muscle, nerve, etc.) consisting of spontaneously or substrate controlled tissue monolayer delamination can be used. Current cell culture bioreactors are for the most part designed for non-adherent cell suspensions or expansions of cells [131,146,173]. These devices do not provide the means of capturing and co-culturing delaminated monolayers of multiple tissue types that are required for the formation of the multi-phasic BLBs.

Bone monolayer growth is carried out in **module 1**, located and sealed into **part 25** of **bioreactor 40**. **Module 1** may be segmented into individual **wells 88** to form multiple monolayers of various shapes and sizes by the addition of silicone **barriers 99** to the **culture substrate 11**. Other barrier materials such as Teflon that do not allow for significant cell adhesion may also be used. **Bioreactor 40**

includes manual or automatic translation elements designed to facilitate bone monolayer capture (**suture 22**) and transfer into co-culture (**component 3)**. Manipulation of **suture 22** arrangements though **culture substrate 11** and tension (controlled via **component 3**) can be used to control construct length and graft tension within delaminated constructs. During bone monolayer formation, MSCs are seeded onto **culture substrate 11** of **module 1**, which preferably consists of a sterile polystyrene culture surface coated with or without cell adhesion proteins such as laminin.

Media exchange of **module 1** is controlled manually with sterile injection of media in an open-environment or automatically with perfused media. The **connecting plate 26** contains **fittings 5** designed to add and remove media contained in each segmented well of **module 1**. MSCs of the bone monolayer growth process contained in **module 1** are seeded at an initial density of approximately 21,000 cells/cm^2. Seeding density may not be critical to the success of this invention, affecting only rate of monolayer formation.

Cells proliferate after seeding, forming a monolayer, and differentiate towards an osteogenic lineage. While additional serum-containing cell culture media and growth factors may be used, a preferred growth medium to optimize cell proliferation and promote robust osteogenic ECM production consists of DMEM supplemented with 20% fetal bovine serum and antibiotics, along with the addition of dex, FGF-b, and ascorbic acid/ L-proline. Growth conditions that must be maintained in **module 1** include a pH of about 7.4, a medium temperature of 37°C, and a sterile air environment consisting of up to 20% O_2. The medium must be exchanged at sufficient rate and volume to prevent depletion of critical media constituents by the growing cells; preferably 50% replaced every two days.

In reference to Figure 5.6, following sufficient ECM matrix production by the seeded cells, a confluent **bone monolayer 9** is formed on the **culture substrate 11** after approximately 5 days at the described seeding density (Figure 5.6A).

Growth-promoting medium is replaced with differentiation medium consisting of DMEM, supplemented with 7% horse serum, antibiotic, transforming growth factor-beta (TGF-b), ascorbic acid / L-proline, and dex to induce cell differentiation, integration, and passive tension that leads to subsequent spontaneous delamination of confluent tissue monolayer. **Bone monolayer 9** delamination within **module 1** is captured on **sutures 22,** forming a 3D **bone construct 10** as shown in Figure 5.6B. **Sutures 22** transverse **modules 1 and 2** and are held in tension by anchoring **spools 7 (**shown in Figure 5.7). The **bone constructs 10** are allowed to mature on **suture 22**; the tissue continues to contract and reorganize the ECM structure while constrained under tension. This maturation phase occurs over approximately 2 days. However longer or shorter times are possible. To facilitate translation and co-culture of the **bone constructs 10**, the **bioreactor 40** is inverted (Figure 5.6C). Following the release of tension in the **sutures 22** by loosening the **anchoring spools 7**, both bone constructs are translated to **ligament culture substrate 20** in **module 2** and secured within **part 32** (Figure 5.6D). Manual or automated translation of the suture via **magnets 8** contained within **component 3** facilitates this transfer (Figure 5.7)**.** In reference to Figure 5.7, tension is re-established in **sutures 22** (not shown) by pulling the **magnets 8** after the anchoring **spool 7** has been re-tightened.

The **sutures 22** required for translation reside within tubes (not shown) used to minimize sharp edges and friction during translation. These tubes reside in **grooves 16** of **parts 25 and 32.** The grooves align the sutures to ensure uniaxial insertion across **modules 1 and 2** and locate insertion into **component 3** to interface with the **anchoring spools 7** and **magnets 8**. Sliding grooves for **magnets 8** are located in **part 37**. **Plates 34 and 35** secure the tubing into the **grooves 16** and anchor **parts 25 and 32** to **component 3,** attached to **connecting plate 26.**

Following translation of bone constructs, MSCs are seeded onto the **ligament culture substrate 20** of **module 2** at an initial density of approximately 21,000 cells/cm^2. The osteogenic medium is replaced with ligament growth medium to promote fibroblastic differentiation and production of ligamentous ECM. This process requires approximately 8 days in culture. The ligamentous medium consists of DMEM supplemented with 20% fetal bovine serum and antibiotics, along with the addition of FGF-b, and ascorbic acid/ L-proline. Ligament medium is exchanged via **fittings 5** attached to the **connecting plate 26**, at 50% of volume every 2 days. Environmental conditions required for ligament growth within **module 2** are identical to **module 1**.

Following formation of a **ligament monolayer 55** upon the ligament **culture substrate 20** (Figure 5.8A), the medium is switched to differentiation medium to further induce matrix production and cell-matrix tension. The ligamentous differentiation medium is composed of DMEM, supplemented with 7% horse serum, antibiotic, transforming growth factor-beta (TGF-b), and ascorbic acid / L-proline. As the **ligament monolayer 55** spontaneously delaminates, **sutures 22** capture it, surrounding the **bone constructs 10** on **substrate 20**. The end result is a multi-phasic **BLB construct 50** that continues to mature (remodel, condense, and develop ECM) over time in culture (Figure 5.8B). This maturation phase requires approximately 1 week, although shorter and longer periods are possible.

The resulting BLB construct can be grafted into the patient at this point or if desired, further conditioned mechanically through the physical manipulation of **sutures 22**. If implanted, the incorporated sutures may be utilized to secure the graft into the patient during the surgical procedure. It is preferable that a fresh BLB construct be used within 3 weeks following formation, as cells and appropriate graft tension are difficult to maintain in culture for extended periods of times. Alternatively, freezing, acellularizing, or other means of preservation may be used to preserve the construct. As will be understood by those skilled in the

art, a skilled practitioner may make many changes in the apparatus described above without departing from the spirit or scope of the device.

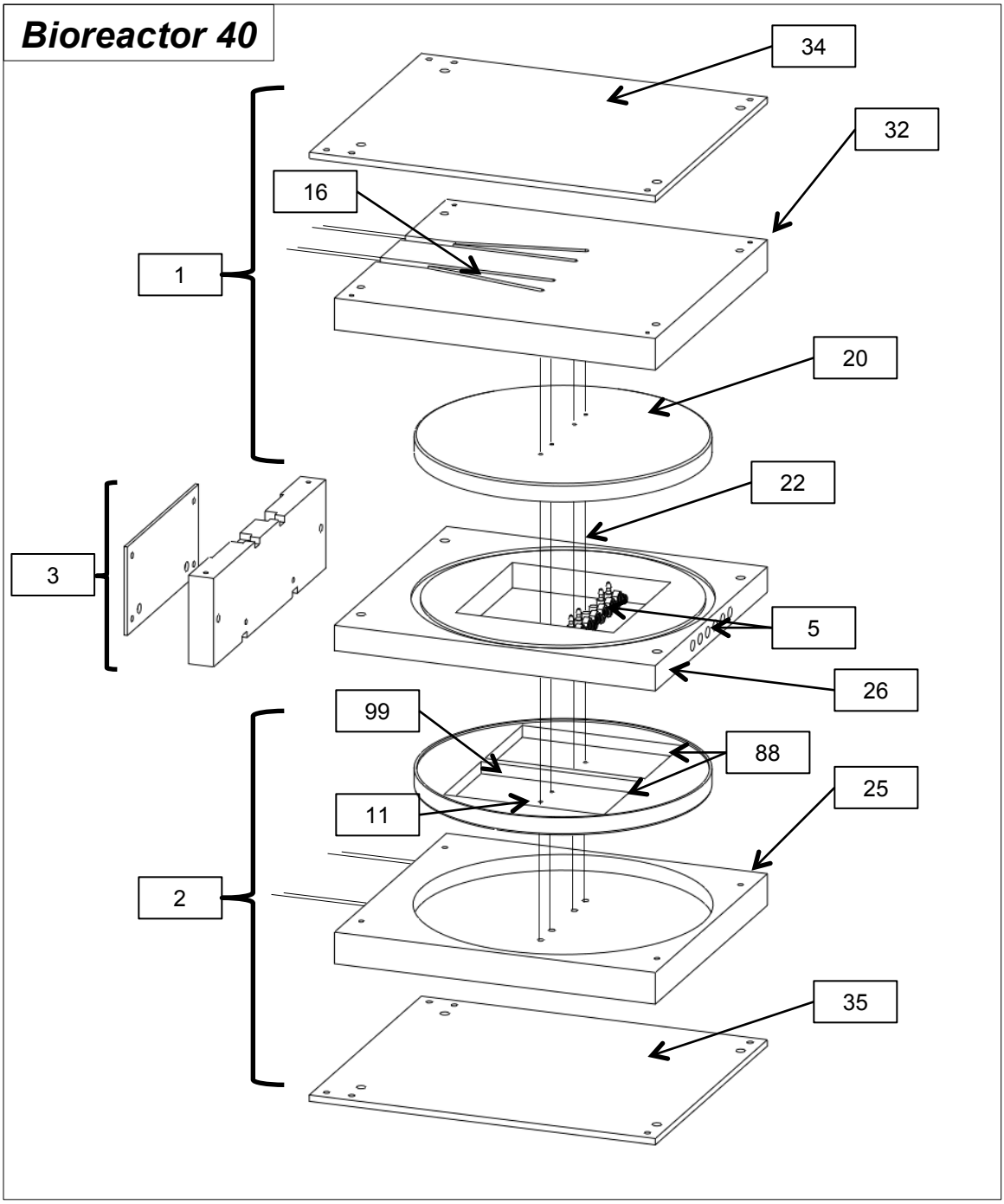

Figure 5.5 Exploded view of the Flip-Plate bioreactor design

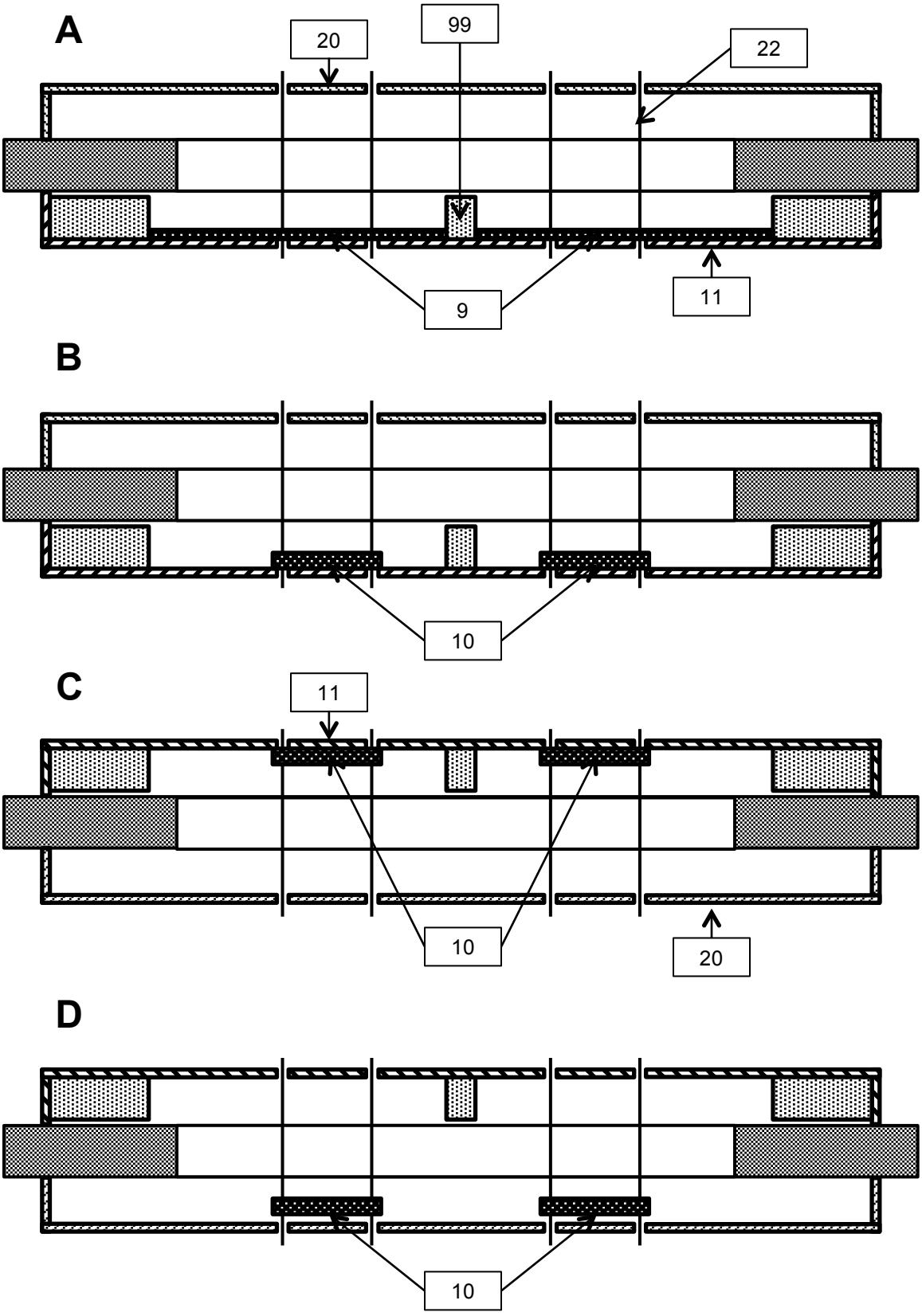

Figure 5.6 Translation of bone constructs within Flip Plate bioreactor. Diagrams A, B, C, and D are cross-sectional views that show the capturing and co-culture process.

Component 3

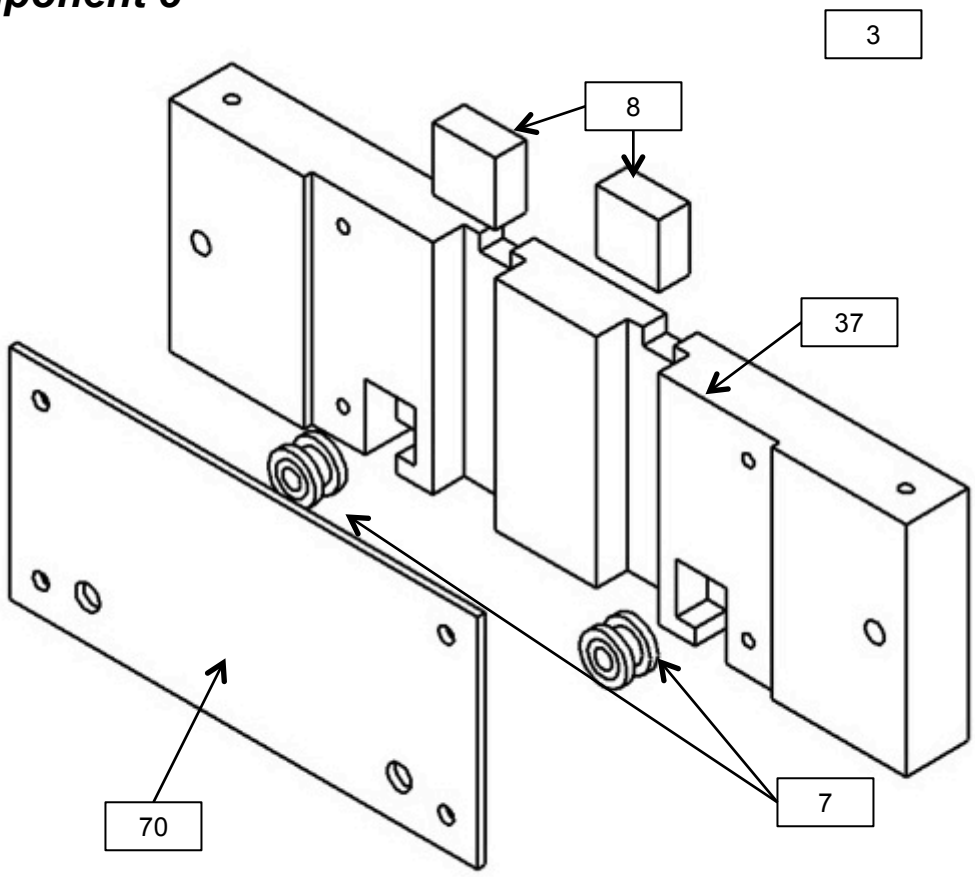

Figure 5.7 Mechanism for tissue translations of the Flip-Plate device shown in a perspective view. Shown as component 3 of Figure 5.5.

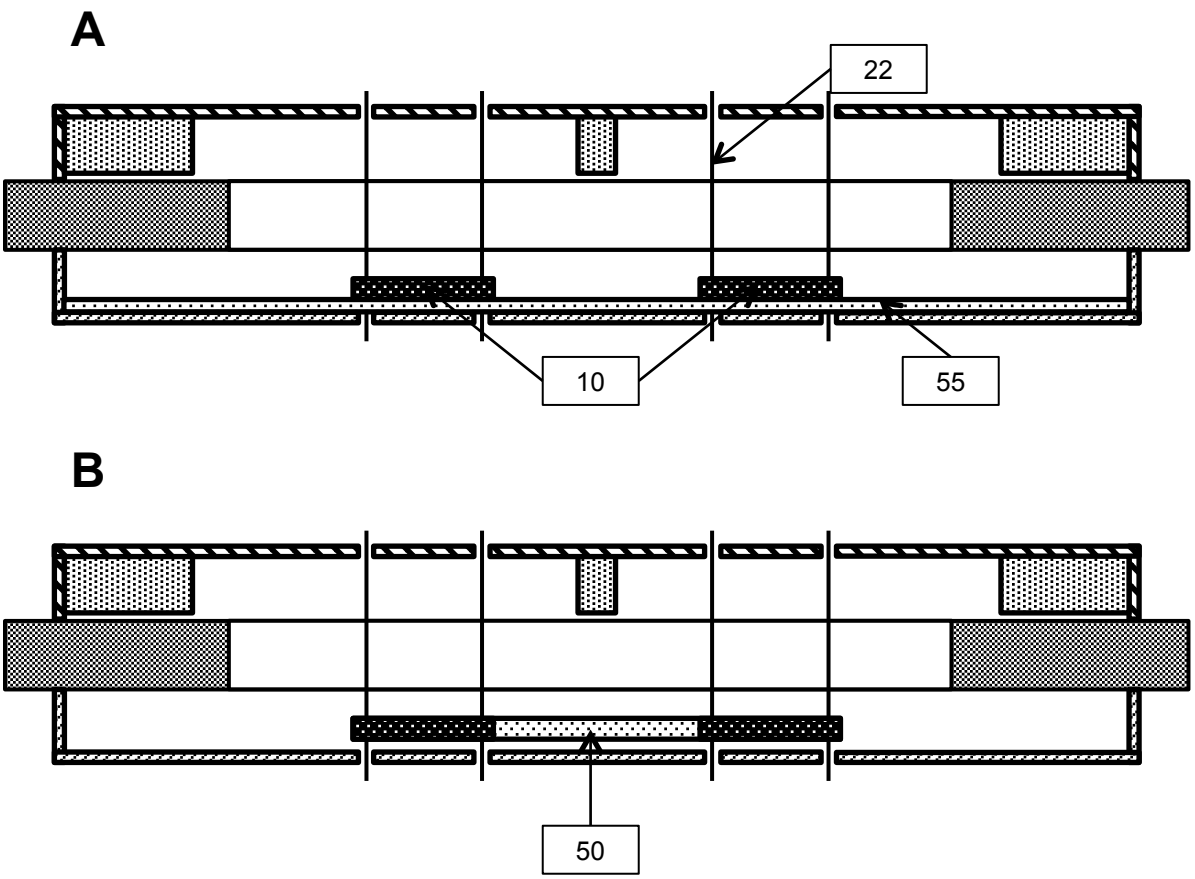

Figure 5.8 Formation of BLB construct within the Flip-Plate bioreactor. Diagrams A and B are cross-sectional views of the BLB captured on suture constraints.

5.10 Construct Evaluation Methodologies

Following successful construct formation, constructs were removed from the bioreactor and evaluated as described below:

5.10.1 Mechanical Testing

Following delamination of the ligament monolayer, the BLB constructs were allowed to fuse, forming a uniform cylindrical construct constrained between the tensioned sutures. Upon removal of the construct from the bioreactor, separate parts of the construct were allocated for mechanics or histological and molecular biology analysis. Approximately half of bone/ligament complex was taken for histology and molecular biology. The rest was attached to a custom-built tensile tester and submerged in DPBS for subsequent tensile testing. The testing set-up can be seen in Figure 5.9. Constructs were secured using custom Velcro grips and incrementally lengthened to approximate the original length within the reactor. Sixty-micron beads were painted onto the surface of the tissue for post analysis digital image correlation to extrapolate the tissue-level strain during testing. The construct was pulled until failure at a rate of 0.01 /sec. Load and strain at failure was recorded. Figure 5.9 is an image of the described testing set-up of the ligament region of the BLB construct. The missing bone region on the right, shown by lack of suture, indicates the region removed for PCR analysis.

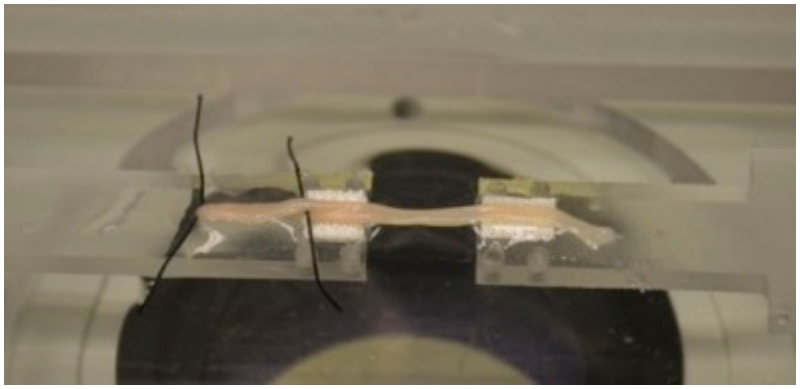

Figure 5.9 BLB on tensile testing set-up

5.10.2 Histological Analysis

For staining, unfixed samples were placed into TBS medium (Triangle Biological Sciences), frozen in cold isopentane, and stored at -80°C until needed. Fixed samples were placed in 4% paraformaldehyde (PFA) for 1 hour. The samples were then placed into 15% sucrose solution for 1 hr at 4°C and then overnight (>12 hrs) in 30% sucrose solution also at 4°C. The constructs were then transferred into TBS medium and frozen over dry ice and stored at -80°C until needed. Samples were cut to obtain cross and longitudinal sections with a cryostat at a thickness of 12 µm, adhered to Superfrost Plus microscopy slides, and used for staining. Sections were stained for general morphology observations with hematoxylin and eosin (H&E). Mineral content of the tissue was determined via alizarin red staining (Sigma), and collagen alignment with picro-sirius red stain.

5.10.3 PCR Analysis – Y Chromosome

Genomic DNA was isolated from respective bone and ligament regions of the BLB tissue samples by proteinase K digestion followed by ethanol precipitation. A PCR-based assay for the ovine-specific Y-chromosome repeat sequence Ucd043 was used to determine the presence of male cells in BLB explant samples [73]. Duplex PCR was performed using SCUcd043.FWD/SCUcd043. REV primers to amplify Ucd043 together with P1- 5EZ/P2-3EZ primers to amplify the ZFY/ZFX locus. P1-5EZ and P2-3EZ primers also provided an internal control for amplification. Sensitivity of the assay was assessed with a dilution panel of 100, 25, and 5 pg of male ovine DNA. Subsequent experimental reactions were carried out with 25 ng of genomic DNA template.

5.11 Results

5.11.1 Flip-Plate Construct Formation

The ability of the Flip-Plate bioreactor to successfully produce a BLB construct without user-dependent manipulation has been demonstrated using the

bioreactor and processes detailed above. Briefly, MSCs induced towards an osteogenic lineage were sterilely delivered into individual wells within module 1 of the device and fed nutrients and growth factors specific to bone formation. A bone monolayer is formed, and as it self-delaminated, a constraint system guided its formation into two 3D cylindrical bone constructs (Figure 5.10A).

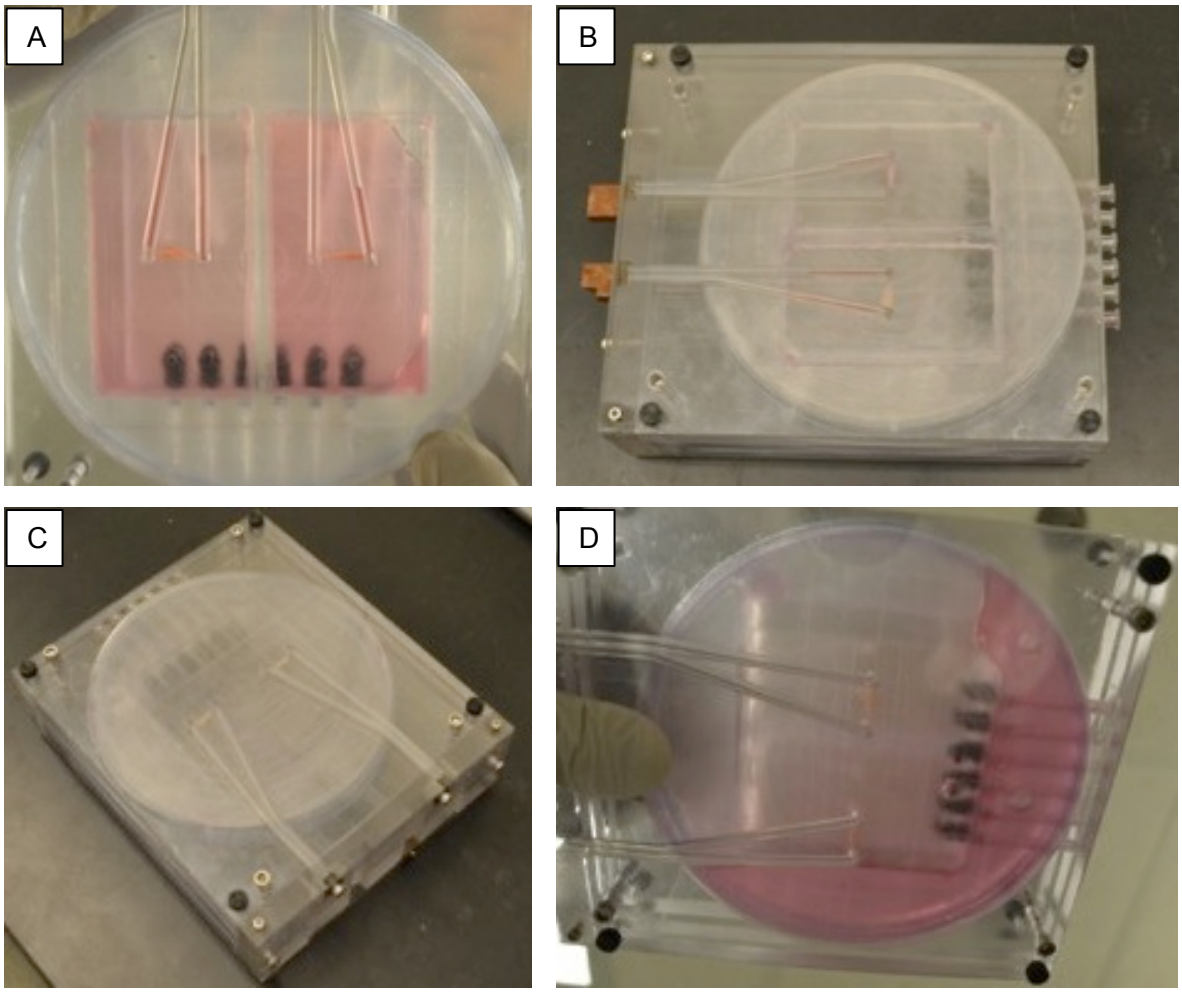

Figure 5.10 Translation of Bone Constructs in Flip-Plate Bioreactor A) Capturing of bone constructs, B) Inversion of device, C) Translation of constructs followed by subsequent, and D) seeding of ligament cells. As a reference, dimensions of bioreactor device are 7 x 6 x 2 inches.

Following formation of bone constructs in module 1, the bioreactor cartridge was inverted, and the bone constructs were translated via magnets along guides to the adjacent unseeded culture surface (Figure 5.10 B, C). Additional MSCs induced towards ligamentous lineage were added to the culture surface (Figure 5.10D), fed nutrients and fibrogenic growth factors, and grown to confluence,

forming a ligament monolayer. At confluence, the ligament monolayer delaminated from the substrate, surrounded the bone constructs (Figure 5.11A), and formed a bone-ligament-bone construct that could be removed from the bioreactor and utilized as an ACL graft (Figure 5.11 B, C).

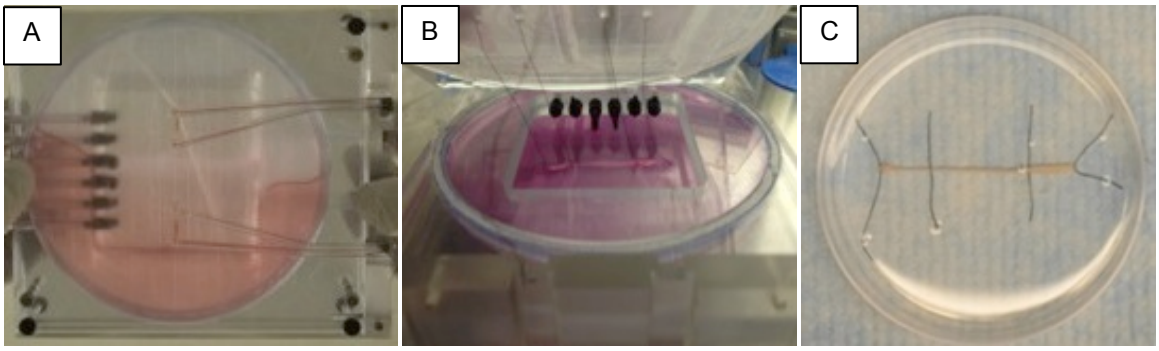

Figure 5.11 Formation of BLB construct within Bioreactor. A) Delamination of ligament, B) Captured BLB construct shown with device opened, and C) BLB construct after removal from bioreactor and placed into separate dish. As a reference, construct length is 6 cm for each image.

5.12 Construct Validation

5.12.1 Mechanics

The ligament region of bioreactor BLB constructs and ligament only controls were mechanically tested until failure at one week following formation. Stress vs. strain data are shown in Figure 5.12. Ligament constructs, formed with the manual process of Aim 2, had a modulus of 0.38±0.12 MPa (n=3) at a physiological strain range of 0.05-0.07. Bioreactor constructs were similar, with an average tissue modulus of 0.32±0.11 MPa (n=3). The mechanics of the bone regions were not evaluated. The relative standard deviation within each group was similar to that reported in Chapter 3, approximately 30%. The diameter of the bioreactor constructs were 1.4±0.6 mm for BLBs (n=3) and 0.91±0.03 mm for ligament only constructs captured on pin-plates (n=3).

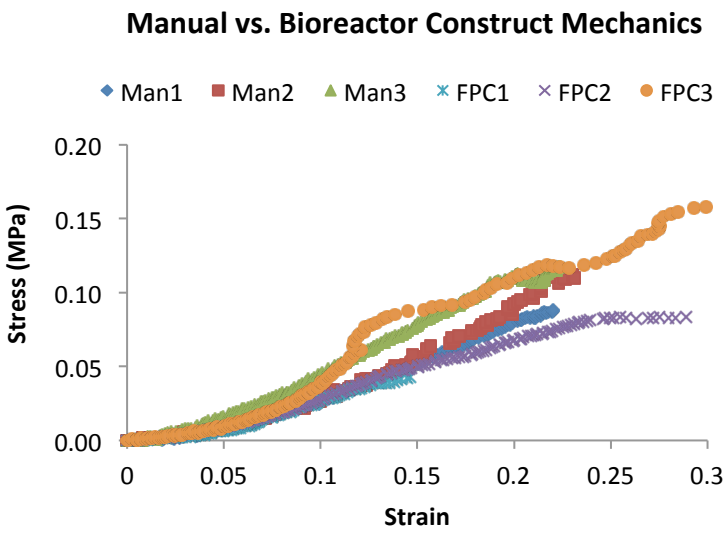

Figure 5.12 Failure Stress-Strain Data of Manual vs. Bioreactor Formed Constructs. Strains are until failure of ligament region of the BLB construct.

5.12.2 Histology

Alizarin red staining shows mineral nodules within the bone regions of the graft that were absent from the ligament region. This was evidence of a bi-modal tissue distribution within the BLB graft (Figure 5.13 A-C). Mineralization was comparable to bone and ligament constructs cultured seperately in osteogenic and fibrogenic media, respectively, demonstrating a capacity of the tissue to maintain a differentiated state while in co-culture. The construct was composed of primarily type 1 collagen and contained viable nuclei thoughout (Figure 5.13 D-F).

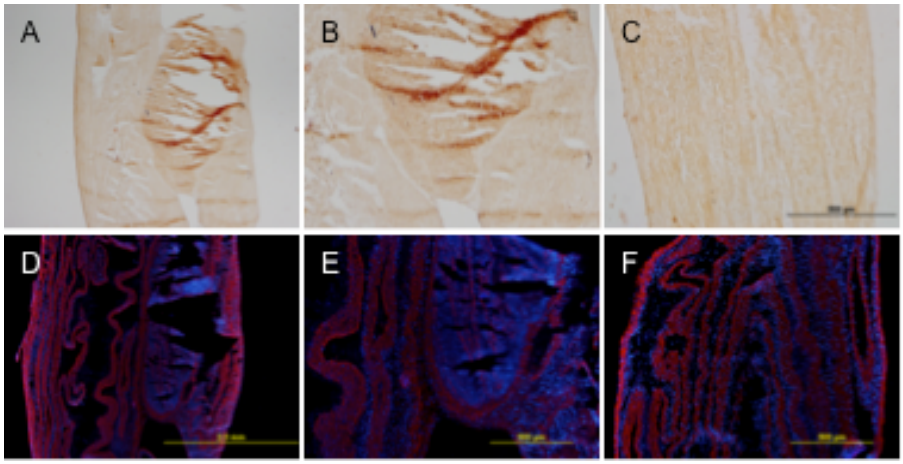

Figure 5.13 Histological Staining of Bioreactor fabrication BLB Constructs A) Alizarin staining of bone region (X4), B) Alizarin staining of bone region (X20), C) Alizarin staining of ligament region, D) Col-1/DAPI of bone region (X4), E) Col-1/DAPI of bone region (X20), and F) Col-1/DAPI of ligament region.

5.12.3 PCR

The PCR analysis demonstrates that co-culture of multiple tissues within a continuous tissue construct was successful. Male Y chromosome was detected in only the bone regions of the construct (Figure 5.14). Female tissue was detected throughout the construct and most highly expressed in the central ligament region (n=2). Both bone and ligament regions contained significant amounts of DNA.

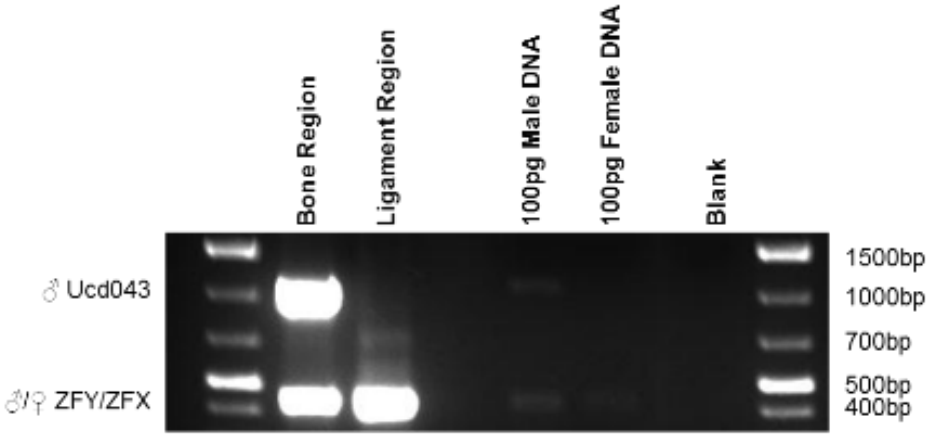

Figure 5.14 PCR Data of Bioreactor Formed BLB Constructs. Bone regions were positive for male cell DNA while ligament regions comprised of female cells were not.

5.13 Discussion

5.13.1 Design Elements

The Flip-Plate bioreactor design successfully meets all previously described design criteria.

Minimize Contamination Risk

The Flip-Plate is designed to be a fully closed system. Although not utilized for the initial proof-of-concept prototype, inclusion of sterile inline attachments for media exchange to the inlet and outlet fittings of the bioreactor device can completely seal the device from the external environment. Being a closed system, perfusion is required for the infusion of temperature and gas controlled media. The use of a perfusion system allows for precise control of culture parameters and the potential for continuous system monitoring and in-line media sampling. Such a system can greatly improve the safety of the device and comply with current CGMP standards.

However, the inclusion of a perfusion system introduces additional variables into the system that can alter cell adherence and growth. It also adds an increased level of complexity to the device requiring additional costs and labor time to implement. For these reasons, the fittings of the bioreactor were left open, exposed to the local environmental condition, creating a semi-closed system. Use of the bioreactor as a semi-closed system still significantly limited external exposure to contamination. This permitted the bioreactor to fully replicate the pre-defined BLB fabrication methodologies to allow cell growth within a sterile incubator at 37C, 95% humidity, and 5%CO_2 and media exchange within a sterile laminar flow hood. The semi-closed bioreactor still provides reduced contamination risk by eliminating direct user-contact with cells and tissue. Cell injection and media exchange are performed only through sterile injection ports via the syringe push-pull system. Despite being slightly exposed to the external environment, no contamination was observed with use of this device. Once the

cells are injected into the device, the two culture surfaces are not taken apart until the final tissue graft has been created and matured.

The entire device is fabricated from FDA compliant materials. Aside from the disposable cell culture surfaces, the entire system can be sterilized by traditional sterilization techniques (autoclaving or ethylene oxide) and reused. Further UV treating of the device following assembly in a laminar flow hood further ensures the sterility of the device prior to use. When fully closed, the device can be used as a container for tissue preservation, storage, and shipping. The overall goal is to deliver the preserved graft within the device so that it can be stored and opened when needed by the surgeon.

Eliminate Manual, User-Depended Processes

Eventually, the bioreactor system will be designed for complete automation. As opposed to our current manual, user-dependent technology utilized in previous BLB fabrication methods, all physical manipulations were performed on the exterior of the device. This eliminated the user-variability associated with forming the 3D BLB graft during the tissue combination process. Smooth and efficient translation of the tissue was achieved by utilizing a magnet to pull the sutures. Though other modes of movement are feasible, the utilization of a magnetic field to provide translation allows the translational mechanism to be completely sealed from the external environment. The end result is a much more consistent manufacturing process not reliant on technician skill.

The eventual attachment of the bioreactor cartridge into a larger mechanical system will allow for automated magnetic manipulation and inversion, or flipping, of the device. If used in combination with an automatic perfusion system, larger quantities of grafts can be fabricated with minimal need for a technician.

Economically Scalable

The lack of reliance upon technician skill or labor through design of an automated system would greatly improve the economic viability of the device with scale. The bioreactor is modular, meaning several bioreactor cartridge systems can be connected in parallel to a single media reservoir and manifold system. This allows for the production of multiple grafts with little additional costs. The Flip-Plate device was also designed to have a relatively small footprint to maximize space and reduce infrastructure costs with large-scale manufacturing. The current dimensions were chosen due to ease of manufacturing. Small profile devices can be achieved through more skillful machining processes such as injection molding.

5.13.2 Performance Requirements

The Flip-Plate bioreactor successfully produced a construct that was morphologically similar to previous work [105], thus demonstrating the successful adaptation of our manual BLB fabrication methods into a semi-closed automated process. The entire construct was continuous with compositionally different tissue at each end. Mineralized matrix was observed in the bone regions of the graft despite the removal of dexamethasone and prolonged exposure to ligament growth medium. Mechanically, despite being similar to the ligament-only controls, the modulus of the ligament region of the graft was approximately an order of magnitude lower than previously data described in section 3.5.5. The reason for this is likely due to the difference in maturation time of only 1 week in the present study. Further studies will investigate whether additional time *in vitro* may improve matrix remodeling and graft mechanics at later time points.

Size disparity was also observed between experiments. Larger 5 mm and 2 mm diameter constructs formed during stage 1 at one-week time points in 100 mm and 150 mm plates, respectively, were not reproduced during Flip-Plate bioreactor experiments. Flip-Plate BLB constructs were approximately 2-3 mm in diameter. Inherent variability in cell ECM synthesis and remodeling likely account

for these differences. Previous work has demonstrated the ability of the BLB construct to significantly grow in size *in vivo* approximating the native tissue dimensions. Despite this feature, the *in vitro* construct must still maintain a consistent and robust diameter to provide sufficient structural integrity during the implantation procedure. Therefore, strategies to maintain construct size, such as alteration of culture surface area, the removal of TGF-B, or release of suture tension, may be needed to prevent excessive tissue condensation and better preserve construct diameter and viability.

Delamination and 3D tissue formation within the Flip-Plate bioreactor was facilitated through the use of tensioned sutures, rather than conventional pin-plates described previously. During both trans-osseous rotator cuff repair and anatomic ACL reconstructive surgery, the tissue-engineered graft is sutured to the periosteum of the bone. The inclusion of the suture during the fabrication process provides adequate material to secure the ends of the graft and anchor the construct during surgery. Inclusion of alternative suture configurations may enhance suture-graft integration and provide additional stability during implantation and fixation to native tissue. Additionally, through automated manipulation of suture tension, mechanical conditioning of the graft could be performed to modulate the maturation and physical properties of the tissue graft.

5.14 Conclusion

In conclusion, the work outlined in this aim demonstrates the feasibility of converting traditional bench-scale tissue culture techniques into a closed, automated bioreactor system. In addition, this work describes and validates a novel bioreactor design for the fabrication of scaffold-free, multi-phasic, co-cultured tissue grafts for musculoskeletal repair. The application of bioreactors for the generation of tissue-engineered products can lower contamination risks and reduce user-dependency, providing a more consistent and economically scalable manufacturing process. The development of cost-effective, scalable,

and regulatory compliant manufacturing procedures early in the research stages of product development and before pre-clinical and clinical trials can significantly lower the technical, regulatory, and financial hurdles limiting the current translation of products within the tissue engineering field.

Chapter 6
Thesis Conclusions and Future Work

6.1 Conclusions

The objectives of this thesis were to evaluate the efficacy of our scaffold-less tissue engineered constructs to regenerate the rotator cuff enthesis following repair and to advance our existing construct fabrication methodologies to more standardized and commercially relevant manufacturing processes. To accomplish these objectives, the research of this thesis was guided by three aims. Aim 1 focused on the repair of full thickness rotator cuff tears following acute and chronic injury, utilizing our scaffold-less 3D construct methodologies. As described in Chapter 2, use of our engineered tissues improved the regeneration of the rotator cuff enthesis compared to existing suture repair techniques. The re-establishment of the native enthesis is critical for modulating loads at the tendon/bone interface and its regeneration may lead to the improvement of repair outcomes following rotator cuff repair.

Aim 2 focused on the standardization of construct fabrication methodologies for uniform, reproducible, and clinically relevant tissue production. As described in Chapter 3, the use of a non-terminal bone marrow aspiration technique, a Ficoll cell isolation method, a defined passaging density, and a novel monolayer capturing “pin-plate”, greatly improved the consistency and efficiency of our manufacturing process. Furthermore, the application of these processes using human derived MSCs successfully demonstrated the feasibly of our methods to fabricate ligament and bone tissues from a clinically relevant cell source without the use of exogenous scaffolding (Chapter 4). The addition of these

manufacturing processes is a significant step towards the translation of these scaffold-less technologies for human use and enables a more efficient process for construct production.

However, to further expedite the commercialization of this technology and to comply with existing FDA manufacturing guidelines, a novel bioreactor system was designed, built, and evaluated as described in Aim 3. Because no existing bioreactor systems existed for the closed, automated manufacturing of multiple tissues within a single chamber, a new Flip-Plate bioreactor device was developed (Chapter 5). The successful fabrication of a BLB construct within a semi-closed chamber, without the need for direct tissue manipulation by a technician, allows for scalable tissue production needed for large scale BLB graft manufacturing. By addressing issues related to the development and manufacturing of tissue engineering technologies early in the manufacturing process, our ability to overcome current challenges that limit the development of new medical products in the field of regenerative medicine is enhanced.

6.2 Future Work

Future work related to this thesis will focus on the continued evaluation of our constructs in a rotator cuff repair model. Specifically, the safety and efficacy of the constructs following implantation must be evaluated as required by the FDA. While the results of Aim 1 were encouraging in a rat rotator cuff repair model, the construct's utility in a large animal model will need to be demonstrated. Additionally, the toxicological response and *in vivo* function of the graft must be investigated before proceeding into clinical trials.

The manufacturing process of our scaffold-less constructs must also be further validated. While the described methodologies are a significant improvement over existing protocols, they lack the sample size and validation needed to effectively demonstrate the safety and reproducibly of the manufacturing process to the

FDA. Moreover, having optimized production of only the ligament region of our BLB graft, future work is needed to optimize methods related to the formation of scaffold-less bone tissues. To facilitate commercial manufacturing of BLB constructs, several fully automated Flip-Plate bioreactors must be built in order to simultaneously produce a large number of constructs at an economical cost. Production of these constructs will be vital for characterizing the attributes of our tissues and establishing product specifications for our BLB grafts. They will also be needed to support future large-scale FDA process validation studies and the widespread clinical use of our product. The research of this thesis presents a new enthesis repair strategy to improve the treatment of musculoskeletal injuries involving the ACL and rotator cuff tendons. By overcoming the current translational challenges related to product development and industrialized manufacturing early in the research process, the work of this thesis will hopefully provide a framework for expediting the clinical and commercial translation of other tissue engineering products in the field.

References

1. Abbasalizadeh S, Baharvand H. Technological progress and challenges towards cGMP manufacturing of human pluripotent stem cells based therapeutic products for allogeneic and autologous cell therapies. Biotechnol. Adv. 2013;31:1600–1623. doi:10.1016/j.biotechadv.2013.08.009

2. Akhtar MA, Bhattacharya R, Ohly N, Keating JF. Revision ACL reconstruction - causes of failure and graft choices. Br. J. Sports Med. 2011 Nov 10;45(15):A15–A16. doi:10.1136/bjsports-2011-090606.49

3. Angeline ME, Rodeo SA. Biologics in the Management of Rotator Cuff Surgery. Clin. Sports Med. 2012;31:645–663. doi:10.1016/j.csm.2012.07.003

4. Apreleva M, Ozbaydar M, Fitzgibbons PG, Warner JJP. Rotator cuff tears: the effect of the reconstruction method on three-dimensional repair site area. Arthroscopy. 2002;18(5):519–26. doi:10.1053/jars.2002.32930

5. Archer R, Williams DJ. Why tissue engineering needs process engineering. Nat. Biotechnol. 2005;23(11):1353–1355.

6. Ardern CL, Webster KE, Taylor NF, Feller JA. Return to sport following anterior cruciate ligament reconstruction surgery: a systematic review and meta-analysis of the state of play. Br. J. Sports Med. 2011 Jun;45(7):596–606. doi:10.1136/bjsm.2010.076364

7. Aurora A, McCarron J, Iannotti JP, Derwin K. Commercially available extracellular matrix materials for rotator cuff repairs: state of the art and

future trends. J. Shoulder Elbow Surg. 2007;16:S171–8. doi:10.1016/j.jse.2007.03.008

8. Badylak SF. The extracellular matrix as a scaffold for tissue reconstruction. Semin. Cell Dev. Biol. 2002 Oct;13(5):377–83.

9. Barber FA, Herbert MA, Coons DA. Tendon augmentation grafts: biomechanical failure loads and failure patterns. Arthroscopy. 2006 May;22(5):534–8. doi:10.1016/j.arthro.2005.12.021

10. Barenius B, Ponzer S, Shalabi A, Bujak R, Norlén L, Eriksson K. Increased risk of osteoarthritis after anterior cruciate ligament reconstruction: a 14-year follow-up study of a randomized controlled trial. Am. J. Sports Med. 2014 May;42(5):1049–57. doi:10.1177/0363546514526139

11. Bartolozzi A, Andreychik D, Ahmad S. Determinants of outcome in the treatment of rotator cuff disease. Clin. Orthop. Relat. Res. 1994 Nov;(308):90–7.

12. Bassett RW, Cofield RH. Acute tears of the rotator cuff. The timing of surgical repair. Clin. Orthop. Relat. Res. 1983 May;(175):18–24.

13. Bedi A, Maak T, Walsh C, Rodeo SA, Grande D, Dines DM, et al. Cytokines in rotator cuff degeneration and repair. J. Shoulder Elb. Surg. 2012;21:218–227. doi:10.1016/j.jse.2011.09.020

14. Benjamin M, Kumai T, Milz S, Boszczyk BM, Boszczyk AA, Ralphs JR. The skeletal attachment of tendons--tendon “entheses”. Comp. Biochem. Physiol. A. Mol. Integr. Physiol. 2002;133:931–945. doi:10.1016/S1095-6433(02)00138-1

15. Benjamin M, McGonagle D. Entheses: Tendon and ligament attachment sites. Scand. J. Med. Sci. Sport. 2009;19:520–527. doi:10.1111/j.1600-0838.2009.00906.x

16. Benjamin M, Toumi H, Ralphs JR, Bydder G, Best TM, Milz S. Where tendons and ligaments meet bone: Attachment sites (’entheses') in relation to exercise and/or mechanical load. J. Anat. 2006;208:471–490. doi:10.1111/j.1469-7580.2006.00540.x

17. Benjamin M. Anatomy and biochemistry of entheses. Ann. Rheum. Dis. 2000 Dec 1;59(12):995–999. doi:10.1136/ard.59.12.995

18. Bicer EK, Lustig S, Servien E, Selmi TAS, Neyret P. Current knowledge in the anatomy of the human anterior cruciate ligament. Knee Surg. Sports Traumatol. Arthrosc. 2010 Aug;18(8):1075–84. doi:10.1007/s00167-009-0993-8

19. Bishop J, Klepps S, Lo IK, Bird J, Gladstone JN, Flatow EL. Cuff integrity after arthroscopic versus open rotator cuff repair: a prospective study. J. Shoulder Elbow Surg. 2006;15(3):290–9. doi:10.1016/j.jse.2005.09.017

20. Björnsson HC, Norlin R, Johansson K, Adolfsson LE. The influence of age, delay of repair, and tendon involvement in acute rotator cuff tears: structural and clinical outcomes after repair of 42 shoulders. Acta Orthop. 2011 Apr;82(2):187–92. doi:10.3109/17453674.2011.566144

21. Blitz E, Viukov S, Sharir A, Shwartz Y, Galloway JL, Pryce BA, et al. Bone ridge patterning during musculoskeletal assembly is mediated through SCX regulation of Bmp4 at the tendon-skeleton junction. Dev. Cell. 2009 Dec;17(6):861–73. doi:10.1016/j.devcel.2009.10.010

22. Bouchie A. Tissue engineering firms go under. Nat. Biotechnol. 2002;20:1178–1179. doi:10.1038/nbt1202-1178

23. Boykin RE, Heuer HJD, Vaishnav S, Millett PJ. Rotator cuff disease – basics of diagnosis and treatment. Rheumatol. Reports. 2010 Mar 8;2(1). doi:10.4081/rr.2010.e1

24. Brandenberger R, Burger S, Campbell A, Fong T, Lapinskas E, Rowley JA. Cell Therapy Bioprocessing. Bio Process Int. 2011;

25. Brown CH, Carson EW. Revision anterior cruciate ligament surgery. Clin. Sports Med. 1999 Jan;18(1):109–71.

26. Burkhart SS, Johnson TC, Wirth MA, Athanasiou KA. Cyclic loading of transosseous rotator cuff repairs: tension overload as a possible cause of failure. Arthroscopy. 1997 Apr;13(2):172–6.

27. Canseco JA, Kojima K, Penvose AR, Ross JD, Obokata H, Gomoll AH, et al. Effect on Ligament Marker Expression by Direct-Contact Co-culture of Mesenchymal Stem Cells and Anterior Cruciate Ligament Cells. Tissue Eng. Part A. 2012;:120924061154007. doi:10.1089/ten.tea.2012.0030

28. Caplan AI. Mesenchymal stem cells. J. Orthop. Res. 1991 Sep;9(5):641–50. doi:10.1002/jor.1100090504

29. Carpenter JE, Thomopoulos S, Flanagan CL, DeBano CM, Soslowsky LJ. Rotator cuff defect healing: a biomechanical and histologic analysis in an animal model. J. Shoulder Elbow Surg. 1998;7(6):599–605.

30. Castro-Malaspina H, Gay RE, Resnick G, Kapoor N, Meyers P, Chiarieri D, et al. Characterization of human bone marrow fibroblast colony-forming cells (CFU-F) and their progeny. Blood. 1980 Aug;56(2):289–301.

31. Chen J, Xu J, Wang A, Zheng M. Scaffolds for tendon and ligament repair: review of the efficacy of commercial products. Expert Rev. Med. Devices. 2009 Jan;6(1):61–73. doi:10.1586/17434440.6.1.61

32. Cho NS, Yi JW, Rhee YG. Arthroscopic biceps augmentation for avoiding undue tension in repair of massive rotator cuff tears. Arthroscopy. 2009 Feb;25(2):183–91. doi:10.1016/j.arthro.2008.09.012

33. Cofield RH, Parvizi J, Hoffmeyer PJ, Lanzer WL, Ilstrup DM, Rowland CM. Surgical repair of chronic rotator cuff tears. A prospective long-term study. J. Bone Joint Surg. Am. 2001 Jan;83-A(1):71–7.

34. Cohen DB, Kawamura S, Ehteshami JR, Rodeo SA. Indomethacin and celecoxib impair rotator cuff tendon-to-bone healing. Am. J. Sports Med. 2006;34:362–369. doi:10.1177/0363546505280428

35. Coons DA, Alan Barber F. Tendon graft substitutes-rotator cuff patches. Sports Med. Arthrosc. 2006 Sep;14(3):185–90.

36. Cooper RR, Misol S. Tendon and ligament insertion. A light and electron microscopic study. J. Bone Joint Surg. Am. 1970 Jan;52(1):1–20.

37. Crawford SN, Waterman BR, Lubowitz JH. Long-term failure of anterior cruciate ligament reconstruction. Arthroscopy. 2013 Sep;29(9):1566–71. doi:10.1016/j.arthro.2013.04.014

38. Davie NL, Brindley D, Culme-Seymour EJ, Mason C. Streamlining Cell Therapy Manufacture. Bio Process Int. 2012;

39. Dejardin LM, Arnoczky SP, Ewers BJ, Haut RC, Clarke RB. Tissue-engineered rotator cuff tendon using porcine small intestine submucosa. Histologic and mechanical evaluation in dogs. Am. J. Sports Med. 2001;29(2):175–84.

40. Derwin KA, Badylak SF, Steinmann SP, Iannotti JP. Extracellular matrix scaffold devices for rotator cuff repair. J. Shoulder Elb. Surg. 2010;19:467–476. doi:10.1016/j.jse.2009.10.020

41. Derwin KA, Baker AR, Spragg RK, Leigh DR, Iannotti JP. Commercial Extracellular Matrix Scaffolds for Rotator Cuff Tendon Repair: Biomechanical, Biochemical, and Cellular Properties. J Bone Jt. Surg Am. 2006;88:2665–2672. doi:10.2106/JBJS.E.01307

42. Derwin KA, Codsi MJ, Milks RA, Baker AR, McCarron JA, Iannotti JP. Rotator cuff repair augmentation in a canine model with use of a woven poly-L-lactide device. J. Bone Joint Surg. Am. 2009 May;91(5):1159–71. doi:10.2106/JBJS.H.00775

43. Dugas JR, Campbell DA, Warren RF, Robie BH, Millett PJ. Anatomy and dimensions of rotator cuff insertions. J. Shoulder Elbow Surg. 2002;11(5):498–503.

44. Eagan MJ, Zuk PA, Zhao K-W, Bluth BE, Brinkmann EJ, Wu BM, et al. The suitability of human adipose-derived stem cells for the engineering of ligament tissue. J. Tissue Eng. Regen. Med. 2011 Sep 22;6:702–709. doi:10.1002/term.474

45. Van Eck CF, Schkrohowsky JG, Ramirez C, Irrgang JJ, Fu FH, Working Z. Failure Rate and Predictors of Failure after Anatomic ACL Reconstruction with Allograft (SS-61). Arthrosc. J. Arthrosc. Relat. Surg. 2011 May;27(5):e62–e63. doi:10.1016/j.arthro.2011.03.065

46. Ellman H, Hanker G, Bayer M. Repair of the rotator cuff. End-result study of factors influencing reconstruction. J. Bone Joint Surg. Am. 1986 Oct;68(8):1136–44.

47. Ersen A, Demirhan M, Atalar AC, Kapicioğlu M, Baysal G. Platelet-rich plasma for enhancing surgical rotator cuff repair: evaluation and comparison of two application methods in a rat model. Arch. Orthop. Trauma Surg. 2014 Mar;134(3):405–11. doi:10.1007/s00402-013-1914-3

48. Fleming BC, Hulstyn MJ, Oksendahl HL, Fadale PD. Ligament Injury, Reconstruction and Osteoarthritis. Curr. Opin. Orthop. 2005 Oct;16(5):354–362.

49. Freeman JW, Woods MD, Laurencin CT. Tissue engineering of the anterior cruciate ligament using a braid-twist scaffold design. J. Biomech. 2007 Jan;40(9):2029–36. doi:10.1016/j.jbiomech.2006.09.025

50. Fu FH, Bennett CH, Ma CB, Menetrey J, Lattermann C. Current trends in anterior cruciate ligament reconstruction. Part II. Operative procedures and clinical correlations. Am. J. Sports Med. 2000;28(1):124–30.

51. Fuchs B, Weishaupt D, Zanetti M, Hodler J, Gerber C. Fatty degeneration of the muscles of the rotator cuff: assessment by computed tomography versus magnetic resonance imaging. J. Shoulder Elbow Surg. 1999;8(6):599–605.

52. Galatz L, Rothermich S, VanderPloeg K, Petersen B, Sandell L, Thomopoulos S. Development of the supraspinatus tendon-to-bone insertion: localized expression of extracellular matrix and growth factor genes. J. Orthop. Res. 2007 Dec;25(12):1621–8. doi:10.1002/jor.20441

53. Galatz LM, Ball CM, Teefey SA, Middleton WD, Yamaguchi K. The outcome and repair integrity of completely arthroscopically repaired large and massive rotator cuff tears. J. Bone Joint Surg. Am. 2004 Mar;86-A(2):219–24.

54. Galatz LM, Charlton N, Das R, Kim HM, Havlioglu N, Thomopoulos S. Complete removal of load is detrimental to rotator cuff healing. J. Shoulder Elbow Surg. 2009;18(5):669–75. doi:10.1016/j.jse.2009.02.016

55. Galatz LM, Griggs S, Cameron BD, Iannotti JP. Prospective longitudinal analysis of postoperative shoulder function : a ten-year follow-up study of full-thickness rotator cuff tears. J. Bone Joint Surg. Am. 2001 Jul;83-A(7):1052–6.

56. Galatz LM, Sandell LJ, Rothermich SY, Das R, Mastny A, Havlioglu N, et al. Characteristics of the rat supraspinatus tendon during tendon-to-bone healing after acute injury. J. Orthop. Res. 2006;24:541–550. doi:10.1002/jor.20067

57. Gao J, Räsänen T, Persliden J, Messner K. The morphology of ligament insertions after failure at low strain velocity: an evaluation of ligament entheses in the rabbit knee. J. Anat. 1996 Aug;189 (Pt 1:127–33.

58. Gartsman GM. Massive, irreparable tears of the rotator cuff. Results of operative debridement and subacromial decompression. J. Bone Joint Surg. Am. 1997 May;79(5):715–21.

59. Gartsman GM. All arthroscopic rotator cuff repairs. Orthop. Clin. North Am. 2001 Jul;32(3):501–10, x.

60. Gazielly DF, Gleyze P, Montagnon C. Functional and anatomical results after rotator cuff repair. Clin. Orthop. Relat. Res. 1994 Jul;(304):43–53.

61. Genin GM, Kent A, Birman V, Wopenka B, Pasteris JD, Marquez PJ, et al. Functional grading of mineral and collagen in the attachment of tendon to bone. Biophys. J. 2009 Aug 19;97(4):976–85. doi:10.1016/j.bpj.2009.05.043

62. Gimbel JA, Van Kleunen JP, Lake SP, Williams GR, Soslowsky LJ. The role of repair tension on tendon to bone healing in an animal model of chronic rotator cuff tears. J. Biomech. 2007 Jan;40(3):561–8. doi:10.1016/j.jbiomech.2006.02.010

63. Gimbel JA, Van Kleunen JP, Mehta S, Perry SM, Williams GR, Soslowsky LJ. Supraspinatus tendon organizational and mechanical properties in a chronic rotator cuff tear animal model. J. Biomech. 2004 May;37(5):739–49. doi:10.1016/j.jbiomech.2003.09.019

64. Goh JC-H, Ouyang H-W, Teoh S-H, Chan CKC, Lee E-H. Tissue-engineering approach to the repair and regeneration of tendons and ligaments. Tissue Eng. 2003 Jan;9 Suppl 1:S31–44. doi:10.1089/10763270360696969

65. Goltry K, Hampson B, Venturi N, Bartel R. Large-scale production of adult stem cells for clinical use. In: Lakshmipathy U, Chesnut J, Thyagarajan B, editors. Emerging Technology Platforms for Stem Cells. John Wiley and Sons, Inc; 2009. p. 153–168.

66. Gore DR, Murray MP, Sepic SB, Gardner GM. Shoulder-muscle strength and range of motion following surgical repair of full-thickness rotator-cuff tears. J. Bone Joint Surg. Am. 1986 Mar;68(2):266–72.

67. Goutallier D, Postel J-M, Gleyze P, Leguilloux P, Van Driessche S. Influence of cuff muscle fatty degeneration on anatomic and functional outcomes after simple suture of full-thickness tears. J. Shoulder Elbow Surg. 2003;12(6):550–4. doi:10.1016/S1058274603002118

68. Goutallier D, Postel JM, Bernageau J, Lavau L, Voisin MC. Fatty muscle degeneration in cuff ruptures. Pre- and postoperative evaluation by CT scan. Clin. Orthop. Relat. Res. 1994 Jul;(304):78–83.

69. Gulotta L V, Kovacevic D, Ehteshami JR, Dagher E, Packer JD, Rodeo SA. Application of bone marrow-derived mesenchymal stem cells in a rotator cuff repair model. Am. J. Sports Med. 2009;37:2126–2133. doi:10.1177/0363546509339582

70. Gulotta L V, Kovacevic D, Packer JD, Deng XH, Rodeo SA. Bone marrow-derived mesenchymal stem cells transduced with scleraxis improve rotator cuff healing in a rat model. Am. J. Sports Med. 2011;39:1282–1289. doi:10.1177/0363546510395485

71. Gulotta L V., Rodeo SA. Growth Factors for Rotator Cuff Repair. Clin. Sports Med. 2009;28:13–23. doi:10.1016/j.csm.2008.09.002

72. Gumucio JP, Korn MA, Saripalli AL, Flood MD, Phan AC, Roche SM, et al. Aging-associated exacerbation in fatty degeneration and infiltration after rotator cuff tear. J. Shoulder Elbow Surg. 2014 Jan;23(1):99–108. doi:10.1016/j.jse.2013.04.011

73. Gutiérrez-Adán A, Cushwa WT, Anderson GB, Medrano JF. Ovine-specific Y-chromosome RAPD-SCAR marker for embryo sexing. Anim. Genet. 1997 Apr;28(2):135–8.

74. Harryman DT, Mack LA, Wang KY, Jackins SE, Richardson ML, Matsen FA. Repairs of the rotator cuff. Correlation of functional results with integrity of the cuff. J. Bone Joint Surg. Am. 1991 Aug;73(7):982–9.

75. Hattrup SJ. Rotator cuff repair: relevance of patient age. J. Shoulder Elbow Surg. 1995;4(2):95–100.

76. Hersche O, Gerber C. Passive tension in the supraspinatus musculotendinous unit after long-standing rupture of its tendon: a preliminary report. J. Shoulder Elbow Surg. 1998;7(4):393–6.

77. Hettrich CM, Rodeo SA, Hannafin JA, Ehteshami J, Shubin Stein BE. The effect of muscle paralysis using Botox on the healing of tendon to bone in a rat model. J. Shoulder Elb. Surg. 2011;20:688–697. doi:10.1016/j.jse.2010.09.016

78. Iannotti J. Full-Thickness Rotator Cuff Tears: Factors Affecting Surgical Outcome. J. Am. Acad. Orthop. Surg. 1994 Mar;2(2):87–95.

79. Iannotti JP, Bernot MP, Kuhlman JR, Kelley MJ, Williams GR. Postoperative assessment of shoulder function: a prospective study of full-thickness rotator cuff tears. J. Shoulder Elbow Surg. 1996;5(6):449–57.

80. Iannotti JP, Codsi MJ, Kwon YW, Derwin K, Ciccone J, Brems JJ. Porcine small intestine submucosa augmentation of surgical repair of chronic two-tendon rotator cuff tears. A randomized, controlled trial. J. Bone Joint Surg. Am. 2006 Jun;88(6):1238–44. doi:10.2106/JBJS.E.00524

81. Ide J, Kikukawa K, Hirose J, Iyama K ichi, Sakamoto H, Fujimoto T, et al. The effect of a local application of fibroblast growth factor-2 on tendon-to-bone remodeling in rats with acute injury and repair of the supraspinatus tendon. J. Shoulder Elb. Surg. 2009;18:391–398. doi:10.1016/j.jse.2009.01.013

82. Ide J, Kikukawa K, Hirose J, Iyama K ichi, Sakamoto H, Mizuta H. The Effects of Fibroblast Growth Factor-2 on Rotator Cuff Reconstruction With Acellular Dermal Matrix Grafts. Arthrosc. - J. Arthrosc. Relat. Surg. 2009;25:608–616. doi:10.1016/j.arthro.2008.11.011

83. Killian ML, Cavinatto L, Galatz LM, Thomopoulos S. The role of mechanobiology in tendon healing. J. Shoulder Elb. Surg. 2012;21:228–237. doi:10.1016/j.jse.2011.11.002

84. Kim HM, Galatz LM, Das R, Havlioglu N, Rothermich SY, Thomopoulos S. The role of transforming growth factor beta isoforms in tendon-to-bone healing. Connect. Tissue Res. 2011;52:87–98. doi:10.3109/03008207.2010.483026

85. Kirschenbaum D, Coyle MP, Leddy JP, Katsaros P, Tan F, Cody RP. Shoulder strength with rotator cuff tears. Pre- and postoperative analysis. Clin. Orthop. Relat. Res. 1993 Mar;(288):174–8.

86. Kovacevic D, Fox AJ, Bedi A, Ying L, Deng X-H, Warren RF, et al. Calcium-phosphate matrix with or without TGF-β3 improves tendon-bone healing after rotator cuff repair. Am. J. Sports Med. 2011;39:811–819. doi:10.1177/0363546511399378

87. Kronberg M, Wahlström P, Broström LA. Shoulder function after surgical repair of rotator cuff tears. J. Shoulder Elbow Surg. 1997;6(2):125–30.

88. Kumagai J, Sarkar K, Uhthoff HK, Okawara Y, Ooshima A. Immunohistochemical distribution of type I, II and III collagens in the rabbit supraspinatus tendon insertion. J. Anat. 1994 Oct;185 (Pt 2:279–84.

89. Lähteenmäki HE, Hiltunen A, Virolainen P, Nelimarkka O. Repair of full-thickness rotator cuff tears is recommended regardless of tear size and age: a retrospective study of 218 patients. J. Shoulder Elbow Surg. 2007;16(5):586–90. doi:10.1016/j.jse.2007.04.001

90. Lehman C, Cuomo F, Kummer FJ, Zuckerman JD. The incidence of full thickness rotator cuff tears in a large cadaveric population. Bull. Hosp. Jt. Dis. 1995 Jan;54(1):30–1.

91. Li X, Xie J, Lipner J, Yuan X, Thomopoulos S, Xia Y. Nanofiber scaffolds with gradations in mineral content for mimicking the tendon-to-bone insertion site. Nano Lett. 2009;9:2763–2768. doi:10.1021/nl901582f

92. Liu W, Lipner J, Xie J, Manning CN, Thomopoulos S, Xia Y. Nanofiber scaffolds with gradients in mineral content for spatial control of osteogenesis. ACS Appl. Mater. Interfaces. 2014;6:2842–2849. doi:10.1021/am405418g

93. Liu YX, Thomopoulos S, Birman V, Li JS, Genin GM. Bi-material attachment through a compliant interfacial system at the tendon-to-bone insertion site. Mech. Mater. 2012;44:83–92. doi:10.1016/j.mechmat.2011.08.005

94. Livak KJ, Schmittgen TD. Analysis of relative gene expression data using real-time quantitative PCR and the 2(-Delta Delta C(T)) Method. Methods. 2001 Dec;25(4):402–8. doi:10.1006/meth.2001.1262

95. Lohmander LS, Englund PM, Dahl LL, Roos EM. The long-term consequence of anterior cruciate ligament and meniscus injuries: osteoarthritis. Am. J. Sports Med. 2007 Oct;35(10):1756–69. doi:10.1177/0363546507307396

96. Longo UG, Lamberti A, Maffulli N, Denaro V. Tendon augmentation grafts: A systematic review. Br. Med. Bull. 2010;94:165–188. doi:10.1093/bmb/ldp051

97. Longo UG, Lamberti A, Petrillo S, Maffulli N, Denaro V. Scaffolds in tendon tissue engineering. Stem Cells Int. 2012 Jan;2012:517165. doi:10.1155/2012/517165

98. Lu HH, Jiang J. Interface tissue engineering and the formulation of multiple-tissue systems. Adv. Biochem. Eng. Biotechnol. 2006;102:91–111. doi:10.1007/b138509

99. Lu HH, Subramony SD, Boushell MK, Zhang X. Tissue engineering strategies for the regeneration of orthopedic interfaces. Ann. Biomed. Eng. 2010;38:2142–2154. doi:10.1007/s10439-010-0046-y

100. Lu HH, Thomopoulos S. Functional attachment of soft tissues to bone: development, healing, and tissue engineering. Annu. Rev. Biomed. Eng. 2013;15:201–26. doi:10.1146/annurev-bioeng-071910-124656

101. Lui P, Zhang P, Chan K, Qin L. Biology and augmentation of tendon-bone insertion repair. J. Orthop. Surg. Res. 2010;5:59. doi:10.1186/1749-799X-5-59

102. Lysaght MJ, Hazlehurst AL. Tissue Engineering: The End of the Beginning. Tissue Eng. 2004;10:309–320. doi:10.1089/107632704322791943

103. Lysaght MJ, Jaklenec A, Deweerd E. Great expectations: private sector activity in tissue engineering, regenerative medicine, and stem cell

therapeutics. Tissue Eng. Part A. 2008;14:305–315. doi:10.1089/tea.2007.0267

104. Ma J, Goble K, Smietana M, Kostrominova T, Larkin L, Arruda EM. Morphological and functional characteristics of three-dimensional engineered bone-ligament-bone constructs following implantation. J. Biomech. Eng. 2009;131:101017. doi:10.1115/1.4000151

105. Ma J, Smietana MJ, Kostrominova TY, Wojtys EM, Larkin LM, Arruda EM. Three-Dimensional Engineered Bone–Ligament–Bone Constructs for Anterior Cruciate Ligament Replacement. Tissue Eng. Part A. 2011;00(00):103–116. doi:10.1089/ten.tea.2011.0231

106. Ma J. Jinjin Thesis. 2012;

107. Manning CN, Kim HM, Sakiyama-Elbert S, Galatz LM, Havlioglu N, Thomopoulos S. Sustained delivery of transforming growth factor beta three enhances tendon-to-bone healing in a rat model. J. Orthop. Res. 2011 Jul;29(7):1099–105. doi:10.1002/jor.21301

108. Mansat P, Cofield RH, Kersten TE, Rowland CM. Complications of rotator cuff repair. Orthop. Clin. North Am. 1997 Apr;28(2):205–13.

109. Marston WA, Hanft J, Norwood P, Pollak R. The efficacy and safety of Dermagraft in improving the healing of chronic diabetic foot ulcers: results of a prospective randomized trial. 2003. doi:10.2337/diacare.26.6.1701

110. Martin I, Simmons PJ, Williams DF. Manufacturing challenges in regenerative medicine. Sci. Transl. Med. 2014;6:232fs16. doi:10.1126/scitranslmed.3008558

111. Mascarenhas R, MacDonald PB. Anterior cruciate ligament reconstruction: a look at prosthetics--past, present and possible future. Mcgill J. Med. 2008 Jan;11(1):29–37.

112. Mason C, Hoare M. Regenerative medicine bioprocessing: building a conceptual framework based on early studies. Tissue Eng. 2007;13:301–311. doi:10.1089/ten.2007.13.ft-307

113. Moffat KL, Wang INE, Rodeo SA, Lu HH. Orthopedic Interface Tissue Engineering for the Biological Fixation of Soft Tissue Grafts. Clin. Sports Med. 2009;28:157–176. doi:10.1016/j.csm.2008.08.006

114. Montgomery SR, Petrigliano FA, Gamradt SC. Biologic augmentation of rotator cuff repair. Curr. Rev. Musculoskelet. Med. 2011;4:221–230. doi:10.1007/s12178-011-9095-6

115. Mosna F, Sensebé L, Krampera M. Human bone marrow and adipose tissue mesenchymal stem cells: a user's guide. Stem Cells Dev. 2010;19:1449–1470. doi:10.1089/scd.2010.0140

116. Murray MM. Current Status and Potential of Primary ACL Repair. Clin. Sports Med. 2009;28:51–61. doi:10.1016/j.csm.2008.08.005

117. Nassos JT, Chudik SC. Arthroscopic rotator cuff repair with biceps tendon augmentation. Am. J. Orthop. (Belle Mead. NJ). 2009 Jun;38(6):279–81.

118. Neer CS, Craig E V, Fukuda H. Cuff-tear arthropathy. J. Bone Joint Surg. Am. 1983 Dec;65(9):1232–44.

119. Neuhuber B, Swanger SA, Howard L, Mackay A, Fischer I. Effects of plating density and culture time on bone marrow stromal cell characteristics. Exp. Hematol. 2008 Sep;36(9):1176–85. doi:10.1016/j.exphem.2008.03.019

120. Nho SJ, Delos D, Yadav H, Pensak M, Romeo AA, Warren RF, et al. Biomechanical and biologic augmentation for the treatment of massive rotator cuff tears. Am. J. Sports Med. 2010 Mar;38(3):619–29. doi:10.1177/0363546509343199

121. Obma PR. Free biceps tendon autograft to augment arthroscopic rotator cuff repair. Arthrosc. Tech. 2013 Jan;2(4):e441–5. doi:10.1016/j.eats.2013.07.002

122. Paxton JZ, Barr K, Grover LM. Current Progress in Enthesis Repair: Strategies for Interfacial Tissue Engineering. Orthop. Muscular Syst. 2012;S1:1–13. doi:10.4172/2161-0533.S1-003

123. Paxton JZ, Donnelly K, Keatch RP, Baar K, Grover LM. Factors affecting the longevity and strength in an in vitro model of the bone-ligament interface. Ann. Biomed. Eng. 2010;38:2155–2166. doi:10.1007/s10439-010-0044-0

124. Pennisi E. Tending tender tendons. Science. 2002 Mar 8;295(5557):1011. doi:10.1126/science.295.5557.1011

125. Persson A, Fjeldsgaard K, Gjertsen J-E, Kjellsen AB, Engebretsen L, Hole RM, et al. Increased risk of revision with hamstring tendon grafts compared with patellar tendon grafts after anterior cruciate ligament reconstruction: a study of 12,643 patients from the Norwegian Cruciate Ligament Registry, 2004-2012. Am. J. Sports Med. 2014 Mar;42(2):285–91. doi:10.1177/0363546513511419

126. Petersen W, Laprell H. Insertion of autologous tendon grafts to the bone: a histological and immunohistochemical study of hamstring and patellar tendon grafts. Knee Surg. Sports Traumatol. Arthrosc. 2000;8:26–31. doi:10.1007/s001670050006

127. Petrigliano FA, McAllister DR, Wu BM. Tissue engineering for anterior cruciate ligament reconstruction: a review of current strategies. Arthroscopy. 2006;22:441–451. doi:10.1016/j.arthro.2006.01.017

128. Phillips JE, Burns KL, Le Doux JM, Guldberg RE, García AJ. Engineering graded tissue interfaces. Proc. Natl. Acad. Sci. U. S. A. 2008 Aug 26;105(34):12170–5. doi:10.1073/pnas.0801988105

129. Von Porat A, Roos EM, Roos H. High prevalence of osteoarthritis 14 years after an anterior cruciate ligament tear in male soccer players: a study of radiographic and patient relevant outcomes. Ann. Rheum. Dis. 2004 Mar;63(3):269–73.

130. Puchtler H, Meloan SN, Terry MS. On the history and mechanism of alizarin and alizarin red S stains for calcium. J. Histochem. Cytochem. 1969 Feb;17(2):110–24.

131. Ratcliffe A, Niklason LE. Bioreactors and bioprocessing for tissue engineering. Ann. N. Y. Acad. Sci. 2002;961:210–215. doi:10.1111/j.1749-6632.2002.tb03089.x

132. Ratcliffe E, Thomas RJ, Williams DJ. Current understanding and challenges in bioprocessing of stem cell-based therapies for regenerative medicine. Br. Med. Bull. 2011;100:137–155. doi:10.1093/bmb/ldr037

133. Rayment EA, Williams DJ. Concise review: Mind the gap: Challenges in characterizing and quantifying cell- and tissue-based therapies for clinical translation. Stem Cells. 2010;28:996–1004. doi:10.1002/stem.416

134. Reinhardt KR, Hetsroni I, Marx RG. Graft selection for anterior cruciate ligament reconstruction: a level I systematic review comparing failure rates and functional outcomes. Orthop. Clin. North Am. 2010 Apr;41(2):249–62. doi:10.1016/j.ocl.2009.12.009

135. Rhee YG, Cho NS, Lim CT, Yi JW, Vishvanathan T. Bridging the gap in immobile massive rotator cuff tears: augmentation using the tenotomized

biceps. Am. J. Sports Med. 2008 Aug;36(8):1511–8. doi:10.1177/0363546508316020

136. Ricchetti ET, Aurora A, Iannotti JP, Derwin KA. Scaffold devices for rotator cuff repair. J. Shoulder Elb. Surg. 2012;21:251–265. doi:10.1016/j.jse.2011.10.003

137. Riley GP, Harrall RL, Constant CR, Chard MD, Cawston TE, Hazleman BL. Glycosaminoglycans of human rotator cuff tendons: changes with age and in chronic rotator cuff tendinitis. Ann. Rheum. Dis. 1994 Jun;53(6):367–76.

138. Riley GP, Harrall RL, Constant CR, Chard MD, Cawston TE, Hazleman BL. Tendon degeneration and chronic shoulder pain: changes in the collagen composition of the human rotator cuff tendons in rotator cuff tendinitis. Ann. Rheum. Dis. 1994 Jun;53(6):359–66.

139. Robertson A, Nutton RW, Keating JF. Current trends in the use of tendon allografts in orthopaedic surgery. J. Bone Joint Surg. Br. 2006 Aug;88(8):988–92. doi:10.1302/0301-620X.88B8.17555

140. Robertson DB, Daniel DM, Biden E. Soft tissue fixation to bone. Am. J. Sports Med. 1986;14(5):398–403.

141. Rodeo SA, Potter HG, Kawamura S, Turner AS, Kim HJ, Atkinson BL. Biologic augmentation of rotator cuff tendon-healing with use of a mixture of osteoinductive growth factors. J. Bone Joint Surg. Am. 2007 Nov;89(11):2485–97. doi:10.2106/JBJS.C.01627

142. Rodeo SA, Suzuki K, Deng XH, Wozney J, Warren RF. Use of recombinant human bone morphogenetic protein-2 to enhance tendon healing in a bone tunnel. Am. J. Sports Med. 1999;27(4):476–88.

143. Rokito AS, Zuckerman JD, Gallagher MA, Cuomo F. Strength after surgical repair of the rotator cuff. J. Shoulder Elbow Surg. 1996;5(1):12–7.

144. Romeo AA, Hang DW, Bach BR, Shott S. Repair of full thickness rotator cuff tears. Gender, age, and other factors affecting outcome. Clin. Orthop. Relat. Res. 1999 Oct;(367):243–55.

145. Roos EM. Joint injury causes knee osteoarthritis in young adults. Curr. Opin. Rheumatol. 2005 Mar;17(2):195–200.

146. Dos Santos FF, Andrade PZ, Da Silva CL, Cabral JMS. Bioreactor design for clinical-grade expansion of stem cells. Biotechnol. J. 2013;8:644–654. doi:10.1002/biot.201200373

147. Schlegel TF, Hawkins RJ, Lewis CW, Motta T, Turner AS. The effects of augmentation with Swine small intestine submucosa on tendon healing under tension: histologic and mechanical evaluations in sheep. Am. J. Sports Med. 2006 Feb;34(2):275–80. doi:10.1177/0363546505279912

148. Schwartz AG, Pasteris JD, Genin GM, Daulton TL, Thomopoulos S. Mineral Distributions at the Developing Tendon Enthesis. PLoS One. 2012;7. doi:10.1371/journal.pone.0048630

149. Sclamberg SG, Tibone JE, Itamura JM, Kasraeian S. Six-month magnetic resonance imaging follow-up of large and massive rotator cuff repairs reinforced with porcine small intestinal submucosa. J. Shoulder Elbow Surg. 2004;13(5):538–41. doi:10.1016/S1058274604001193

150. Shaw HM, Benjamin M. Structure-function relationships of entheses in relation to mechanical load and exercise: Review. Scand. J. Med. Sci. Sport. 2007;17:303–315. doi:10.1111/j.1600-0838.2007.00689.x

151. Shaw R. Industrializing Stem Cell Production. Bio Process Int. 2010;:10–15.

152. Shearn JT, Kinneberg KR, Dyment NA, Galloway MT, Kenter K, Wylie C, et al. Tendon tissue engineering: progress, challenges, and translation to the clinic. J. Musculoskelet. Neuronal Interact. 2011;11:163–173.

153. Smietana MJ, Syed-Picard FN, Ma J, Kostrominova T, Arruda EM, Larkin LM. The effect of implantation on scaffoldless three-dimensional engineered bone constructs. Vitr. Cell. Dev. Biol. - Anim. 2009;45:512–522. doi:10.1007/s11626-009-9216-3

154. Smith L, Xia Y, Galatz LM, Genin GM, Thomopoulos S. Tissue-Engineering Strategies for the Tendon/Ligament-to-Bone Insertion. Connect. Tissue Res. 2012;53:95–105. doi:10.3109/03008207.2011.650804

155. Spalazzi JP, Boskey AL, Pleshko N, Lu HH. Quantitative Mapping of Matrix Content and Distribution across the Ligament-to-Bone Insertion. PLoS One. 2013;8. doi:10.1371/journal.pone.0074349

156. Spalazzi JP, Dagher E, Doty SB, Guo XE, Rodeo SA, Lu HH. In vivo evaluation of a tri-phasic composite scaffold for anterior cruciate ligament-to-bone integration. In: Annual International Conference of the IEEE Engineering in Medicine and Biology - Proceedings. 2006. p. 525–528.doi:10.1109/IEMBS.2006.259296

157. Spalazzi JP, Dagher E, Doty SB, Guo XE, Rodeo SA, Lu HH. In vivo evaluation of a multiphased scaffold designed for orthopaedic interface tissue engineering and soft tissue-to-bone integration. In: Journal of Biomedical Materials Research - Part A. 2008. p. 1–12.doi:10.1002/jbm.a.32073

158. Spalazzi JP, Doty SB, Moffat KL, Levine WN, Lu HH. Development of controlled matrix heterogeneity on a triphasic scaffold for orthopedic interface tissue engineering. Tissue Eng. 2006;12:3497–3508. doi:10.1089/ten.2006.12.ft-286

159. Spalazzi JP, Vyner MC, Jacobs MT, Moffat KL, Lu HH. Mechanoactive scaffold induces tendon remodeling and expression of fibrocartilage markers. In: Clinical Orthopaedics and Related Research. 2008. p. 1938–1948.doi:10.1007/s11999-008-0310-8

160. Sugimoto Y, Takimoto A, Akiyama H, Kist R, Scherer G, Nakamura T, et al. Scx+/Sox9+ progenitors contribute to the establishment of the junction between cartilage and tendon/ligament. Development. 2013;140:2280–8. doi:10.1242/dev.096354

161. Tempelhof S, Rupp S, Seil R. Age-related prevalence of rotator cuff tears in asymptomatic shoulders. J. Shoulder Elbow Surg. 1999;8(4):296–9.

162. Thomopoulos S, Genin GM, Galatz LM. The development and morphogenesis of the tendon-to-bone insertion - what development can teach us about healing -. J. Musculoskelet. Neuronal Interact. 2010;10:35–45.

163. Thomopoulos S, Hattersley G, Rosen V, Mertens M, Galatz L, Williams GR, et al. The localized expression of extracellular matrix components in healing tendon insertion sites: an in situ hybridization study. J. Orthop. Res. 2002 May;20(3):454–63. doi:10.1016/S0736-0266(01)00144-9

164. Thomopoulos S, Marquez JP, Weinberger B, Birman V, Genin GM. Collagen fiber orientation at the tendon to bone insertion and its influence on stress concentrations. J. Biomech. 2006;39:1842–1851. doi:10.1016/j.jbiomech.2005.05.021

165. Thomopoulos S, Williams GR, Gimbel JA, Favata M, Soslowsky LJ. Variation of biomechanical, structural, and compositional properties along the tendon to bone insertion site. J. Orthop. Res. 2003;21:413–419. doi:10.1016/S0736-0266(03)00057-3

166. Thomopoulos S, Williams GR, Soslowsky LJ. Tendon to bone healing: differences in biomechanical, structural, and compositional properties due to a range of activity levels. J. Biomech. Eng. 2003 Feb;125(1):106–13.

167. Thomopoulos S. The role of mechanobiology in the attachment of tendon to bone. IBMS Bonekey. 2011;8:271–285. doi:10.1138/20110515

168. Tuoheti Y, Itoi E, Yamamoto N, Seki N, Abe H, Minagawa H, et al. Contact area, contact pressure, and pressure patterns of the tendon-bone interface after rotator cuff repair. Am. J. Sports Med. 2005 Dec;33(12):1869–74. doi:10.1177/0363546505278256

169. Vitale MA, Vitale MG, Zivin JG, Braman JP, Bigliani LU, Flatow EL. Rotator cuff repair: an analysis of utility scores and cost-effectiveness. J. Shoulder Elbow Surg. 2007;16(2):181–7. doi:10.1016/j.jse.2006.06.013

170. Vunjak-Novakovic G, Altman G, Horan R, Kaplan DL. Tissue engineering of ligaments. Annu. Rev. Biomed. Eng. 2004;6:131–156. doi:10.1146/annurev.bioeng.6.040803.140037

171. Walton JR, Bowman NK, Khatib Y, Linklater J, Murrell GAC. Restore orthobiologic implant: not recommended for augmentation of rotator cuff repairs. J. Bone Joint Surg. Am. 2007 Apr;89(4):786–91. doi:10.2106/JBJS.F.00315

172. Waltrip RL, Zheng N, Dugas JR, Andrews JR. Rotator cuff repair. A biomechanical comparison of three techniques. Am. J. Sports Med. 2003;31(4):493–7.

173. Wang T, Gardner B, Lin Z, Rubenson J, Wang A, Kirk TB, et al. Bioreactor design for tendon/ligament engineering. Tissue Eng. Part B Rev. 2012;:121017044711003. doi:10.1089/ten.TEB.2012.0295

174. Wang X, Wenk E, Zhang X, Meinel L, Vunjak-Novakovic G, Kaplan DL. Growth factor gradients via microsphere delivery in biopolymer scaffolds for osteochondral tissue engineering. J. Control. Release. 2009;134:81–90. doi:10.1016/j.jconrel.2008.10.021

175. Wendt D, Riboldi SA, Cioffi M, Martin I. Potential and bottlenecks of bioreactors in 3D cell culture and tissue manufacturing. Adv. Mater. 2009;21:3352–3367. doi:10.1002/adma.200802748

176. Williams DJ, Sebastine IM. Tissue engineering and regenerative medicine: manufacturing challenges. IEE Proc. Nanobiotechnol. 2005;152:207–210. doi:10.1049/ip-nbt:20050001

177. Williams DJ, Thomas RJ, Hourd PC, Chandra A, Ratcliffe E, Liu Y, et al. Precision manufacturing for clinical-quality regenerative medicines. Philos. Trans. R. Soc. A Math. Phys. Eng. Sci. 2012;370:3924–3949. doi:10.1098/rsta.2011.0049

178. Williams DJ. Overcoming manufacturing and scale-up challenges. Regen. Med. 2011 Nov;6(6 Suppl):67–9. doi:10.2217/rme.11.63

179. Woo SL, Buckwalter JA. AAOS/NIH/ORS workshop. Injury and repair of the musculoskeletal soft tissues. Savannah, Georgia, June 18-20, 1987. J. Orthop. Res. 1988 Jan;6(6):907–31. doi:10.1002/jor.1100060615

180. Wopenka B, Kent A, Pasteris JD, Yoon Y, Thomopoulos S. The tendon-to-bone transition of the rotator cuff: a preliminary Raman spectroscopic study documenting the gradual mineralization across the insertion in rat tissue samples. Appl. Spectrosc. 2008 Dec;62(12):1285–94. doi:10.1366/000370208786822179

181. Würgler-Hauri CC, Dourte LM, Baradet TC, Williams GR, Soslowsky LJ. Temporal expression of 8 growth factors in tendon-to-bone healing in a rat

supraspinatus model. J. Shoulder Elbow Surg. 2007;16(5 Suppl):S198–203. doi:10.1016/j.jse.2007.04.003

182. Yamanaka K, Matsumoto T. The joint side tear of the rotator cuff. A followup study by arthrography. Clin. Orthop. Relat. Res. 1994 Jul;(304):68–73.

183. Yates EW, Rupani A, Foley GT, Khan WS, Cartmell S, Anand SJ. Ligament tissue engineering and its potential role in anterior cruciate ligament reconstruction. Stem Cells Int. 2012;doi:10.1155/2012/438125

184. Yilgor C, Yilgor Huri P, Huri G. Tissue engineering strategies in ligament regeneration. Stem Cells Int. 2012;doi:10.1155/2012/374676

185. Zhang L, Tran N, Chen HQ, Kahn CJF, Marchal S, Groubatch F, et al. Time-related changes in expression of collagen types I and III and of tenascin-C in rat bone mesenchymal stem cells under co-culture with ligament fibroblasts or uniaxial stretching. Cell Tissue Res. 2008;332:101–109. doi:10.1007/s00441-007-0564-6

186. Zhang X, Bogdanowicz D, Erisken C, Lee NM, Lu HH. Biomimetic scaffold design for functional and integrative tendon repair. J. Shoulder Elb. Surg. 2012;21:266–277. doi:10.1016/j.jse.2011.11.016

187. Zumstein MA, Jost B, Hempel J, Hodler J, Gerber C. The clinical and structural long-term results of open repair of massive tears of the rotator cuff. J. Bone Joint Surg. Am. 2008 Nov;90(11):2423–31. doi:10.2106/JBJS.G.00677